TURUN
YLIOPISTO
UNIVERSITY
OF TURKU

MOLECULAR IMAGING OF AUTOIMMUNE MYOCARDITIS USING NEW PET TRACERS IN EXPERIMENTAL MODELS

Arghavan Jahandideh

TURUN YLIOPISTON JULKAISUJA – ANNALES UNIVERSITATIS TURKUENSIS
SARJA – SER. D OSA – TOM. 1832 | MEDICA – ODONTOLOGICA | TURKU 2024

TURUN
YLIOPISTO
UNIVERSITY
OF TURKU

MOLECULAR IMAGING OF AUTOIMMUNE MYOCARDITIS USING NEW PET TRACERS IN EXPERIMENTAL MODELS

Arghavan Jahandideh

TURUN YLIOPISTON JULKAISUJA – ANNALES UNIVERSITATIS TURKUENSIS
SARJA – SER. D OSA – TOM. 1832 | MEDICA – ODONTOLOGICA | TURKU 2024

University of Turku

Faculty of Medicine
Department of Clinical Physiology and Nuclear Medicine
Doctoral Programme in Clinical Research
Turku PET Centre

Supervised by

Professor Antti Saraste, MD, PhD
Heart Center and Turku PET Centre
University of Turku and
Turku University Hospital
Turku, Finland

Professor Anne Roivainen, PhD
Turku PET Centre and Turku Center for
Disease Modeling
University of Turku
Turku, Finland

Reviewed by

Johanna Magga, PhD
Research Unit of Biomedicine and
Internal Medicine, Faculty of Medicine,
University of Oulu, Finland

Kalle Sipilä, MD, PhD
Department of Clinical Physiology and
Nuclear Medicine, Tampere University
Hospital, Tampere, Finland

Opponent

Professor Kirsi Timonen, MD, PhD
Department of Clinical Physiology and
Nuclear Medicine, Hospital Nova of
Central Finland, Jyväskylä, Finland

ISBN 978-951-29-9994-1 (PRINT)
ISBN 978-951-29-9995-8 (PDF)
ISSN 0355-9483 (Print)
ISSN 2343-3213 (Online)
Painosalama Oy, Turku, Finland 2024

To my family

UNIVERSITY OF TURKU
Faculty of Medicine
Department of Clinical Physiology and Nuclear Medicine
Turku PET Centre
ARGHAVAN JAHANDIDEH: Molecular Imaging of Autoimmune Myocarditis Using New PET Tracers in Experimental Models
Doctoral Dissertation, 155 pp.
Doctoral Programme in Clinical Research
November 2024

ABSTRACT

Diagnosis of myocarditis is challenging because of non-specific clinical presentation of the disease. ^{18}F-FDG PET/CT detects cardiac inflammation. However, non-specific physiological myocardial ^{18}F-FDG uptake impairs the diagnostic accuracy. Current imaging techniques lack specificity for detecting active myocardial inflammation. This study evaluates the efficacy of three Positron Emission Tomography (PET) tracers for identifying myocardial inflammation in experimental autoimmune myocarditis (EAM) rat model and their potential applications in human cardiac sarcoidosis (CS).

Myocarditis was induced by immunizing rats with porcine cardiac myosin in complete Freund's adjuvant. Control rats were injected with Freund's adjuvant alone. Three PET tracers were used in three studies followed by *in vivo* PET/computed tomography (CT) imaging and *ex vivo* autoradiography to study tracers' uptake. Tissue sections of EAM rats and myocardial autopsy samples of patients with CS were studied for folate receptor β (FR-β) and vascular adhesion protein-1 (VAP-1) expression. The first tracer, ^{18}F-FOL, targets FR-β on activated macrophages. The second tracer, [^{68}Ga]Ga-NODAGA-RGD, targets αvβ3 integrin, which is upregulated during angiogenesis and inflammation. The third tracer, [^{68}Ga]Ga-DOTA-Siglec-9, targets VAP-1 associated with leukocyte trafficking. PET/CT imaging with these tracers showed increased uptake in inflamed myocardium compared to non-inflamed myocardium and healthy controls. This uptake was confirmed by *ex vivo* autoradiography. FR-β and VAP-1 were expressed in human cardiac sarcoid lesions.

In conclusion, ^{18}F-FOL, [^{68}Ga]Ga-NODAGA-RGD, and [^{68}Ga]Ga-DOTA-Siglec-9 PET tracers show potential for detecting myocardial inflammation, with potential applicability in human cardiac sarcoidosis.

KEYWORDS: positron emission tomography; inflammation; myocarditis; folate receptor; angiogenesis; αvβ3 integrin; vascular adhesion protein-1

TURUN YLIOPISTO
Lääketieteellinen tiedekunta
Kliininen fysiologia ja isotooppilääketiede
ARGHAVAN JAHANDIDEH: Autoimmuunitulehduksellisen
Sydänlihastulehduksen molekyylikuvaus Uusilla PET-merkkiaineilla
Kokeellisissa Malleissa
Väitöskirja, 155 s.
Kliininen tohtoriohjelma
Marraskuu 2024

TIIVISTELMÄ

Sydänlihastulehduksen diagnosointi on haastavaa vaihtelevan taudinkuvan vuoksi. Positroniemissiotomografia (PET) –tutkimus käyttäen merkkiaineena 18F-fluorideoksiglukoosia ([^{18}F]FDG) auttaa vakavien tautimuotojen diagnostiikassa. Fysiologinen ^{18}F-FDG:n kertyminen sydänlihakseen saattaa kuitenkin heikentää tutkimuksen diagnostista tarkkuutta. Tässä tutkimuksessa selvitettiin kokeellisessa mallissa kolmen uuden PET- merkkiaineen käyttöä sydänlihastulehduksen selvittelyssä ja niiden potentiaalista hyödyntämistä sydänlihassarkoidoosia sairastavien potilaiden diagnostiikassa.

Tutkittavat merkkiaineet olivat ^{18}F-FOL, joka tunnistaa aktivoituneiden makrofagien folaattireseptori beetan, [^{68}Ga]Ga-NODAGA-RGD, joka tunnistaa verisuonten uudismuodostuksessa ja tulehduksessa aktivoituvan αvβ3 integriinireseptorin, sekä [^{68}Ga]Ga-DOTA-Siglec-9, joka tunnistaa leukosyyttien verisuonten adheesioproteiini VAP-1:n. Kokeellisessa mallissa sydänlihastulehdus aiheutettiin immunisoimalla rotat sian sydänmyosiinilla, minkä jälkeen tehtiin PET-tutkimus ja merkkiaineiden kertymää tutkittiin sydänlihasnäytteissä. Folaattireseptori beetan ja VAP-1:n ilmenemistä määritettiin myös potilasnäytteissä. Kaikki tutkitut merkkiaineet kertyivät tulehtuneeseen sydänlihakseen kokeellisessa mallissa, mikä havaittiin PET-tutkimuksessa. Folaattireseptori beeta ja VAP-1 ilmenivät myös sydänlihastulehdusta sairastavien potilaiden sydänlihaksessa.

Yhteenvetona ^{18}F-FOL, [^{68}Ga]Ga-NODAGA-RGD ja [^{68}Ga]Ga-DOTA-Siglec-9 ovat lupaavia PET-tutkimukseen soveltuvia sydänlihastulehduksen merkkiaineita kokeellisessa mallissa.

AVAINSANAT: positroniemissiotomografia; tulehdus; myokardiitti; folaattireseptori; angiogeneesi; αvβ3 integriinireseptori; verisuonten adheesioproteiini-1

Table of Contents

Abbreviations

[^{18}F]FDG	Glucose analog 2-deoxy-2-[^{18}F]fluoro-*D*-glucose
ACE	Angiotensin-converting enzyme
AV	Atrioventricular
BBB	Bundle branch blocks
CCL5	Chemokine ligand 5
CFA	Complete Freund's adjuvant
CMR	Cardiac magnetic resonance
CS	Cardiac sarcoidosis
CXCL9	Chemokine ligand 9
DCM	Dilated cardiomyopathy
DHODH	Dihydroorotate dehydrogenase
EAM	Experimental autoimmune myocarditis
ECG	Electrocardiography
EMB	Endomyocardial biopsy
ERS	European Respiratory Society
FR-β	Folate receptor β
GCM	Giant cell myocarditis
ICD	Implantable cardiac defibrillator
IFA	Incomplete Freund's adjuvant
IFN-γ	Interferon gamma
IL-6	Interleukin-6
IMPDH	Inosine monophosphate dehydrogenase
iNOS	Inducible nitric oxide synthase
IV	Intravenous
JAK	Janus kinase
JCS	Japanese Circulation Society
JMHW	Japanese Ministry of Health and Welfare
LGE	Late gadolinium enhancement
LV	Left ventricle
MGCs	Multinucleated Giant Cells
MHC I	Major histocompatibility complex I

MHC II	Major histocompatibility complex II
MMF	Mycophenolate mofetil
MMP-9	Matrix Metalloproteinase-9
PET	Positron Emission Tomography
ROS	Reactive oxygen species
RV	Right ventricle
sIL-2R	Serum markers like soluble interleukin-2 receptor
SP1	Subproject 1
SP2	Subproject 2
SP3	Subproject 3
sST2	Soluble Suppression of Tumorigenicity 2
TCR	T cell receptors
Th	T helper
Th1	Type 1 T helper
TNF-α	Tumor necrosis factor alpha
T_{reg}	Regulatory T cells
VAP-1	Vascular adhesion protein-1

List of Original Publications

This dissertation is based on the following original publications, which are referred to in the text by their Roman numerals:

I Arghavan Jahandideh, Sauli Uotila, Mia Ståhle, Jenni Virta, Xiang-Guo Li, Ville Kytö, Päivi Marjamäki, Heidi Liljenbäck, Pekka Taimen, Vesa Oikonen, Jukka Lehtonen, Mikko I. Mäyränpää, Qingshou Chen, Philip S. Low, Juhani Knuuti, Anne Roivainen and Antti Saraste. Folate Receptor β-Targeted PET Imaging of Macrophages in Autoimmune Myocarditis. *Journal of Nuclear Medicine*, 2020, 61(11):1643-1649.

II Arghavan Jahandideh, Mia Ståhle, Jenni Virta, Xiang-Guo Li, Heidi Liljenbäck, Olli Moisio, Juhani Knuuti, Anne Roivainen , Antti Saraste. Evaluation of [^{68}Ga]Ga-NODAGA-RGD for PET Imaging of Rat Autoimmune Myocarditis. *Frontiers in Medicine*, 2021, 8:783596.

III Arghavan Jahandideh, Jenni Virta, Xiang-Guo Li, Heidi Liljenbäck, Olli Moisio, Jesse Ponkamo, Noora Rajala, Marion Alix, Jukka Lehtonen, Mikko I Mäyränpää, Tiina A Salminen, Juhani Knuuti, Sirpa Jalkanen, Antti Saraste, Anne Roivainen. Vascular adhesion protein-1-targeted PET imaging in autoimmune myocarditis. *Journal of Nuclear Cardiology*, 2023, 30(6):2760-2772.

1 Introduction

Autoimmune myocarditis stands as a significant challenge in the realm of cardiovascular diseases, incorporating conditions like cardiac sarcoidosis (CS) and giant cell myocarditis (GCM). These disorders, marked by immune-driven inflammation of the heart muscle, present notable complexities in diagnosis and treatment.

CS, initially described in 1929, has gained recognition as a distinct entity within the spectrum of sarcoidosis-related manifestations (Ayoub et al., 2015). GCM first documented in 1905, emerged as a distinct autoimmune disorder characterized by aggressive myocardial inflammation (Saltykow, 1905; DeFilippis et al., 2015; Kandolin et al., 2015; Ekström et al., 2016). Over the decades, advancements in medical science have gradually elucidated the pathophysiological mechanisms underlying these conditions, paving the way for improved diagnostic and therapeutic approaches. CS affects 5% of patients with systemic sarcoidosis (Birnie et al., 2016). Despite its rarity, GCM predominantly affects young to middle-aged adults, with a reported incidence of 0.007-0.02% based on autopsy data (Ekström et al., 2016; Birnie et al., 2016; Whitehead, 1965, Okada & Wakafuji, 1985). The incidence of GCM in Finland was 5.6% among those with fatal myocarditis in Finnish autopsy registry between 1970 and 1998 (Kytö et al., 2005).

The clinical manifestations of autoimmune myocarditis are heterogeneous, ranging from subtle symptoms to life-threatening complications. CS may present with arrhythmias, conduction disturbances, heart failure, or sudden cardiac death, often mimicking other cardiovascular disorders (Kandolin et al., 2015; Birnie et al., 2017). Similarly, GCM typically manifests as acute heart failure, arrhythmias, or conduction abnormalities (DeFilippis et al., 2015; Cooper et al.,1997). The varied clinical phenotypes of these conditions underscore the importance of a comprehensive diagnostic approach. While CS generally carries a favourable prognosis with appropriate immunosuppressive therapy, GCM is associated with a higher mortality rate, particularly in the acute phase (Cooper et al.,1997; Okura et al., 2003). Timely diagnosis, aggressive management, and long-term surveillance are essential for optimizing outcomes and minimizing disease-related complications. Accurate diagnosis of autoimmune myocarditis relies on a combination of clinical

evaluation, imaging modalities, histological analysis, and laboratory investigations. Endomyocardial biopsy remains the gold standard for confirming the diagnosis of autoimmune myocarditis, revealing characteristic histopathological features. However, it is an invasive procedure with several drawbacks, including sampling error and low sensitivity (Birnie et al., 2017; Kandolin et al., 2013; Kadkhodayan et al., 2016).

Advanced imaging techniques, including cardiac magnetic resonance imaging (CMR) and PET, play a pivotal role in assessing myocardial inflammation and disease extent. Key features of myocardial inflammation, including edema, hyperemia, and fibrosis, can be visualized and quantified using specialized CMR sequences such as late gadolinium enhancement (LGE) (Matoh et al., 2008). However, CMR has variable sensitivity and specificity in detection of active inflammation and early stages of autoimmune myocarditis (Friedrich et al., 2009).

PET imaging offers unique insights into the inflammatory processes underlying autoimmune myocarditis by targeting specific molecular pathways involved in immune response. Using radiotracers such as glucose analog 2-deoxy-2-[^{18}F]fluoro-*D*-glucose ([^{18}F]FDG), PET imaging can visualize and quantify myocardial glucose metabolism, which is heightened during inflammation (Schatka & Bengel, 2014; Youssef et al., 2012; Okumura et al., 2004). However, PET relies on the uptake of [^{18}F]FDG by inflammatory cells and the physiological uptake of [^{18}F]FDG by normal myocardium and surrounding tissues may impair its diagnostic accuracy (Youssef et al., 2012; Jeserich et al., 2009; Wu et al., 2013). Thus, novel diagnostic PET radiotracers are under development to improve the detection and characterization of autoimmune myocarditis, providing insights into the underlying molecular mechanisms of myocardial inflammation and tissue injury.

This thesis investigates folate receptor beta (FR-β), αvβ3 integrin and vascular adhesion protein-1 (VAP-1) as new imaging biomarkers in experimental autoimmune myocarditis (EAM) rat model.

2 Review of the Literature

2.1 Myocarditis

Myocarditis is a cardiac inflammatory disease associated with myocardial inflammation and myocyte necrosis. It can be divided into three stages including acute, sub-acute and chronic, which may either cause focal inflammatory lesions or diffuse inflammation in the myocardium. Myocarditis can be caused by multiple mechanisms, including a viral or a non-viral infection, cardiotoxic agents, or autoimmune diseases.

2.1.1 Infectious myocarditis

Viruses are the most common pathogens causing myocarditis, including enteroviruses like Coxsackie B, parvovirus B19 (PVB19) (Tam, 2006; Keramari et al., 2022), human herpesvirus (HHV), adenovirus, influenza A virus, cytomegalovirus, Epstein–Barr virus, hepatitis C virus, and HIV (Barbarinia & Barbaro, 2003; Magnani & Dec, 2006; Watanabe et al., 2019; Schultz et al., 2009). Other infectious causes include bacterial pathogens (e.g., diphtheria or tuberculosis), fungi (e.g., *Aspergillus, Candida or Actinomyces)*, protozoa (e.g., *Trypanosoma cruzi)* and helminths (Brociek et al., 2023; Crum-Cianflone, 2008).

The acute stage of viral myocarditis is usually defined by viral cytotoxicity, while the sub-acute stage is defined by autoimmune mediated injury followed by activation of B cells and T cells, and production of cardiac autoantibodies. Chronic myocarditis is characterized by diffuse myocardial fibrosis that may lead to ventricular arrhythmias, conduction disturbances and inflammatory cardiomyopathy associated with cardiac dysfunction (Sozzi et al., 2022).

Viral myocarditis being by far the most common type of myocarditis, is usually associated with full recovery without leaving any complications. A study on 672 672 Finnish men at a mean age of 20 years in military service over a 20-year period revealed 98 cases with acute viral myocarditis, with none of them presenting with heart failure or cardiomyopathy (Karjalainen & Heikkilä, 1999).

2.1.2 Cardiotoxic Agents Causing Myocarditis

The use of certain drugs such as cocaine, amphetamines, ethanol, antipsychotic medications (lithium, clozapine) immunotherapeutic and chemotherapeutic agents (trastuzumab, anthracyclines, cyclophosphamide) may resulted in toxic myocarditis over time. Additionally, exposure to heavy-metal toxicity, such as with lead, copper, and iron, can contribute to this condition, which may ultimately lead to congestive heart failure and dilated cardiomyopathy (Havakuk et al., 2017; Kilgallen et al., 1998; Shah & Moreb, 2019; Upadhrasta et al., 2019).

2.1.3 Metabolic and Endogenous Causes of Myocarditis

Metabolic disturbances such as thyrotoxicosis, pheochromocytoma, beriberi, and hemochromatosis can cause damage the heart muscle, cardiac inflammation, and potentially leading to myocarditis. These conditions, if left unmanaged, can lead to significant cardiac complications, including congestive heart failure and dilated cardiomyopathy. (Klein et al., 2007; Prejbisz et al., 2011; Lonsdale, 2006; Barton et al., 2018).

2.1.4 Autoimmune Myocarditis

Autoimmune myocarditis is a type of myocarditis where the immune system attacks the heart muscle. It can manifest as various subtypes, including giant cell myocarditis (GCM), lymphocytic myocarditis, pleomorphic myocarditis, eosinophilic myocarditis, hypersensitivity reactions to a drug, allograft rejection after a cardiac transplant, or in association with immunologic syndromes such as sarcoidosis, systemic lupus erythematosus, rheumatoid arthritis, inflammatory bowel disease, Kawasaki disease, Churg-Strauss syndrome, Wegener’s granulomatosis, celiac disease, type 1 diabetes mellitus, systemic sclerosis, thyrotoxicosis, myasthenia gravis, and polymyositis.

2.2 Cardiac Sarcoidosis and Giant Cell Myocarditis

Sarcoidosis is an inflammatory systemic disease that typically affects organs such as the heart, lungs, and kidneys. Cardiac sarcoidosis (CS) is marked by fibrosis and infiltration of immune cells, leading to the formation of non-necrotizing myocardial granulomatous lesions composed of epithelioid cells, T lymphocytes, and multinucleated giant cells (MGCs) derived from macrophages (van Maarsseveen et al., 2009; Cooper et al., 1997; Lagana et al., 2010). CS can result in atrioventricular (AV) block, heart failure, ventricular arrhythmias, and sudden cardiac death (Maisch, 2019). Historically, CS was first reported in a patient with

systemic sarcoidosis in 1929 (Ayoub et al., 2015). For decades, it was estimated that only 12% of cardiac sarcoidosis (CS) cases were diagnosed, as clinical examination was the primary diagnostic method, and advanced imaging techniques were not yet widely available to improve detection rates. (Doughan & Williams, 2006; Matsui et al., 1976).

While CS shares similarities with other chronic autoimmune conditions like giant cell myocarditis (GCM), the two diseases differ in underlying mechanisms and pathology. Both CS and GCM, though rare compared to viral myocarditis, are associated with significant risks and poor outcomes. The systemic and immune-mediated nature of CS continues to pose challenges in both diagnosis and management.

GCM is another type of myocarditis histologically characterized by MGCs and necrotic cardiomyocytes, distinguishing it from CS. However, differentiating CS and GCM based on clinical symptoms is not possible (Saltykow, 1905; Bogabathina et al., 2012). A case study revealed that GCM and CS are a spectrum of pathology rather than distinct pathological entities (Bogabathina et al., 2012). Giant cells are multinucleated inflammatory cells produced by the fusion of CD68 macrophages. GCM was first described in 1905 (Saltykow, 1905) and it is a rare, rapid onset and frequently fatal disorder if it remains untreated. It usually affects young to middle-aged adults. The clinical sequelae of CS and GCM are progressive heart failure, ventricular arrhythmias, AV block and sudden death (DeFilippis et al., 2015; Kandolin et al., 2015; Birnie et al., 2017; Cooper et al.,1997). Considering CS and GCM as two different diseases or two manifestations of the same disorder has been controversial (Nordenswan et al., 2021).

2.2.1 Epidemiology of CS and GCM

CS is commonly found in 5% of patients with sarcoidosis (Birnie et al., 2016). However, the reported prevalence of CS varies in different studies depending on the study population and the type of performed study: clinical, autopsy report or imaging. An imaging study in the U.S. showed cardiac involvement in 2.3% (17 patients) of 736 sarcoidosis patients (Mehta et al., 2008). Similarly, an imaging Swedish study revealed cardiac involvement in 2.3% (22 patients) of 1017 patients with lung sarcoidosis (Darlington et al., 2014). In total 1.5 to 3% of all patients undergone cardiac transplantation were due to CS (Akashi et al., 2012; Zhang et al., 2012; Roberts et al., 2014). In a report of 2950 autopsies, only 2 cases (0.006%) had CS (Abeler, 1979). Two other post-mortem studies showed 20 –27% of myocardial involvement in sarcoidosis patients (Matsui et al., 1976; Sharma, 2008). The

incidence of CS in patients with systemic sarcoidosis was up to 50% in Japanese patients (Sharma, 2008; Iwai et al., 1994). Finally, some imaging studies have found CS in 3.7 to 49% of patients with extracardiac sarcoidosis (Matoh et al., 2008; Mehta et al., 2008; Smedema et al., 2005; Nagai et al., 2014; Patel et al., 2011; Vignaux et al., 2002; Dhôte et al., 2003).

GCM is a rare cardiac disease, but determination of its actual burden is challenging due to insufficient existing epidemiologic data. A study in 1965 reported 3 GCM cases out of 12,815 autopsies from 1950 to 1963 at Oxford Infirmary (Whitehead, 1965). The incidence of GCM at the Japanese autopsy registry was 25 out of 377,841 cases between 1958 and 1977 (Okada et al., 1985). According to a study on the Finnish autopsy registry between 1970 and 1998, the incidence of GCM was 8 (5.6%) out of 142 cases with autopsy confirmed fatal myocarditis (Kytö et al., 2005). The largest multicenter registry data between 1982 and 1997, from about 40 centers worldwide, reported 73 patients diagnosed with GCM (Okura et al., 2003). A study carried out in Finland found 46 cases of GCM between 1991 and 2015 (Ekström et al., 2016).

2.2.2 Pathophysiology of CS and GCM

Sarcoidosis is characterized by the formation of non-necrotizing granulomas in various organs. After the lymphoid and respiratory systems, the cardiovascular system is the third most commonly involved organ system in sarcoidosis. In the heart, sarcoid granulomas usually are formed in the myocardium of the left ventricular free wall followed by the septum, right ventricle, and atria. Histologically, CS granulomas are non-necrotizing, tight, and epithelioid. These granulomas are without a great deal of lymphocytic inflammation and contain epithelioid macrophages to form MGCs, which may contain Schaumann bodies or asteroid bodies. Schaumann bodies are intracellular calcified proteins inclusions within MGCs that supports the diagnosis in 70–88% of the CS cases. Asteroid bodies are stellate-shaped inclusions in MGCs with several rays radiating from the central core that supports the diagnosis in only 2–9% of the CS cases (Rosen, 2022).

Pathologically, GCM ventricular biopsy shows prominent myocyte necrosis and a diffuse inflammatory infiltrate containing MGCs, macrophages, lymphocytes, plasma cells, eosinophils and few neutrophils on light microscopy. Some fibrosis or tissue granulation may be present in inflammatory lesions (Xu & Brooks, 2016). Differentiation of CS and GCM is challenging and may cause confusion due to several shared histopathological features. The lack of granulomas and the presence of eosinophils in GCM is a clue to the diagnosis. Fibrosis is significantly more common in CS (Ekström et al., 2020).

In order to form MGCs, macrophages differentiate into epithelioid cells, develop secretory and bactericidal features, lose some phagocytic properties, and fuse together (Iannuzzi et al., 2007). The etiology of GCM is not yet fully understood, although it seems that autoimmunity has a crucial role in the pathogenesis. According to observations in both human tissue and experimental animal models it seems that GCM is mediated by T lymphocytes (DeFilippis et al., 2015). It can be induced in Lewis rats by autoimmunization with cardiac myosin (Kodama et al., 1990), whereby the inflammatory lesions are dominated by T lymphocytes and macrophages (DeFilippis et al., 2015). Studies showed that short-term therapy with anti-alpha beta T-cell receptor antibodies and cyclosporine (an immunosuppressant that inhibits activated T cells) both delay disease onset in an experimental rat model (Kodama et al., 1990; Hanawa et al., 1994; Zhang et al., 1993). Furthermore, long-term immunosuppressive therapy in humans can increase transplant-free survival rate by more than 19 years (Kandolin et al., 2013; Maleszewski et al., 2015). However, the role of macrophages in the pathophysiology of GCM and the disease progression requires further study.

2.2.3 Animal Models of Autoimmune Myocarditis

The first heart-specific autoimmunity induction in animals was reported in 1958 (Kaplan, 1958). In 1990, an experimental EAM rat model with similarities to the human GCM was established (Kodama et al., 1990). Histologically, MGCs, characteristic of both CS and GCM, are present in this model. In the study (Kodama et al., 1990), Lewis rats were immunized twice, 7 days apart, with human cardiac myosin (a dominant autoantigen in autoimmune myocarditis) emulsified in complete Freund's adjuvant (CFA), via footpad injection. Three weeks after the first immunization all rats developed severe myocarditis. EAM is the most widely used animal model for studying autoimmune myocarditis, as it mimics the severe autoimmune inflammation that leads to inflammatory cardiomyopathy, allowing to study the full spectrum of the disease, including its progression to dilated cardiomyopathy (DCM) (Kodama et al., 1990; Kodama et al., 1992). The peak of inflammation in this animal model occurs at 21 days after their first immunization, followed by a gradual decline thereafter (Błyszczuk, 2019). In addition to the EAM model, other types of animal models used to study autoimmune myocarditis include transgenic models, viral-induced models, spontaneous models, and T-cell transfer models (Kishimoto et al., 2003; Fairweather et al., 2007; Yoshida et al., 1999; Wada et al., 2001).

2.2.4 Genetic Factors in CS and GCM

Genetic factors and predisposition are crucial in the development of autoimmune myocarditis. In animal models, the disease can only be induced in susceptible strains, and the development of the disease is highly dependent on the genetic background of the animal. Mice with *A.SW*, *BALB/c*, *ABY/SnJ* or *A/J* genetic backgrounds, and Lewis rats are susceptible to developing autoimmune myocarditis, while C57BL/6 mice are resistant (Błyszczuk, 2019). Genetic factors are crucial in the susceptibility to sarcoidosis. A study on 210 twin pairs with at least one proband with sarcoidosis showed a higher risk (80-fold) of developing sarcoidosis in monozygotic twins (Sverrild et al., 2008). Another study revealed almost 5-fold increased risk of sarcoidosis among first and second-degree relatives of sarcoidosis patients (Rybicki et al., 2001). Moreover, the incidence of CS development in different ethnics supports the genetic influence (Sato et al., 2010). Different human leucocyte antigen (HLA) gene complexes, located on the chromosome 6, are associated with different phenotypes of sarcoidosis (Sato et al., 2010).

A human study that investigated the expression of 115 different genes in GCM, compared to non-failing hearts, (Kittleson et al., 2005) found upregulation of almost all of the genes that were mostly involved in immune response, regulation of transcription, metabolism and signal transduction. Particularly genes involved in the Th1 immune response (Kittleson et al., 2005). Increased expression of chemokine ligand 5 (CCL5) and chemokine ligand 9 (CXCL9), which are involved in the type 1 T helper (Th1) cells response in GCM, provided evidence for the important role of Th1-specific immune activation in GCM (Kittleson et al., 2005).

2.3 Immune cells in CS and GCM

The term myocarditis is pathologically and clinically related to inflammation of the myocardium. This immune-cell condition was first described by a physician Joseph Friedrich Sobernheim in 1837 (Sobernheim et al., 1837), but there were objections from cardiologists Sir Thomas Lewis and Paul White, because the term was confused with other cardiovascular conditions (Olsen, 1985). Nowadays, several immune mechanisms underlying myocarditis have been clarified, with evidence that various cytokines produced by T lymphocytes and macrophages are important in autoimmune myocarditis (Arango Duque & Descoteaux, 2014; Gutierrez et al., 2014). Granulomas formation in CS is the result of Th-1 lymphocyte immune response in which, Th-1 lymphocytes generate cytokines causing oligoclonal proliferation of T cells. Th-1 lymphocyte immune response also causes macrophage activation and pro-inflammatory T-cell response (Fuse et al., 2003; Hunninghake & Crystal, 1981).

2.3.1 T Cells in CS and GCM

Immature lymphocytes develop into T cells in the thymus and then further in secondary lymphoid organs such as lymph nodes, spleen, appendix, tonsils and Peyer's patches. T cells are crucial for cellular immunity. T cell receptors (TCR) can bind to the antigen fragments, which are linked to the major histocompatibility complex I or II (MHC I, MHC II). CD8+ T cells (cytotoxic T cells) are present at the site of inflammation. Regulatory T cells (T_{reg}) and T helper cells (Th) are the predominant subtypes of CD4+ T cells that are present in the lesions with an important role in adaptive immunity by differentiation into Th1 and Th2 effector cells after initial activation by an antigen. Th1 cells promote inflammation via pro-inflammatory cytokines, while Th2 cells contribute to tissue healing by producing anti-inflammatory cytokines. At the disease onset, high expression of interferon gamma (IFN-γ), tumor necrosis factor alpha (TNF-α) and other cytokines produced by CD4+ Th1 cells stimulate the differentiation of monocytes into pro-inflammatory macrophages, which consequently promote the maintenance of pro-inflammatory Th1 and Th17 lymphocytes by producing pro-inflammatory cytokines, such as TNF-α, IL-1β, IL-6, IL-12, and IL-23 (Arango Duque & Descoteaux, 2014; Gutierrez et al., 2014; Saidha et al., 2012; Okuda et al., 2016). A study showed that cooperation between Th1 and Th17 cells is essential for the transition from autoimmune myocarditis to dilated cardiomyopathy (Nindl et al., 2012). In contrast, Th2 lymphocytes produce IL-13 and IL-4 cytokines that induce the anti-inflammatory polarization in macrophages.

2.3.2 Macrophages in CS and GCM

Macrophages, (discovered in 1884 by Ilya Metchnikoff) are another important cell type present in myocardial lesions in CS and GCM. Blood monocytes, that are derived from the bone marrow, migrate out of the bloodstream and infiltrate tissues. However, whether the bone marrow is the only source of macrophages is still debated. Monocyte differentiation into macrophages occurs in various tissues under different pathological conditions. The spleen has been noted as another source of inflammatory monocytes (Cochain & Zernecke, 2015). Furthermore, a study showed that some of the tissue-resident macrophages arise during embryonic development, with subsequent proliferation in the tissues (Ginhoux & Jung, 2014). With inflammation, there are many factors that affect macrophage phenotype profile and polarization states. Changes in phenotype leads to an adjustment in the gene transcription, followed by expression of different surface molecules and the secretion of different cytokines. Two major subtypes of macrophages exhibit different polarization, including classically activated pro-inflammatory (M1) and alternatively activated anti-inflammatory (M2) types. However, this division does not cover the

full spectrum of macrophage polarization. M1 subtype corresponds with the Th1 response in T cells while M2 subtype corresponds with the Th2 response. M1 macrophages produce proinflammatory cytokines such as IFN-γ, TNF-α, IL-1β, IL-6, IL-12, and chemokine receptor ligands, and initiate an immune response at the site of inflammation (Arango Duque & Descoteaux, 2014; Gutierrez et al., 2014). They also activate inducible nitric oxide synthase (iNOS) and produce reactive oxygen species (ROS), which further participate in the recruitment of new inflammatory cells from the bloodstream and lipid oxidation, respectively. M2 macrophages contribute to tissue healing and control the proliferation of T lymphocytes by producing anti-inflammatory cytokines (Arango Duque & Descoteaux, 2014); they are further divided into M2a, M2b and M2c subtypes, which have different roles. M2a subtype, which is induced by IL-4 and IL-13, secretes fibronectin and TGF-β, contributing to wound healing. M2b and M2c are induced by IL-1β, immune complexes, IL-10 and glucocorticoids; they clean apoptotic cells and are believed to have an immunoregulatory role (Arango Duque & Descoteaux, 2014; Colin et al., 2014; Mosser & Edwards, 2008). Finally, prolonged inflammation leading to myocyte necrosis followed by fibrosis can result in organ dysfunction.

2.3.3 MGCs in CS and GCM

It was previously thought that MGCs in myocarditis are of myogenic origin. Light and electron microscopic studies show the presence of myofibrils, lipofuscin granules and intercalated disks in their cytoplasm (Tubbs et al.,1980; Boesen & Hansen, 1981; Collyns, 1959; Tesluk, 1956; Davies et al., 1975; Pyun et al., 1970). In 1985, and later in 1987, two different immunohistochemical studies reported evidence for macrophage-originated MGCs (Theaker et al., 1985; Hales et al., 1987), and a study using the EAM rat model in 1991 showed that MGCs in myocarditis are derived from macrophages (Kodama et al., 1991), whereby stained MGCs were completely negative for muscle-fibers marker (HHF35), and all the lymphocyte markers (Kodama et al., 1991). It also revealed that most of the rats immunized with cardiac myosin and CFA supplemented with *M tuberculosis* developed GCM, while those immunized with incomplete Freund's adjuvant (IFA) followed by *Bordetella pertussis* vaccine developed myocarditis without MGCs (Kodama et al., 1991). More recent studies show that monocyte/macrophages can fuse to form MGCs (Brodbeck & Anderson, 2009). The most prominent type of MGCs are osteoclasts, which are important in bone resorption (Miron et al., 2016). Various phenotypes of MGCs exist according to the chemical nature and size of the inducing agent. Interestingly, an *in vitro* research model of human tuberculous granulomas showed that high-virulence mycobacteria (such as *M. tuberculosis*) can induce large MGCs with the size of 15 or more nuclei per cell, which are strongly capable of antigen presentation, but

incapable of phagocytosis; low virulence mycobacterium species (such as *M. smegmatis* or *M. avium*) can induce lower numbers of nuclei per cell and are capable of phagocytosis (Lay et al., 2007). Even more recent studies show that the change in macrophage polarization from M1 to M2 may occur during the formation of M1-MGCs and M2-MGCs (Brodbeck & Anderson, 2009; Miron et al., 2016).

2.4 Pharmacological Treatment of Inflammation in CS and GCM

In recent years, there have been notable achievements in pharmacological treatments aiming to suppress inflammatory response and to improve cardiac function in CS patients. Corticosteroids alone or often in combination with other immunosuppressive agents, such as methotrexate or azathioprine, are considered the first-line treatment for CS patients. Corticosteroids are anti-inflammatory agents suppressing cytokine production and consequently inhibiting immune cell activation. In severe CS cases, administration of additional immunosuppressive agents is crucial. There is a strong recommendation in The European Respiratory Society (ERS) guidelines for the use of immunosuppressive therapy in CS patients with abnormal cardiac function (Baughman et al., 2021).

Methotrexate is the most widely used second-line therapy in CS patients (Baughman et al, 2000; Lower & Baughman, 1990). It is a folic acid antagonist inhibiting the metabolism of purine and pyrimidine, as well as inhibiting the synthesis of amino acid and polyamine (Gerke, 2020). There are several observational and retrospective studies supporting the use of methotrexate in CS patients (Nagai et al., 2014; Stievenart et al., 2022; Terasaki et al., 2019).

The guidelines of both The Japanese Circulation Society (JCS) (Terasaki et al., 2019) and the ERS (Rahaghi et al, 2020) mention azathioprine as a second-line immunosuppressive agent that may be used alone or in combination with corticosteroids in patients with CS. Azathioprine inhibits purine synthesis mainly through its active metabolite, 6-mercaptopurine. It blocks the enzyme inosine monophosphate dehydrogenase (IMPDH), which reduces lymphocyte proliferation and function. However, despite its efficacy in CS patients some recent studies revealed an increased risk of infection with azathioprine (Vorselaars et al., 2013; Rossides et al., 2021).

Mycophenolate mofetil (MMF) is another possible medication to use in CS patients. It is an inosine monophosphate dehydrogenase (IMPDH) enzyme inhibitor, which works by suppressing both cellular mediated immune responses and antibody formation and blocking the migration of lymphocytes and monocytes into the site of inflammation (Allison, 2005; Yashima & Ohgane, 2001; Allison & Eugui, 2000). A

study on 77 CS patients treated with corticosteroids alone (n= 32) or with a combination of corticosteroids and MMF (n= 45) showed similar improvement in both treated groups but the combination therapy group required significantly less corticosteroids (Griffin et al., 2021).

Leflunomide is an immunosuppressive disease-modifying medication used in inflammatory disorders. It is a pyrimidine synthesis inhibitor exerting its effect by inhibiting mitochondrial enzyme dihydroorotate dehydrogenase (DHODH) (Fox et al., 1999; Herrmann et al., 2000). There are no randomized or prospective studies evaluating leflunomide treatment in CS patients. However, some studies on sarcoidosis patients showed leflunomide can be useful in sarcoidosis patients who are intolerant to other therapies (Sahoo et al., 2011; Baughman & Lower, 2004).

There are several case reports about application of intravenous (IV) cyclophosphamide in CS patients (Demeter, 1988; Chapelon-Abric et al., 2017; Fazelpour et al., 2021). Cyclophosphamide was approved by the FDA as an alkylating agent for the treatment of neoplasms by accelerating programmed cell death (Ogino & Tadi, 2022) At lower doses, cyclophosphamide suppresses the immune response by inhibiting the activity of T-cells, decreasing the secretion of IL-12 and interferon-gamma (IFN-γ), and increasing secretion of IL-4 and IL-10 (Cacoub et al., 2020). A recent study on 157 CS patients revealed that cyclophosphamide treatment was associated with a reduced risk of disease relapse (Ogino & Tadi, 2022).

Anti-TNF-α agents, such as infliximab and adalimumab are inhibiting pro-inflammatory cytokines. They showed some benefits in patients with severe extra-CS, who were intolerant of or refractory to corticosteroids (Harper et al., 2019; Chung et al., 2003). However, their application in patients with heart failure is limited, due to its cardiotoxicity (Kotyla, 2018; Mann et al., 2004).

Janus kinase (Jak) inhibitors are a promising new treatment approach for sarcoidosis patients, that work by targeting Janus kinase enzymes and modulate immune response pathways. However, their safety and long-term effects are still unknown (Wang et al., 2020).

Pharmacological treatment plans for GCM are highly individualized, depending on a patient's symptoms, disease severity, and the underlying cause. There are no international guidelines on the management of GCM, and only a limited number of studies address its treatment. Generally, the treatment of GCM involves immunosuppressive medication including, corticosteroid therapy alone or in combination with other immunosuppressive agents such as cyclosporine, prednisone, and azathioprine. This aims to reduce inflammation and is combined with cardiac-specific treatment for heart failure, conduction disturbances and

arrhythmias (Cooper et al., 1997; Cooper et al., 2008). The immunosuppressive agents mycophenolate mofetil, methotrexate, rituximab, and intravenous immunoglobulins may be used as second-line treatments (Ammirati et al., 2016). A multicenter international study in 1997 showed that early immunosuppressive therapy with corticosteroids, cyclosporine and azathioprine, increased transplant-free survival rate from 3.0 to 12.3 months after symptom onset (Cooper et al., 1997). Another multi-center study of immunosuppression therapy with cyclosporine and steroids in the patients with microscopically confirmed GCM revealed a significant reduction in the inflammatory cells and necrosis of the tissue after 4 weeks of treatment (Wang et al., 2020). At one-year follow-up, two patients had received a heart transplantation and one had died due to recurrence of GCM after stopping immunosuppressive treatment (Wang et al., 2020). A small study of five immunosuppressive-treated GCM patients found better short-term and long-term survival rates, although 6 months of immunosuppressive therapy had no effect on left ventricular function (Ammirati et al., 2016). A more recent study (2015) revealed histological improvements in repeated endomyocardial biopsy (EMB) after treatment with multiple immunosuppressants (Maleszewski et al., 2015). One preclinical study indicated a benefit of cyclosporine, prednisolone and aspirin therapy in an EAM rat model (Cooper et al., 1997). However, the therapeutic efficacy of immunosuppressive therapy in GCM patients is controversial (Obi et al., 2022), would benefit from closer investigation through prospective randomized trials. Furthermore, a more effective therapeutic approach for GCM remains to be developed.

2.5 Clinical Features and Diagnosis of CS and GCM

CS may occur with extra-cardiac sarcoidosis involvement, but cardiac inflammation degree does not correspond to extra-cardiac inflammation degree (Roberts et al., 2014; Blankstein et al., 2014; Tavora et al., 2009). Sarcoid granulomas typically affect myocardium and epicardium in CS patients, whereby the left ventricle (LV) free wall (96%), intraventricular septum (73%), right ventricle (RV) free wall (46%), right atrium (11%), and left atrium (7%) may be involved (Matsui et al., 1976; Roberts et al., 1977; Birnie et al., 2014).

There are wide range of non-specific clinical symptoms that may be present in CS patients, including palpitations, presyncope, or syncope, and dyspnea. Active inflammation in the heart may lead to conduction abnormalities, ventricular arrhythmias, and heart failure (Kim et al., 2009; Yazaki et al., 2001).

Complete AV-block is the most frequent kind of conduction abnormality that is present in 15-45% of CS patients (usually at a younger age) (Okura et al., 2003; Matsui et al., 1976; Nagai et al., 2015; Sekhri et al., 2011). Bundle branch blocks (BBB) are another type of conduction abnormalities that are present in CS patients (Yazaki et al., 1998; Schuller et al., 2011).

Ventricular arrhythmias in CS patients are challenging to treat. They may start from asymptomatic ventricular premature beats and may lead to ventricular fibrillation (Koplan et al., 2006; Jefic et al., 2009). Implantable cardiac defibrillators (ICDs) have been used for secondary prevention in CS patients with history of ventricular arrhythmias, ventricular fibrillation and sudden cardiac arrest. Furthermore, ICDs are increasingly used for primary prevention in patients with CS without history of arrhythmias. A study including 45 CS patients with an ICD and cardiac involvement confirmed with CMR and/or [^{18}F]FDG PET, reported an incidence rate of 15% per year for ventricular tachyarrhythmias (Betensky et al., 2012). A bigger multicentral study including 235 CS patients, reported corresponding ICD therapy rate of 36.2% during 4 years follow up (Kron et al., 2013).

Congestive heart failure with reduced LV systolic function may occur in advanced CS, because of granulomatous infiltration, inflammation and fibrosis of the myocardium (Zipse & Sauer, 2014). In some old studies, with insufficient diagnostic methods, heart failure was the common first manifestation of CS with reported incidence of 25-75% (Yazaki et al., 2001; Sekhri et al., 2011; Zipse & Sauer, 2014; Fleming & Bailey, 1986). More recent studies with current diagnostic methods, that provide earlier diagnosis of the disease, reported incidence of 13-18% for systolic dysfunction in CS patients (Mehta et al., 2008; Schuller et al., 2011).

GCM is typically seen in young to middle-aged previously healthy individuals, with a mean age of onset of 43 years (Cooper et al.,1997). It has been estimated to account for approximately 17% of all myocarditis fatalities (Gadela et al., 2021). The disease progresses rapidly, with time from symptom onset to hospitalization ranging from 2 weeks to 6 weeks (Birnie et al., 2017; Litovsky et al., 1996; Elezkurtaj et al., 2013). In an international multicenter GCM study group of 63 patients, 89% of the 63 patients either died or underwent heart transplantation, with a median survival of 5.5 months from the onset of symptoms without gender predominance (Cooper et al.,1997).

In the era of modern therapy, which includes effective immunosuppression and the use of ICDs, CS presents as a slowly progressive cardiomyopathy in the majority of patients (Kandolin et al., 2015). However, there is still controversy about GCM, the more aggressive form of the disease, which is associated with a 5-year survival

of <50% (Kandolin et al., 2015; Ekström et al., 2016). Importantly, CS is associated with high risk of ventricular arrhythmias, which is associated with heart failure and sudden cardiac death (80%). In 57-100% of patients with heart failure undergoing transplantation, CS diagnosis is missed (Akashi et al., 2012; Zhang et al., 2012; Cooper et al., 2008). In an international multicenter study of 73 GCM patients, the transplant-free survival probability at 5 years was 10% overall, and 21.9% after diagnosis (Okura et al., 2003). A more recent study of 46 patients, reported that the transplant-free survival probability at 5 years was 42% (Ekström et al., 2016). Maleszewski *et al*. reported that the combined rate of death, transplantation, ventricular-assist device placement, and GCM recurrence of 47% at 5 years, and a prolonged transplant-free survival rate of over 19 years beyond initial diagnosis with long-term immunosuppression (Maleszewski et al., 2015).

The prompt and precise diagnosis of CS and/or GCM is essential for effective treatment and patient outcomes. Owing to their infrequent prevalence and non-specific clinical presentations, these disorders present notable obstacles in diagnosis. The clinically sufficient diagnosis of GCM depends on histologic demonstration of MGCs and fused epithelioid histiocytes with multiple nuclei, with cardiac imaging indicating the myocardial involvement and the exclusion of other diseases with a similar histologic or clinical picture (Perkel et al., 2013).

The diagnosis of CS and GCM typically begins with a comprehensive clinical assessment, involving a detailed medical history and physical examination. Symptoms such as chest pain, dyspnea, palpitations, and syncope may indicate potential cardiac involvement. However, these symptoms lack specificity and can resemble those of various cardiac and non-cardiac conditions, posing challenges to clinical diagnosis (Roberts et al., 2014; Akashi et al., 2012; Ekström et al., 2019).

In recent years, there has been increasing interest in identifying biomarkers for diagnosing and predicting outcomes in CS and GCM. Serum markers like soluble interleukin-2 receptor (sIL-2R), angiotensin-converting enzyme (ACE), cardiac troponins, Natriuretic Peptides, C-Reactive Protein, Galectin-3, Interleukin-6 (IL-6), Matrix Metalloproteinase-9 (MMP-9), and Soluble Suppression of Tumorigenicity 2 (sST2) have shown potential in reflecting disease activity and prognosis (Iannuzzi et al., 2007; Yasutake et al., 200; Cao et al., 2019; Lok et al., 2013; Belperio et al., 2001; Dieplinger et al., 2015). However, further validation is needed to ascertain their diagnostic accuracy and clinical usefulness.

Electrocardiography (ECG) serves as a fundamental tool for evaluating cardiac electrical activity and identifying conduction abnormalities (Ekström et al., 2019; Zipse & Sauer, 2013). ECG findings in patients with CS and GCM can vary based on the extent and location of myocardial involvement. Common abnormalities

include AV conduction disturbances such as AV-block, BBB, and intraventricular conduction delays (Ekström et al., 2019). ECG findings in CS and GCM lack specificity, although conduction abnormalities and arrhythmias are frequently observed (Mehta et al., 2008; Schuller et al., 2011).

Echocardiography serves as the primary imaging modality, offering real-time visualization of the heart. In patients with CS and GCM, echocardiography plays a pivotal role in detecting myocardial involvement, assessing ventricular function, and identifying complications, such as pericardial effusion and valvular abnormalities (Mehta et al., 2008; Burstow et al., 1989). Common echocardiographic findings in CS include regional wall motion abnormalities, LV dysfunction, and diastolic dysfunction (Mehta et al., 2008; Yazaki et al., 1998). In GCM, echocardiography may reveal focal or diffuse LV wall thickening, reduced LV systolic function, and pericardial effusion, although these findings lack specificity and may overlap with other cardiomyopathies (Uemura et al., 2005; Benotti et al., 1980).

Although histological diagnosis is recommended by the various guidelines, including Japanese Ministry of Health and Welfare (JMHW) guideline, expert consensus recommendation and current guidelines of the American Thoracic Society/European Respiratory Society, advanced imaging modalities are frequently needed (Kim et al., 2009; Hiraga et al., 1993; Statement on sarcoidosis, 1999).

2.5.1 Diagnostics Biopsies

In extra-cardiac sarcoidosis patients, lymph node or lung biopsy is initially performed due to the higher sensitivity and lower procedural risk (Birnie et al., 2017). However, in CS patients, EMB has low sensitivity due to the focal nature of the disease and non-caseating granulomas have been found only in 25% of the CS patients' biopsies (Birnie et al., 2016; Ardehali et al., 2005).

Historically, GCM diagnosis were only made at autopsy. Since the 1980s, EMB has been considered as the ultimate diagnostic tool for the disease, revealing the histological hallmarks of MGCs, myocyte necrosis, lymphocytes and intact or degranulated eosinophils (Okura et al., 2003; Elezkurtaj et al., 2013; Cooper, 2007). EMB remains the gold standard for diagnosing GCM, allowing direct histological examination of myocardial tissue, with a sensitivity of 80-85%, particularly in severe cases (Elezkurtaj et al., 2013; Cooper, 2007; Shields et al., 2002). However, 20% of EMB give false-negative results (Darlington et al., 2014).

Imaging-guided EMB, and multiple and repeated EMBs can increase the diagnostic yield of EMB (Yilmaz et al., 2010). However, many physicians avoid performing it due to its low availability, high cost, and the risks of an invasive

procedure. Moreover, there may be sampling errors due to the focal localization of inflammatory lesions, which can limit the sensitivity (Birnie et al., 2017; Kandolin et al., 2013; Kadkhodayan et al., 2016). The limitations of EMB as the gold standard for diagnosing myocarditis have highlighted the need for novel non-invasive diagnostic approaches.

2.5.2 Cardiac Magnetic Resonance Imaging (CMR)

Cardiac MRI is a noninvasive technique that gives high-resolution measurements, which can be used in diagnosis of myocardial injury (Friedrich et al., 2009). However, in order to diagnose inflammation, the standard MRI may not be feasible because it has low sensitivity and specificity for detecting active inflammation. Thus, late gadolinium enhancement (LGE) imaging by using gadolinium contrast agents with CMR is now the preferred method of imaging in the diagnosis of myocarditis. Gadolinium chelate contrast agent, is a biologically inert substance that only distributes in extracellular matrix; it does not cross intact cell membranes (Matoh et al., 2008). In damaged or inflamed myocardium, it accumulates in the extracellular matrix in consequence of increased extracellular volume, extracellular edema and slow washout kinetics (Matoh et al., 2008). In diagnosing CS, the sensitivity and specificity of LGE-CMR range from 75-100% and 77-92%, respectively, compared to the modified JMHW guidelines, with positive and negative predictive values of 55% and 100%, respectively (Ohira et al., 2008; Tezuka et al., 2015; Yoshida et al., 2013). In 17 diagnostic studies on GCM, LGE-CMR, which enables visualization of myocyte necrosis and myocardial fibrosis, demonstrated an average specificity of 96% and sensitivity of 68% (Kotanidis et al., 2018; Lagan et al., 2018). However, the diagnostic accuracy of LGE varies considerably between the studies, with specificity of 39-100% and sensitivity of 30-95%, reflecting the heterogeneity of the studied populations, disease stage and time of imaging (Kotanidis et al., 2018; Lagan et al., 2018). A 2012 study of 5 histologically-proven cases of GCM indicated the widespread pattern of LGE distribution in all layers of the myocardium on CMR imaging with underlying inflammation and/or fibrosis (Leong et al., 2012). In another study, in 2016, 24 out of 25 patients (96%) had abnormal myocardial LGE on MRI indicating myocardial inflammation (Ekstrom et al., 2016). Despite its high specificity, LGE imaging alone can have variable sensitivity for tissue characterization in GCM depending on the study design, the time of imaging in relation to GCM stage, patient selection and the method of validation, which can impair the diagnostic accuracy (Shields et al., 2002). Moreover, early-stage focal myocarditis, healing myocarditis and diffuse or borderline GCM may not lead to observable LGE (Friedrich et al., 2009). A 2006 study found that 95% of patients with EMB-proved active myocarditis demonstrated visible LGE, whereas only 40%

of patients with EMB-proved healing myocarditis had visible LGE (Mahrholdt et al., 2006). Therefore, LGE-CMR alone is not sufficient to diagnose GCM, but LGE-CMR-guided EMB can provide better diagnostic accuracy (Friedrich et al., 2009).

2.5.3 Positron Emission Tomography (PET) of Inflammation

PET/computed tomography (PET/CT) imaging is another feasible non-invasive approach for diagnosis of myocarditis, with high sensitivity. It uses target-specific molecules as radioactive tracers (Turkington, 2001; Bengel et al., 2009). PET imaging technique has been widely used in the detection of various conditions such as cancer, cardiovascular disease and neurological disorders. Moreover, it shows promise in the detection of immune-cell infiltration and diagnosis of myocarditis even at an initial stage (Schatka & Bengel, 2014). PET imaging is a three dimensional (3D), powerful, non-invasive and quantitative. This repetitive molecular imaging technique uses targeted probes labeled with positron-emitting radionuclides to detect and monitor disease processes in living patients.

PET tracers are a small-molecule, peptide or antibody agents labeled with a positron-emitting radionuclides, such as ^{11}C, ^{13}N, ^{15}O, ^{18}F or ^{68}Ga, which will bind to a molecular target of interest and causes gamma (γ) radiation, which is detectable by the PET camera (Turkington, 2001; Bengel et al., 2009). Over time, the positron-emitting radionuclide accumulates at the target site and can be measured as a function of time within a region of interest (ROI). Radioactive decay causes the radionuclide to emit a positron, which collides with a nearby electron, resulting in the creation of a pair of 511 kilo-electron volt (gamma) photons that travel in opposite directions. These photons are detected and the accumulated tracer can be localized in the tissue by PET scanner detectors, and reconstructed to a 3D image (Turkington, 2001; Bengel et al., 2009).

2.5.3.1 [^{18}F]FDG PET Imaging of Inflammation

Currently, glucose analog [^{18}F]-2-fluoro-2-deoxy-*D*-glucose ([^{18}F]FDG), in which the oxygen in C2 position is replaced with fluorine-18, is the most commonly used PET tracer for imaging of cardiac inflammation. [^{18}F]FDG PET imaging can detect active cardiac inflammation by assessing the metabolic activity of the inflammatory cells for anatomical localization to guide EMB and diagnose myocarditis. Under aerobic conditions, healthy myocardium uses predominantly free fatty acids in its metabolism (Schatka & Bengel, 2014). [^{18}F]FDG is transported into the cells by glucose transport proteins (GLUT) and when absorbed, it undergoes phosphorylation by hexokinase enzyme. [^{18}F]FDG cannot enter into glycolysis and therefore it is trapped inside the cells. At the site of macrophage-mediated inflammation,

accumulation of [^{18}F]FDG accumulation indicates an active inflammatory condition (Youssef et al., 2012; Okumura et al., 2004; Mc Ardle et al., 2013). Inflammatory cells, including neutrophils and macrophages, express high levels of glucose transporters, particularly GLUT1 and GLUT3 (Jamar et al., 2013).

Werner et al. recently highlighted the application of [^{18}F]FDG PET in assessing disease activity in autoimmune myocarditis (Werner et al., 2019). However, the use of [^{18}F]FDG PET in giant cell myocarditis (GCM) remains relatively unexplored. A recent study reported serial PET imaging in a GCM case, revealing [^{18}F]FDG uptake in the heart without evidence of extracardiac inflammation (Lamacie et al., 2020). Interestingly, similar patterns are also observed in patients with cardiac sarcoidosis (CS).

A single-center study in 2016 showed that 93% of patients with GCM had focal uptake of [^{18}F]FDG (Ekstrom et al., 2016), and a [^{18}F]FDG PET/MRI study in 2018 revealed that [^{18}F]FDG PET is in good agreement with CMR with reported sensitivity of 74% and specificity of 97% for PET compared to CMR (Nensa et al., 2018). A meta-analysis of 17 studies, which included 891 patients with suspected cardiac sarcoidosis (CS), found that PET had a sensitivity of 84% and a specificity of 83% (Kim et al., 2020). A recent meta-analysis revealed that sensitivity of [^{18}F]FDG PET in diagnosis of CS is significantly decreased when patients had been treated with anti-inflammatory agents before imaging compared to non-treated patients (82% vs 94%). However, specificity did not differ significantly (Aitken et al., 2022).

Cardiac PET is typically paired with whole-body imaging to detect extracardiac involvement. [^{18}F]FDG PET has high accuracy for detecting of cardiac inflammation and provides valuable prognostic information. However, to identify [^{18}F]FDG pathological uptake, it is essential to suppress the non-specific physiological myocardial [^{18}F]FDG uptake through a combination of fasting and dietary changes. Recent SNMMI-ASNC guidelines for patient preparation, recommend changing the patient's diet to a high-fat, low-carbohydrate and protein-permitted diet in combination with prolonged (12-18 hr) fasting, and intravenous administration of unfractionated heparin 15 min before [^{18}F]FDG administration (Chareonthaitawee et al., 2017). However, incomplete suppression of physiological glucose uptake, which can occur in up to 20% of patients, may impair [^{18}F]FDG PET diagnostic accuracy (Youssef et al., 2012; Jeserich et al., 2009). Another major disadvantage of [^{18}F]FDG PET is the risk of obtaining false-positive result, because it cannot discriminate tumor tissue from inflammation (Youssef et al., 2012). For these reasons, new, more specific PET tracers are needed.

A recent meta-analysis of 37 studies demonstrated, that both LGE-CMR and ^{18}F-FDG PET are predictive of major adverse cardiac events in CS. However, LGE-CMR is considered the initial imaging modality to assess prognosis in CS with higher odds ratio compared to [^{18}F]FDG PET (odds ratio, 8.0 vs 2.1) (Aitken et al., 2023).

2.5.3.2 Other PET Imaging Studies in CS and GCM

To overcome limitations of [^{18}F]FDG PET, several recent studies have investigated potential alternative tracers with greater specificity for detecting cardiac inflammation to diagnose the disease, to monitor the response to therapy and to investigate the pathophysiology of the disease. Recent PET tracers for the imaging of inflammation in autoimmune myocarditis are presented in Table 1.

The radiolabeled [^{11}C]-methionine, a marker of amino acid transport, protein synthesis and routinely used in oncology, has shown promising result for the detection of autoimmune myocarditis in rat model of experimental autoimmune myocarditis (Maya et al., 2016).

The 18-kDa translocator protein (TSPO), is a biomarker of brain injury and cancer, is overexpressed in myocardial inflammatory lesions. Therefore, various translocator protein (TSPO)-selective PET radiotracers including [^{18}F]fluoromethyl-PBR28, [^{18}F]CB251, ^{18}F-FDPA and [125I]-IodoDPA-713 were investigated in EAM rats and mice with coxsackievirus B3 (CVB3) myocarditis to detect myocardial inflammation. The results suggest that the TSPO ligands are potential cardiac inflammation imaging agents and can detect myocardial inflammation (Kim et al.,2018, Mou et al., 2022; Fairweather et al., 2014).

Mannosylated human serum albumin (MSA), which was initially developed for lymph node imaging, is a new approach for detecting myocarditis. Mannose residue receptor (MR) is expressed in anti-inflammatory macrophages, and ^{68}Ga-NOTA-MSA has detected myocardial inflammation in EAM rats (Lee et al.,2017).

Another recent approach is to target fibroblast activation protein alpha (FAP-α), a protease with endopeptidase activity, which is upregulated in cardiomyopathies. ^{68}Ga-labeled fibroblast activation protein inhibitor (^{68}Ga-FAPI) has been used in patients to detect immune checkpoint inhibitors (ICI)-associated myocarditis in oncology (Finke et al., 2021). The result showed ^{68}Ga-FAPI can identify affected patients with ICI-associated myocarditis at an early stage (Finke et al., 2021).

The G protein-coupled receptors known as somatostatin receptors (SSTRs), are diagnostic and therapeutic targets in oncology, that also have applications for detecting myocarditis (Kircher et al., 2020). Somatostatin receptor-type 2 (SSTR2A) is highly expressed on activated pro-inflammatory macrophages and offers a

potential imaging target for detecting inflammation. ^{68}Ga-DOTATOC PET/CT detected ICI-associated myocarditis in patients (Boughdad et al., 2021).

Macrophages are the most abundant cell type in GCM lesions (Cihakova & Rose,2008) thereby representing an attractive target for identifying active inflammation. αvβ3 integrin, expressed by macrophages and angiogenic endothelial cells, is another potential target to identify inflammation (Grönman et al., 2017). Vascular adhesion protein-1 (VAP-1) is an endothelial cell surface molecule associated with many inflammatory conditions, making it a potential target for *in vivo* imaging of inflammation. Upon inflammatory stimulus, VAP-1 is rapidly translocated from intracellular storage granules to the endothelial cell surface (Salmi et al., 1992; Elo et al., 2018; Siitonen et al., 2017; Virtanen et al., 2015).

Table 1. Recent PET radioligands for imaging of inflammation in myocarditis. Own drawing.

Target	**Myocarditis type**	**PET tracer**	**Application of PET imaging**
L-type amino acid transporter	Autoimmune myocarditis	^{11}C-methionine	Pre-clinical (Maya et al., 2016)
TSPO	Autoimmune myocarditis	[^{18}F]Fluoromethyl-PBR28 [^{18}F]CB251	Pre-clinical (Kim et al.,2018)
TSPO	Autoimmune myocarditis	^{18}F-FDPAmou	Pre-clinical (Mou et al., 2022)
TSPO	Viral myocarditis	[125I]-IodoDPA-713	Pre-clinical (Fairweather et al., 2014)
Macrophage mannose receptor	Autoimmune myocarditis	^{68}Ga-NOTA-MSA	Pre-clinical (Lee et al.,2017)
FAP-α	ICI-associated myocarditis	^{68}Ga-FAPI	Clinical ((Finke et al., 2021)
SSTRs	ICI-associated myocarditis	^{68}Ga-DOTATOC	Clinical (Boughdad et al., 2021)

TSPO = Translocator protein, MSA = Mannosylated human serum albumin, FAP-α = Fibroblast activation protein alpha, SSTRs = Somatostatin receptors, ICI = Immune checkpoint inhibitors

2.6 Folate Receptors Targeting in Inflammation

Folic acid, also known as vitamin B9, was developed in the 1940s for the treatment of anemia. It is a dietary supplement for folates. In the body, folic acid is first converted into dihydrofolate and then to tetrahydrofolate (THF; the biologically active form) via dihydrofolate reductase enzyme (DHFR). THF plays an important role in various body and cell functions including DNA synthesis, repair and methylation, cell division and growth, and formation of red blood cells. It contributes to the formation of essential nucleotides and amino acids in the cell and protein metabolism (Hoffbrand & Weir, 2001).

The folate receptor (FR) is a 38-kDa glycosylphosphatidylinositol-anchored protein that binds to folate ligands on the cell membrane and transports them into the cell via invagination of the plasma membrane followed by a endocytic vesicle (endosome) formation. This migrates into the cell cytoplasm and becomes acidified to a pH of ~ 6.5 in order to release the folate ligand (Yang et al., 2017; Rothberg et al., 1990). Currently, five different cell membranes FRs have been discovered, including FR-α, FR-β, FR-γ, FR-δ and rebinding protein (Rtbdn).

FR-α is encoded by the FOLR1 gene and is generally expressed on the apical surface of certain polarized epithelial cells, including those of the kidney proximal tubule cells, choroid plexus, uterus, fallopian tubes, epididymis, type I and II pneumocytes in the lungs, the acinar cells of the breast, trophoblasts in the placenta and the salivary and bronchial glands (Kamen et al., 1988; Weitman et al., 1992; Garin-Chesa et al., 1993; Buist et al., 1995; Wu et al., 1999). FR-α has a high affinity for folate and its derivatives and is over-expressed in various malignancies originating from epithelial cells, such as ovary, uterus, cervix, breast, colon, kidney, testicular choriocarcinoma, malignant pleural mesothelioma, non-functioning pituitary adenocarcinoma and ependymal brain tumors (Buist et al., 1995; Wu et al., 1999; Campbell et al., 1991; Ross et al., 1994; Toffoli et al., 1997; Parker et al., 2005). Most FRs on normal tissue are inaccessible due to the intercellular junctions of the epithelia, therefore administered folate-targeted agents cannot affect most epithelia except the epithelia of cancer and kidney cells (Fernández et al., 2017).

FR-β is transcribed by FOLR2 gene, having 68% sequence homology with FOLR1. It is expressed in placenta, thymus, spleen, normal myelopoiesis, hematopoietic-originated cells and malignant cells such as leukemias (Ross et al., 1994; Salazar & Ratnam, 2007; Puig-Kröger et al., 2009; Wibowo et al., 2013). On myelomonocytic lineage, FR-β can be co-expressed with macrophage/monocyte differentiation markers such as CD13, CD14, CD11b and CD33, but it is not co-expressed with lymphocytes differentiation markers like CD3 and CD19 (Wibowo et al., 2013; Reddy et al., 1999). A 2009 study revealed that it is usually co-expressed

with cell-differentiation markers of an activated-state of macrophages (CD80, CD86, Ly-6C/G); human macrophages without these activation markers expressed few FR (Xia et al., 2009). Taken together, FR-β expression is highly associated with activation of macrophages and monocytes during acute and chronic inflammation, which is implicated in the pathogenesis of various human inflammatory diseases, such as rheumatoid arthritis, atherosclerosis, systemic lupus erythematosus, Crohn's disease, pulmonary disease, ulcerative colitis, diabetes, glomerulonephritis, psoriasis, sarcoidosis, osteoarthritis, encephalomyelitis, interstitial lung disease, and myocardial infarction (Hu et al., 2019; Varghese et al., 2007; Tsuneyoshi et al., 2012; Paulos et al., 2004; Silvola et al., 2018; Yi , 2016; Elo et al., 2019; Schniering et al., 2019; Ni et al., 2016; Shen et al., 1995).

FR-γ is encoded by the *FOLR3* gene and has 71% and 79% sequence homology with *FOLR1* and *FOLR2*, respectively. *FOLR3* has two polymorphic variants resulting in two different protein receptors with short and long polypeptide. FR-γ is upregulated in normal and malignant hematopoietic cells such as bone marrow, thymus and spleen as well as cancer cells in the ovary, cervix and uterus (Shen et al., 1994; Crown, 2013).

FR-δ is encoded by the *FOLR4* gene. It has been isolated from the cells of different animals, including mouse, zebrafish, lizard and chicken (Spiegelstein et al., 2000), but not yet from human cells, although the *FOLR4* gene has been isolated on chromosome 11 (Crown, 2012).

Rtbdn protein is the most recently discovered receptor in this family. Encoded by *Rtbdn* gene on chromosome 19, it is expressed on various cells in the body, particularly on retinal cells and on the nervous and secretory cells. The protein has similar homology with riboflavin-binding proteins and is therefore, believed to contribute to the binding of retinoids and other carotenoids (Italiani et al., 2015).

Macrophages are important immune cells involved in inflammatory responses (Mathias et al., 2003), and various studies have proved that activated macrophages, which express FR-β on their surface, are involved in the pathogenesis of a variety of inflammatory diseases. Therefore, FR-β expressed on activated macrophages is a unique diagnostic and therapeutic target for the diagnosis and treatment of macrophage-mediated inflammatory diseases. The process involves the attachment of the folate (folic acid), to a molecule, imaging agent, or drug to form a "folate conjugate". Several different folate conjugates have been developed (Siegel et al., 2003; Reddy et al., 2004; Turk et al., 2002).

Radiolabeled folate derivatives have been used to detect and diagnose inflammation in various inflammatory disorders. The first imaging studies of inflammatory diseases with a folate radiotracer were performed in 2002 on adjuvant-

induced arthritic rats and in 2004 on arthritic dogs with a folate radiotracer, showing that 99mTc-EC20 could selectively detect inflamed arthritic joints (Turk et al., 2002; Paulos et al., 2004). An imaging study using folate-conjugated imaging agents on a murine asthma model revealed that the folate-conjugated imaging agents can selectively target FR-expressing macrophages (Shen et al., 2013; yala-Lopez et al., 2010). Two different recent studies have shown that aluminum [^{18}F]fluorine-labeled 1,4,7-triazacyclononane-1,4,7- triacetic acid conjugated folate (^{18}F-FOL) can detect inflammation in atherosclerotic mice and in rats with autoimmune encephalomyelitis (Silvola et al., 2018; Elo et al., 2019).

FR-targeted imaging with folate-conjugated radiopharmaceuticals has also been performed in human patients to detect osteoarthritis and rheumatoid arthritis (Xia et al., 2009; Kraus et al., 2016; Yi, 2016). However, the potential of ^{18}F-FOL has not been studied for *in vivo* imaging of cardiac inflammation in EAM rats or humans with autoimmune myocarditis.

2.6.1 Folate Receptor-β Targeted Immunotherapy

FR-β targeted therapy represents a cutting-edge approach in the treatment of inflammatory diseases, leveraging the unique properties of folate receptors β (FR-β) to deliver therapeutic agents directly to cancer or inflamed tissues. FR-β targeted therapy offers a promising alternative to conventional treatments, potentially reducing side effects and improving efficacy. FR-β targeted therapy in inflammatory diseases exploits the overexpression of FR-β on activated macrophages involved in the inflammatory process. The specificity of FR-β targeted therapy is particularly beneficial in chronic inflammatory conditions, where long-term therapy is often required, and side effects can significantly affect the patient's quality of life. Additionally, targeted therapy can potentially allow for lower doses of therapeutic agents to be used.

Various folate-drug conjugates have been designed for inflammation therapy. Hapten, for example, has a low molecular weight and high immunogenic properties, which make it a great molecule to be linked to folate (Paulos et al., 2006). Folate-hapten conjugate of fluorescein isothiocyanate (FITC) was utilized for FR-β targeted immunotherapy in animal models of rheumatoid arthritis and systemic lupus erythematosus and resulted in reduction of disease symptoms by eliminating FR-positive activated macrophages in inflammatory lesions (Tsuneyoshi et al., 2012; Yi et al., 2009). A study on a rat model of rheumatoid arthritis showed folate-hapten conjugates of FITC, dinitrophenyl (DNP) and trinitrophenyl (TNP) exerted therapeutic effect resulting in reduction of disease symptoms (Furusho et al., 2012). Moreover, administration of recombinant immunotoxin to atherosclerotic ApoE-/-

mice, decreased the severity of the atherosclerosis symptoms by targeting FR-β expressing macrophages (Garcia et al., 2021). FR-β targeted *in vivo* imaging and immunotherapy of inflammatory diseases are summarized in Table 2. Up to date, FR-β targeted therapy has been successful for treating various macrophage-mediated inflammatory diseases including rheumatoid arthritis, atherosclerosis, multiple sclerosis, and systemic lupus erythematosus, (Table 2).

FR-β targeted therapy is a promising approach which can potentially be applied for the treatment of autoimmune myocarditis. Aminopterin (AMT), a derivative of folic acid, is a potent inhibitor of the enzyme dihydrofolate reductase (DHFR). DHFR plays a crucial role in the synthesis of nucleotides, which are necessary for DNA replication and cell division. By inhibiting DHFR, AMT can suppress the immune system's overactivity by reducing the proliferation of inflammatory cells. However, its application has largely been limited in favor of methotrexate (a less toxic analogue), due to the serious side effects including liver toxicity, kidney damage, and suppression of bone marrow, leading to decreased blood cell counts. While methotrexate is a more tolerable agent with less toxicity, AMT has much higher potency and pharmacological properties which have led to a renewed interest for its clinical development for immunotherapy (Lu et al., 2021; Mezu-Ndubuisi et al., 2021).

Table 2. FR-β targeted *in vivo* imaging and immunotherapy. Own drawing.

Application	Diseases	Animal models/Human	References
Imaging	Rheumatoid arthritis	Rat	(Turk et al., **2002**)
	Rheumatoid arthritis	Dog	(Paulos et al., 2004)
	Rheumatoid arthritis	Human	(Xia et al., 2009)
	Osteoarthritis	Human	(Kraus et al., 2016)
	Asthma	Mice	(Shen et al., 2013)
	Atherosclerosis	Mice	(Yala-lopez et al., 2010)
	Atherosclerosis	Mice	(Silvola et al., 2018)
	Autoimmune encephalomyelitis	Rat	(Elo et al., 2019)
IMMUNOTHERAPY	Rheumatoid arthritis	Rat/Mice	(Yi et al., 2009; Paulos et al., 2006)
	Systemic lupus erythematosus	Mice	(Varghese et al., 2007)
	Atherosclerosis	Mice	(Furusho et al., 2012)

2.7 αvβ3 Integrin Targeting in Inflammation

Integrins are heterodimeric transmembrane receptors that mediate cell-cell and cell-extracellular matrix contacts. Integrins consist of α- and ß-subunits, comprising at least 24 subtypes of integrins. αvβ3 integrin is a cell membrane glycoprotein receptor which facilitates the trans-endothelial migration of leukocytes to the site of inflammation. Furthermore, αvβ3 integrin signaling modulates the generation of inflammatory cytokines and chemokines, affecting the inflammatory response (Mezu-Ndubuisu et al., 2021; Pang et al., 2003).

αvβ3 integrin is highly upregulated during angiogenesis in endothelial cells, making it a potential target for imaging angiogenesis related conditions (Sherif et al., 2012; Brooks et al.,1994;). Angiogenesis, which is known as the formation of new capillaries from pre-existing vessels, is associated with pathogenesis of cancer (Aguilar-Cazares et al., 2019), ischemic heart disease (Wu et al., 2018), as well as many inflammatory diseases, such as rheumatoid arthritis (Marrelli et al., 2011; Elshabrawy et al., 2015), diabetic retinopathy (Rezzola et al.,2020), psoriasis

(Guérard & Pouliot, 2012), pulmonary sarcoidosis or fibrosis (Antoniou et al., 2006; Ziora et al., 2015) and atherosclerosis (Camaré et al., 2017; Antonov et al., 2004). αvβ3 integrin also plays a role in macrophage inflammatory responses and myofibroblast differentiation (Antonov et al., 2011; Sarrazy et al., 2014). Integrin triple peptide motif arginine-glycine-aspartic acid (RGD) has been known to bind with the αvβ3 integrin. RGD-based ligands can bind to many integrin heterodimers and have been used in diagnosis and treatment of various angiogenesis involved diseases (Kapp et al., 2017). Radiolabelled RGD derivatives can be used to detect αvβ3 integrin expression in cancer, inflammation, and cardiovascular diseases (Van Der Gucht et al., 2016; Chen et al., 2016; Kiugel et al., 2014; Eo et al., 2016). Various ^{68}Ga-labeled RGD peptides have been developed and used in preclinical and clinical studies (; Gao et al., 2012; Higuchi et al., 2008; Laitinen et al., 2013; Menichetti et al., 2013). A study has shown, that ^{68}Gallium-labeled 1,4,7-triazacyclononane-1-glutaric acid-4,7-diacetic acid conjugated RGD peptide ([^{68}Ga]Ga-NODAGA-RGD), was able to detect αvβ3 integrin expression after ischemic myocardial injury (Grönman et al., 2017). RGD motif containing tracers also can be utilized to monitor the effects of angiogenesis inducing therapies (Cai et al., 2016) or imaging other characteristics of LV remodeling such as myofibroblasts (Van den Borne et al., 2008). However, evaluation of αvβ3 integrin targeted imaging as a novel tool for the *in vivo* imaging of cardiac inflammation in autoimmune myocarditis remains to be studied.

2.8 VAP-1 Targeting in Inflammation

Vascular adhesion protein-1 (VAP-1) is primarily expressed on endothelial cells in the microvasculature and circulates in a soluble form. Under normal conditions, VAP-1 is stored within intracellular granules but translocates to the endothelial surface during inflammation. It plays a pivotal role in immune cell trafficking by facilitating leukocyte adhesion and extravasation. As a primary amine oxidase (AOC-3), VAP-1 produces hydrogen peroxide and aldehydes, which enhance leukocyte activation and migration into inflamed tissues. Elevated VAP-1 levels are linked to various conditions, including arthritis, multiple sclerosis, diabetes, and atherosclerosis (Jaakkola et al., 2000; Merinen et al., 2005; Airas et al., 2006).

The extracellular N-terminal domain of VAP-1 is responsible for its adhesive properties, while the stalk region anchors it to the cell membrane, ensuring proper positioning. Soluble VAP-1 (sVAP-1) results from the proteolytic cleavage of membrane-bound VAP-1 and retains its amine oxidase activity. Elevated sVAP-1 levels may indicate ongoing inflammation and tissue damage, making it a potential biomarker for disease monitoring (Kurkijärvi et al., 1998; Kurkijärvi et al., 2000; Kivi et al., 2009).

Sialic acid-binding immunoglobulin-like lectins 9 (Siglec-9) and 10 (Siglec-10) are leukocyte ligands for VAP-1, expressed on monocytes and granulocytes (Kurkijärvi et al., 1998; Aalto et al., 2011; Ahtinen et al., 2014). A Gallium-68-labelled peptide, 1,4,7,10-tetraazacyclododecane-N,N′,N″,N‴-tetraacetic acid conjugated to a sialic acid-binding Siglec-9 motif (^{68}Ga-DOTA-Siglec-9), has been utilized as a PET tracer for in vivo imaging of inflammation and cancer (Ahtinen et al., 2014; Silvola et al., 2016; Shen et al., 2015). This tracer shows promise for PET imaging of cardiac inflammation, particularly in experimental autoimmune myocarditis (EAM) rat models.

3 Aims

The overall aim of this study was to evaluate novel molecular imaging methods for the detection of cardiac inflammation in EAM rat model.

This study consists of 3 subprojects and the specific aim for each subproject is described below:

1. Subproject 1 (SP1): The aim of this subproject was to evaluate the feasibility of the FR-β targeting radiotracer ^{18}F-FOL for PET imaging of myocardial inflammation in EAM rat model.

2. Subproject 2 (SP2): The aim of this subproject was to study the expression of αvβ3 integrin in myocardial inflammatory lesions and evaluate the feasibility of detecting myocardial inflammation in EAM rat model using αvβ3 targeted [^{68}Ga]Ga-NODAGA-RGD PET.

3. Subproject 3 (SP3): The aim of this subproject was to evaluate the feasibility of VAP-1-targeted [^{68}Ga]Ga-DOTA-Siglec-9 imaging for the detection of myocardial inflammation in EAM rat model.

4 Materials and Methods

4.1 Ethical Issues

4.1.1 Animal Studies

All animal experiments received approval from the National Animal Experiment Board in Finland and the Regional State Administrative Agency for Southern Finland (license numbers ESAVI/968/04.10.07/2018 and ESAVI/37123/2020).

The experiments were conducted in accordance with European Union legislation on animal experimentation. Animals were housed under standard conditions with a 12-hour light–dark cycle and had free access to water and food at the Central Animal Laboratory of the University of Turku.

All procedures were carried out under isoflurane anesthesia (1.5–2.5%) and buprenorphine analgesia (0.03 mg/kg) was administered twice a day for 2 days after immunization.

4.1.2 Human Samples

The use of human tissues was approved by the hospital ethical review board (HUS317/13/03/01/2015 and HUS/1068/2016), the National Authority for Medicolegal Affairs (4615/ 06.01.03.01/2016), and the National Institute for Health and Welfare (THL/691/5.05.00/2016) (Ekström et al., 2019).

4.2 EAM Rat Model and Study Outline

Autoimmune myocarditis was induced in male Lewis rats (n = 62; age 6–8 weeks, weight 286.7 ± 28 g; Janvier Labs, France) by subcutaneous injections of 5 mg/mL pig cardiac myosin (M0531; Sigma Aldrich) in an equal volume of complete Freund's adjuvant supplemented with 1 mg/ml heat-killed dried *Mycobacterium tuberculosis* (F5881; Sigma Aldrich), twice (day 0 and day 7), either into the footpad (n = 13 in SP1) or the hock of the left foot. To enhance immunization, the rats also received an intraperitoneal injection of 250 ng/mL pertussis toxin (P2980; Sigma

Aldrich) on day 0. Control rats were injected with the adjuvant alone. All procedures were performed under isoflurane anesthesia, giving buprenorphine analgesia (0.03 mg/kg) twice a day for 2 days after immunization. The numbers of animals in each study and the imaging experiments performed for each group are shown in Table 3.

PET imaging was performed 3 weeks after the first immunization (day 21). Either contrast-enhanced CT or [^{18}F]FDG/PET imaging was performed for localization of the myocardium. In SP3, anti-VAP-1 polyclonal antibody (1 mg/kg) was injected intravenously 10 minutes before sacrifice into six immunized rats and two controls to facilitate detection of luminal VAP-1 by immunofluorescence. Following PET imaging, the rats were euthanized, blood was collected via cardiac puncture, and plasma was separated by adding an anticoagulant followed by centrifugation. Various organs, including the heart, were excised, weighed, and analyzed for radioactivity using a gamma counter (Triathler 3"; Hidex) to assess tracer biodistribution. The heart tissues were either embedded in an optimal cutting-temperature compound and frozen or fixed in 10% formaldehyde and embedded in paraffin. Hearts were sectioned into serial transverse cryosections of 20 µm and 8 µm, or 4 µm paraffin-embedded sections, at 1 mm intervals from base to apex for autoradiography, histology, and immunostaining.

Table 3: Study design and numbers of rats in each study and imaging experiment. Own drawing.

Tracers	**SP1 (^{18}F-FOL)**		**SP2 ([^{68}Ga]Ga-NODAGA-RGD)**		**SP3 ([^{68}Ga]Ga-DOTA-Siglec-9)**	
Total number (n)	24		19		19	
	15 immunized	6 controls	8 immunized	8 controls	9 immunized	6 controls
In vivo PET/CT with the specific tracer (n)	15*	6	8**	8	9**	6
In vivo [^{18}F]FDG PET (n)	10	3	6	5	3	0
Histologically proven myocardial inflammatory lesions (n)	7	0	7	0	8	0
Ex vivo autoradiography (n)	7	6	7	8	8	6
Ex vivo gamma counting (n)	7	6	7	8	8	6
Anti-VAP-1 polyclonal antibody injection 10 min before sacrifice (n)	0	0	0	0	6***	2***
Number immunized with inflammatory lesions for blocking or negative-control peptide (n)	3		3		4	
In vivo PET/CT dynamic blocking followed by ex vivo autoradiography and gamma counting (n)	3		0		0	
In vivo negative-control peptide followed by *ex vivo* autoradiography and gamma counting (n)	0		3		4***	
In vitro blocking of the tissue sample (n)	3		0		3	

In vivo blocking study: *in vivo* competition assay with 100-fold molar excess of folate glucosamine injected 10 min before ^{18}F-FOL. *In vitro* blocking study: *in vitro* competition assay in the presence or absence of 100-fold molar excess of folate glucosamine (*SP1)* and with or without 10 minutes

pre-incubation with a 100-fold molar excess of non-labeled DOTA-Siglec-9 peptide as a blocker (*SP3).* n = number. *10 had a static scan and all others a dynamic scan. ** 4 had a dynamic scan and all others a static scan. ***A dose of 1 mg/kg of anti-VAP-1 polyclonal antibody was injected intravenously 10 min before sacrifice to detect surface-bound VAP-1 by immunofluorescence.

4.3 Human Myocardial Samples

In SP1, 5 myocardial autopsy samples from 5 patients who died of CS and 1 myocardial sample from an explanted heart due to sarcoidosis, were cut into serial 4 μm paraffin sections. Hematoxylin and eosin (H&E) staining was performed for general histology. For immunohistochemistry, adjacent serial 4-μm paraffin sections were stained with an anti-FR-β antibody to study localization of FR-β and an anti-CD68 antibody to detect macrophages. Double immunofluorescence staining was performed with an anti-CD68 antibody and with an anti-FR-β antibody (Shen et al., 2015).

In SP3, myocardial samples from 2 patients who died of CS and 1 myocardial sample from an explanted heart because of sarcoidosis were used. Hearts were cut into serial 4 μm paraffin sections. H&E staining was performed for general histology. For immunohistochemistry, adjacent serial 4-μm paraffin sections were stained with an anti-CD68 antibody to detect macrophages and polyclonal anti-VAP-1 antibody produced in rabbits against recombinant human VAP-1 (Bono et al., 1998) were used to detect VAP-1.

All antibodies used for immunohistochemical staining are listed in Table 4.

4.4 Radiochemistry

The PET tracers were synthetized at the Radiochemistry Laboratory of Turku PET Centre. The [^{18}F]FDG was acquired from batches synthetized with a standard protocol for clinical applications.

4.4.1 Synthesis of ^{18}F-FOL

The preparation of ^{18}F-FOL ([^{18}F]AlF-NOTA-folate) was conducted as described in previous studies (Silvola et al., 2018; Elo et al., 2019). Radiolabeling commenced by adding [^{18}F]-fluoride (3.2–3.4 GBq) in 50 μL of physiological saline to a reaction vessel containing 25 μL of sodium acetate buffer (pH 4.0, 1M) and 2 mM aluminum chloride ($AlCl_3$). This mixture was kept at room temperature for 3 minutes, followed by the addition of 250 μg of NOTA-folate in 50 μL of water and 125 μL of acetonitrile. The reaction was heated at 100 °C for 15 minutes, then diluted with 1

mL of water containing 0.2% formic acid. The resulting mixture was purified using high-performance liquid chromatography (HPLC) with a semi-preparative C18 column (Jupiter 250×10 mm; Phenomenex Inc., Torrance, CA, USA) equipped with both UV (254 nm) and radioactivity detectors. Solvent A was water with 0.1% formic acid, and solvent B was acetonitrile with 0.1% formic acid. The elution gradient transitioned from 8% B to 21% B over 20 minutes at a flow rate of 4 mL/min. Potassium bicarbonate ($KHCO_3$) solution (1 M) was added to the collected HPLC fraction to adjust the pH to 5.5, after which the solvents were evaporated. The final formulation was in phosphate-buffered saline (PBS) containing 8% ethanol and 7% polypropylene glycol, with a radioactivity concentration of less than 400 MBq/mL. The product underwent sterile filtration (0.22 μm, Millipore) before being used for PET studies. The total radiosynthesis time ranged from 75 to 88 minutes from the end of bombardment, with a radiochemical purity exceeding 95% and a molar activity of 34 ± 9.3 GBq/μmol. The radiochemical yield, corrected for decay, was 57% ± 9.2%.

To assess the *in vivo* stability and plasma protein binding of ^{18}F-FOL, blood samples were collected from three control rats and four immunized rats 80 minutes post-injection. Plasma was separated by centrifugation (2,100 × g for 4 minutes at 4 °C), and proteins were precipitated by adding an equal volume of acetonitrile, followed by another round of centrifugation. The radioactivity concentration in both the precipitated protein and the supernatant was measured using a 1480 Wizard 3″ (Perkin Elmer/Wallac, Turku, Finland). The supernatant was further filtered through a 0.45-μm Minispike filter (Waters Corporation, USA) for HPLC analysis. The HPLC analysis of plasma samples used a semi-preparative C18 column (Jupiter 250×10 mm; Phenomenex Inc., Torrance, CA, USA) with UV (254 nm) and radioactivity detectors. Solvent A consisted of water with 0.1% trifluoroacetic acid (TFA), and solvent B was acetonitrile with 0.1% TFA. The gradient elution ranged from 7% B to 22% B over 15 minutes at a flow rate of 5 mL/min. The fraction of radioactivity corresponding to the intact tracer in plasma was 91% ± 2.3%.

4.4.2 Synthesis of ^{68}Ga-NODAGA-RGD

The preparation of ^{68}Ga-NODAGA-RGD followed previously described methods (Grönman et al., 2017). For synthesizing the ^{68}Ga-labeled 1,4,7-triazacyclononane-1-glutaric acid-4,7-diacetic acid-conjugated RGD peptide (^{68}Ga-NODAGA-RGD), the NODAGA-RGD peptide (cyclo[L-arginylglycyl-L-aspartyl-D-tyrosyl-N6-([[4,7-bis(carboxymethyl)-1,4,7-triazonan-1-yl]acetyl])-L-lysyl]; product number 9805) was sourced from ABX Advanced Biochemical Compounds GmbH, Radenberg, Germany. The ^{68}Ga was obtained from a ^{68}Ge/^{68}Ga generator (Eckert & Ziegler, Valencia, CA, USA) through elution with 0.1 M hydrochloric acid. A 500

µL aliquot of the ^{68}Ga eluate was mixed with 18 mg of sodium acetate to achieve a pH of 5, followed by the addition of 10 nmol of NODAGA-RGD (dissolved in deionized water to make a 1 mM stock solution). The reaction mixture was heated at 100 °C for 15 minutes without further purification.

The radiochemical purity of [^{68}Ga]NODAGA-RGD was assessed using reversed-phase HPLC with a Jupiter C18 column (4.6 × 150 mm, 300 Å, 5 µm; Phenomenex, Torrance, CA, USA) at a flow rate of 1 mL/min and detection at 220 nm. Solvent A was water with 0.1% TFA, and Solvent B was acetonitrile with 0.1% TFA. The elution gradient was programmed as 97/3 (A/B) for 0–5 minutes, changing to 0/100 from 5–15 minutes. The HPLC system included LaChrom instruments (Hitachi; Merck, Darmstadt, Germany) connected to a Radiomatic 150TR radioisotope detector (Packard, Meriden, CT, USA). The resulting radiochemical purity was ≥99%, and the molar activity was 18 ± 7.3 GBq/µmol (n = 9).

4.4.3 Synthesis of [^{68}Ga]DOTA-Siglec-9

[^{68}Ga-DOTA-Siglec-9 was prepared according to previously described procedures (Siitonen et al., 2017). A cyclic peptide, CARLSLSWRGLTLCPSK, with disulfide-bridged cysteines consisting of residues 283 to 297 from the Siglec-9 and 8-amino-3,6-diooxaoctanoyl linker (polyethylene glycol derivative) between DOTA chelator and peptide (Peptide Specialty Laboratories GmbH), was labeled with ^{68}Ga as previously described. The radiochemical purity determined by reversed-phase radio-HPLC was 95% and the molar activity was 25.8 ± 8.3 GBq/lmol.

The [^{68}Ga]Ga-DOTA control peptide was derived from the cyclic [^{68}Ga]Ga-DOTA-Siglec-9 peptide CARLSLSWRGLTLCPSK by mutating Arg3, Trp8, and Arg9 to alanines. These residues were selected since the double-mutated R3A/R9A peptide does not bind human VAP-1 (hVAP-1) (Silvola et al., 2016). Trp8 was additionally mutated to alanine since its predicted binding site is not conserved in human VAP-1 or rat VAP-1. Thereafter, the residues in the resulting CAALSLSAAGLTLCPSK peptide were scrambled manually by avoiding Siglec-9-derived amino-acid repeats and by distributing polar residues throughout the sequence to avoid hydrophobic patches. The constructed [^{68}Ga]Ga-DOTA control, CSALATGLSALALCPSK, the R3A/R9A, and the [^{68}Ga]Ga-DOTA-Siglec-9 peptides were docked into the homology model for rat VAP-1 (rVAP-1) with Gold24 using the pyridazinone inhibitor in the crystal structure of hVAP-1 (Protein Data Bank (PDB) ID 4bty (Bligt-Linden et al., 2013) as the center of the binding site. The rVAP-1 model was created with Modeller26 using the published sequence alignment (Lopes de Carvalho et al., 2018) and hVAP-1 structure (PDB ID 4bty). Additionally, all peptides were docked into hVAP-1 for comparison. Docking of the peptides to

hVAP-1 and rVAP-1 resulted in 10 binding modes for each peptide. Trp8 in the [^{68}Ga]Ga-DOTA-Siglec-9 peptide binds close to the specificity pocket of hVAP-1 (Asp180, Thr210, and Leu177) (Bligt-Linden et al., 2013; Lopes de Carvalho et al., 2018). This binding site is not conserved in rVAP-1, where the corresponding residues are Gln180, Lys210 and Gln177) (Bligt-Linden et al., 2013). Trp8 in the docked [^{68}Ga]Ga-DOTA-Siglec-9 and R3A/R9A peptides binds near Gln180 and Gln177 in rVAP-1, whereas the constructed [^{68}Ga]Ga-DOTA control with scrambled sequence and without any tryptophanes does not interact with these residues.

4.5 *In Vivo* PET/CT Imaging

In vivo imaging studies were conducted on isoflurane-anesthetized rats (induction at 4-5% and maintenance at 1.5-2%) using a small animal PET/CT device (Inveon Multimodality; Siemens Medical Solutions) as outlined in previous research (Ståhle et al., 2020). Following this, 300 µL of an intravascular iodinated contrast agent (eXia™ 160XL; Binitio Biomedical Inc.) was administered intravenously, and high-resolution CT imaging was performed immediately after PET, as previously detailed (Eo et al., 2016). Body temperature was maintained with a heating pad, and blood glucose levels were monitored using a glucometer (Bayer Contour, Bayer AG, Leverkusen, Germany).

In SP1, rats received 50 ± 1.5 MBq of ^{18}F-FOL via the tail vein. Imaging consisted of either a 60-minute dynamic PET acquisition (frames: 6 × 10 s, 4 × 60 s, 5 × 300 s, and 3 × 600 s) or a 10-minute static PET acquisition starting at 30 minutes post-injection. For myocardium visualization, a 40-minute static [^{18}F]FDG PET acquisition (50 ± 2.6 MBq) starting at 20 minutes post-injection was conducted the day before the ^{18}F-FOL study.

In SP2, rats were injected with 50.8 ± 2.8 MBq [^{68}Ga]Ga-NODAGA-RGD intravenously. This was followed by either a 10-minute static PET acquisition starting at 60 minutes post-injection or a 90-minute dynamic PET acquisition beginning at the time of injection (frames: 6 × 10 s, 4 × 60 s, 5 × 300 s, and 6 × 600 s) to analyze tracer kinetics. Additionally, a 40-minute static [^{18}F]FDG PET acquisition (38.5 ± 2.9 MBq) starting at 20 minutes post-injection was performed the day before the [^{68}Ga]Ga-NODAGA-RGD study for myocardium localization.

In SP3, rats were injected with 50.4 ± 2.3 MBq [^{68}Ga]Ga-DOTA-Siglec-9 via the tail vein. Imaging options included a 30-minute static PET acquisition starting at 30 minutes post-injection or a 60-minute dynamic PET acquisition starting at the time of injection (frames: 6 × 10 s, 4 × 60 s, 5 × 300 s, and 6 × 600 s) to study tracer kinetics. For myocardium visualization, a 40-minute static [^{18}F]FDG PET

acquisition (40.4 ± 1.6 MBq) starting at 20 minutes post-injection was performed the day before the [^{68}Ga]Ga-DOTA-Siglec-9 study.

The PET data were reconstructed using an iterative three-dimensional ordered subset expectation maximization with maximum a priori (OSEM3D/SP-MAP) algorithm, with 2 OSEM iterations and 18 MAP iterations, including attenuation and dead time correction, targeting a resolution of 1.5 mm, and a matrix size of 128 × 128. Regions of interest (ROIs) of uniform size were defined in the PET images co-registered with CT or [^{18}F]FDG images using Carimas 2.9 software (Turku PET Centre, Turku, Finland) (Eo et al., 2016; Ståhle et al., 2020). ROIs were drawn in the left ventricular (LV) myocardium. In immunized rats, ROIs were placed in myocardial regions roughly corresponding to inflammatory lesions identified in histology. In control rats, ROIs were placed in the septal wall to measure tracer uptake in non-lesioned myocardium. The mean standardized uptake value (SUVmean) was compared between histologically inflamed and non-inflamed myocardial regions, determined by consensus of two blinded readers. Additional ROIs were drawn in the liver, lung, kidney, foreleg muscle, inferior vena cava, and LV (to measure blood radioactivity). Decay-corrected time-activity curves were generated for rats with dynamic datasets.

4.5.1 Kinetic Modeling

In SP1, Logan, Patlak, and compartmental modeling were performed to study the tracer uptake kinetics, and parametric images were acquired as previously described (Kiugel et al., 2014; Ståhle et al., 2020). Metabolite-corrected plasma time activity curves were used as input functions. Image-derived blood curves measured in the vena cava and LV cavity were converted into metabolite-corrected plasma curves using the group median plasma-to-blood ratio and percent of ^{18}F-FOL measured in the metabolite analysis. After tracer injection, distribution volume (DV) and Ki were calculated as the slope of the plot 5–60 min. Parametric images of DV were obtained using Logan plots and modeling images, and the data were compared with standardized uptake values.

4.6 Ex Vivo Autoradiography of Tissue Sections

Ex vivo digital autoradiography was performed on 20 µm cryosections of the myocardium of the imaged rats at 100 minutes (SP1 and SP2) and 70 minutes (SP3) post-injection, to quantify the tracer uptake in tissue sections in more detail. The cryosections were air-dried and placed under a radiation-sensitive imaging plate (Fuji Imaging Plate BAS-TR2025, Fuji Photo Film Co., Ltd., Tokyo, Japan) for a specific time depending on the radionuclide decay, and then scanned with a Fuji

Analyser BAS-5000 (internal resolution of 25 μm, Fuji, Tokyo, Japan). Thereafter, the 20 μm sections were stained with H&E. Multiple ROIs were drawn in the inflamed and non-inflamed myocardium in co-registered autoradiographs and images of H&E stainings of the same sections using TINA^{TM} 2.10f software (Raytest Isotopenmessgeräte GmbH., Straubenhardt, Germany). Inflamed myocardium was defined as the presence of inflammatory cell infiltrate and signs of myocyte necrosis in the H&E-stained section. Non-inflamed myocardium was defined as the absence of both inflammation in the H&E-stained section and CD68 positive macrophages in a serial tissue section. The whole area of histologically inflamed myocardium was sampled, whereas the non-inflamed myocardium was sampled using multiple, uniformly sized ROIs. The results are as average photo-stimulated luminescence per square millimeter (PSL/mm^2).

4.7 Specificity of Tracer Binding

In SP1, to study the specificity of ^{18}F-FOL uptake, an *in vivo* blocking study was carried out with IV injection of a 100-fold excess of FR-β ligand folate glucosamine ($C_{25}H_{30}N_8O_{10}$; 100 μL) 10 minutes before ^{18}F-FOL injection. *In vitro* binding study of ^{18}F-FOL in myocardial tissue sections from 3 immunized rats was performed in the presence or absence of a 100-fold excess of folate glucosamine as described earlier (Schniering et al., 2019) to further evaluate the specificity of the tracer.

In SP2, to assess the specificity of [^{68}Ga]Ga-NODAGA-RGD uptake in cardiac inflammatory lesions, uptake of a non-specific control peptide [^{68}Ga]Ga-DOTA-E[c(RGEfK)]2 was studied in three immunized rats (weight in g, 310.3 ± 6.6). The rats were IV injected with 52.4 ± 0.8 MBq [^{68}Ga]Ga-DOTA-E[c(RGEfK)]2 and euthanized at 90 min post-injection. Then, tracer biodistribution was studied and *ex vivo* autoradiography of 20 μm cryosections of the myocardium was performed as described above.

In SP3, *in vivo* [^{68}Ga]Ga-DOTA-control peptide binding study was carried out in four immunized rats (weight, 298.7 ± 9.5 g). The rats were IV injected with 40.8 ± 5.8 MBq [^{68}Ga]Ga-DOTA-control peptide and were euthanized at 70 minutes post-injection, after which biodistribution analysis and *ex vivo* autoradiography were performed on 20 μm cryosections of the myocardium. To further assess the specificity of the tracer binding, an *in vitro* binding study of [^{68}Ga]Ga-DOTA-Siglec-9 in cardiac tissue sections from three immunized rats was performed with or without 10 minutes pre-incubation with a 100-fold molar excess of non-labeled DOTA-Siglec-9 peptide as a blocker. Total and blocked binding of [^{68}Ga]Ga-DOTA-Siglec-9 was studied by digital autoradiography.

4.8 *Ex Vivo* Biodistribution

Ex vivo biodistribution study was performed in parallel to autoradiography study. After 100 minutes (SP1 and SP2) and 70 minutes (SP3) of tracer accumulation, the selected tissues including the heart, blood, intestine, kidney, liver, lung, lymph node, muscle, plasma, pancreas, spleen, thymus, white adipose tissue, urine and bone marrow (only in SP1) were excised, weighed, and measured for total radioactivity utilizing a gamma counter (Triathler 3", Hidex Oy, Turku, Finland). The radioactivity measurements were normalized for injected dose, animal weight, decay, and tissue sample weight. Results were expressed as SUV.

4.9 Histology, Immunohistochemistry, and Immunofluorescence

General histology and relevant inflammatory markers were examined in all studies. The typical staining protocol included heat-mediated antigen retrieval, usually in citrate buffer, a blocking reagent such as 1% bovine serum albumin in PBS/Tween, incubation with primary antibody for 60 minutes or overnight, followed by appropriate secondary antibodies. For general histology, 20 μm cryosections were stained with hematoxylin and eosin (H&E). All antibodies used for immunohistochemical and immunofluorescence staining are listed in Table 4.

In SP1, for immunohistochemistry, adjacent serial 4 μm paraffin sections were stained with antibodies against FR-β, CD3 to detect lymphocytes, and CD68 to detect macrophages. Additionally, antibodies against iNOS and CD206 were used to detect pro-inflammatory (M1-polarized) and anti-inflammatory (M2-polarized) macrophages, respectively. To study the co-localization of FR-β with macrophage subsets, double immunofluorescence stainings were performed on cryosections. The cryosections were stained with biotinylated anti-FR-β antibody detected with Streptavidin Alexa Fluor™ 488 conjugate, followed by staining with either anti-CD68, anti-iNOS, or anti-CD206 antibodies.

In SP2, adjacent serial 8 μm cryosections were stained with monoclonal mouse anti-rat CD68 to detect macrophages, monoclonal mouse anti-rat CD61 to detect the integrin β3 chain, polyclonal rabbit anti-rat CD31 to detect endothelial cells, and monoclonal mouse anti-α-smooth muscle actin (α-SMA) antibody to detect myofibroblasts.

In SP3, 8 μm cryosections were stained with monoclonal mouse anti-rat CD68 to detect macrophages, polyclonal CD31 to detect vascular endothelium, and monoclonal mouse anti-actin α-smooth muscle to detect α-smooth muscle actin (α-SMA) in myofibroblasts, with appropriate peroxidase-conjugated secondary

antibodies. 3,3'-Diaminobenzidine (DAB) was used as a chromogen. Immunofluorescence staining with anti-VAP-1 antibody was performed on 8 μm cryosections to detect VAP-1. Heart cryosections from rats that received intravenous anti-VAP-1 antibody (clone 174-5, 1 mg/kg in saline) 10 minutes before sacrifice (five immunized and two controls) were incubated with fluorescein isothiocyanate (FITC)-conjugated anti-mouse IgG, followed by Alexa Fluor 488-conjugated anti-FITC and Hoechst. Heart cryosections from other rats (four immunized and four controls) were incubated with polyclonal rabbit anti-human anti-VAP-1 antibody (also recognizes rat VAP-1), followed by Alexa Fluor 488-conjugated goat anti-rabbit IgG secondary antibody.

Additional H&E and immunohistochemical staining with monoclonal mouse anti-rat CD68 and polyclonal anti-VAP-1 antibodies were performed on 4 μm paraffin-embedded sections and 8 μm cryosections of thymus, white adipose tissue, spleen, and bone marrow from immunized rats that received intravenous anti-VAP-1 antibody (clone 174-5, 1 mg/kg in saline) 10 minutes before sacrifice.

Table 4: Antibodies used in immunohistochemical and immunofluorescence staining studies. Own drawing.

Antibody	Clone	Dilution	Study	Manufacturer
Rat sections				
Immunohistochemistry				
FR-β	Polyclonal rabbit anti-rat, orb317614	1:200 (Paraffin)	SP1	Biorbyt Cambridge, UK
CD68	Monoclonal mouse anti-rat, MCA341R	1:10000 (Cryo)	SP1	AbD Serotec Munich, Germany
CD68	Monoclonal mouse anti-rat, MCA341GA	1:2000 (Paraffin) 1:1000 (Cryo)	SP1, SP2, SP3	Bio-Rad California, USA
iNOS	Polyclonal rabbit anti-rat, ab15323	1:350 (Paraffin)	SP1	Abcam Cambridge, UK
CD206	Polyclonal rabbit anti-rat anti-mannose receptor, ab64693	1:5000 (Paraffin)	SP1	Abcam Cambridge, UK
CD3	Monoclonal rabbit anti-rat, 2GV6	1:1 (Paraffin)	SP1	Ventana Arizona, USA
CD61	monoclonal mouse anti-rat, MCA1773	1:500 (Cryo)	SP2	Bio-Rad California, USA
CD31	polyclonal rabbit anti-rat, NB100-2284	1:200 (Cryo)	SP2, SP3	Novus Biologicals, Centennial, CO, USA
α-SMA	monoclonal mouse, A5228-200	1:12000 (Cryo)	SP2, SP3	Sigma-Aldrich, St. Louis, MO, USA
Immunofluorescence				
FR-β	Biotinylated anti-human FR-β, m909	1:50 (Cryo)	SP1	Non-commercial (Shen et al., 2014)

Streptavidin	Alexa Fluor™ 488 conjugate S32354	1:200 (Cryo)	SP1	Thermo Fisher Massachusetts, USA
Streptavidin	Alexa Fluor™ 488 conjugate A11029	5 mg/mL (Cryo)	SP3	Thermo Fisher Massachusetts, USA
Hoechst				
CD68	Monoclonal mouse anti-rat, MCA341R	1:1000 (Cryo)	SP1	AbD Serotec Munich, Germany
iNOS	Polyclonal rabbit anti-rat, ab15323	1:1000 (Cryo)	SP1	Abcam Cambridge, UK
CD206	Polyclonal rabbit anti-rat, ab64693	1:1000 (Cryo)	SP1	Abcam Cambridge, UK
VAP-1	Polyclonal rabbit anti-human	1:10000 (Cryo)	SP3	Non-commercial (Bono et al., 1998)
FITC-conjugate	Anti-mouse IgG, F28883	1:100 (Cryo)	SP3	Sigma-Aldrich, St. Louis, MO, USA
Human tissue sections				
Immunofluorescence				
FR-β	Biotinylated anti-human FR-β, m909	1:50 (Paraffin)	SP1	Non-commercial (Shen et al., 2014)
Streptavidin	Alexa Fluor™ 488 conjugate S32354	1:200 (Paraffin)	SP1	Thermo Fisher Massachusetts, USA
Streptavidin	Alexa Fluor™ 488 conjugate goat anti-rabbit IgG, A11034	1:200 (Paraffin)	SP3	Life Technologies, California, USA
CD68	Monoclonal mouse anti-human, M0876	1:200 (Paraffin)	SP1	Dako, Agilent Technologies Inc., California, USA
VAP-1	Polyclonal rabbit anti-human	1:10000 (Paraffin)	SP3	Non-commercial (Bono et al., 1998)

4.10 Statistical Analyses

Data are presented as mean ± standard deviation (SD). Paired or non-paired Student's t-test was applied for single comparisons between two groups with normally distributed data. The Mann–Whitney U test and Kolmogorov–Smirnov tests were applied to single comparisons between non-normally distributed data. Normality distribution assumption was checked with the Shapiro–Wilk test, and assumption of variance equality was checked with Fisher's F test. Spearman's rank test (rs) was used to analyze correlation between two continuous variables. GraphPad Prism 6 Software. was used to perform the analyses, and the statistical significance threshold was $P < 0.05$.

5 Results

5.1 Histology

5.1.1 Experimental Autoimmune Myocarditis Induces Inflammatory Lesions Presenting FR-β, αvβ3 Integrin and VAP-1

In SP1, histological analysis of the rat hearts indicated focal cardiac inflammatory lesions in ten out of eighteen immunized rats (56%), six resulting from hock injections and four from footpad injections. No lesions were identified in the six control rats. These inflammatory lesions were predominantly located near the epicardium and exhibited myocyte necrosis along with dense infiltration of inflammatory cells. CD68-positive macrophages were the main cell type present in the lesions, comprising both M1- and M2-polarized macrophages. CD3-positive lymphocytes were also observed but to a lesser extent. Outside the inflammatory lesions, the myocardium appeared normal under microscopic examination, and CD68 staining was minimal. Immunohistochemistry revealed a significant presence of FR-β-positive cells within the lesions, but not in the unaffected myocardium (Figure 1). Double immunofluorescence staining confirmed the co-localization of FR-β with CD68-positive macrophages, which were predominantly M1-polarized.

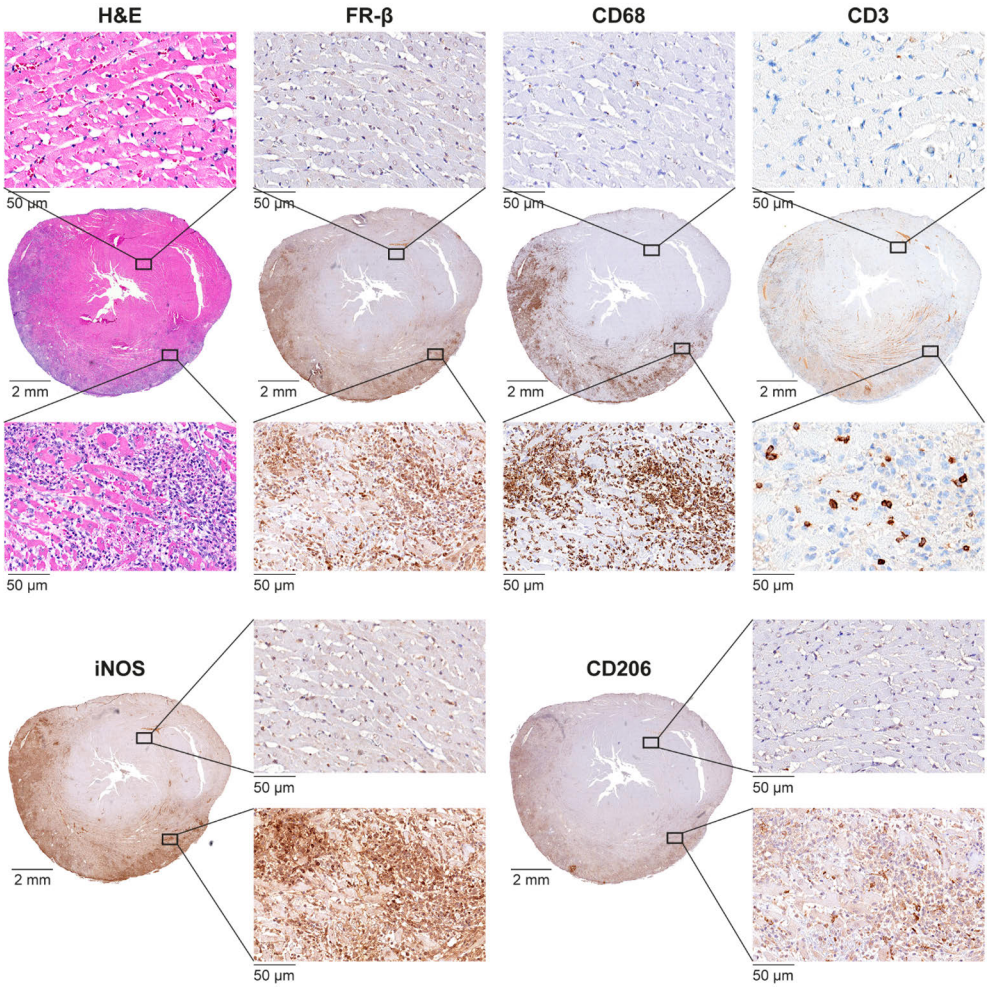

Figure 1. An inflammatory myocardial lesion in a rat with autoimmune myocarditis identified by hematoxylin and eosin (H&E) staining. Immunostaining revealed folate receptor β (FR-β) co-localized with CD68-positive macrophages. Additionally, scattered CD3-positive lymphocytes were observed. Staining with antibodies against inducible nitric oxide synthase (iNOS) indicated the presence of M1-polarized macrophages, while staining with antibodies against CD206 revealed a smaller presence of M2-polarized macrophages. From original publication I.

In the SP2, histological analysis revealed that seven out of eight immunized rats (87.5%) exhibited extensive cardiac inflammatory lesions, while none of the eight control rats showed any inflammatory lesions. These lesions were marked by

significant infiltration of inflammatory cells and myocyte necrosis. Immunohistochemical staining identified CD68-positive macrophages as the predominant inflammatory cells within the lesions. Additionally, positive α-SMA staining indicated the presence of myofibroblasts, and CD31-positive staining demonstrated the existence of a capillary network within the inflammatory areas. CD61 (β3 integrin marker) staining overlapped with CD31-positive areas, revealing capillary-like structures with positive staining (Figure 2).

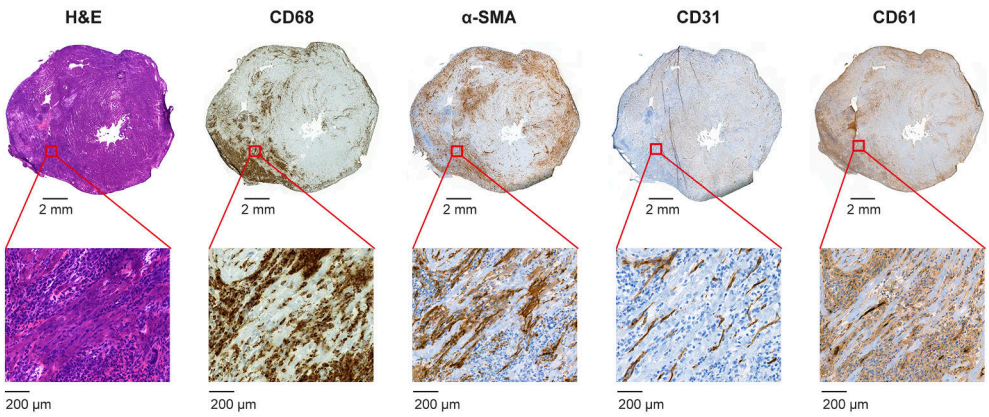

Figure 2. Histology of myocardial inflammatory lesions in a heart cross-section from an immunized rat. Hematoxylin and eosin (H&E) staining reveals diffuse inflammation and a large inflammatory lesion in the inferior wall of the left ventricle, extending to the right ventricular wall, characterized by infiltrating inflammatory cells and myocyte necrosis. Immunostaining (brown) demonstrates dense infiltrates of CD68-positive macrophages, numerous α-smooth muscle actin (α-SMA)-positive myofibroblasts, and a substantial capillary network of CD31-positive endothelial cells. CD61 antibody staining indicates that some capillaries express integrin β3. From original publication II.

In SP3, representative histological, immunohistochemical, and immunofluorescence stainings of rat myocardium 21 days post-immunization are depicted in Figure 3. Histological analysis confirmed multiple myocardial lesions in eight out of nine immunized rats (88%), whereas no lesions were observed in the six control rats. These lesions were characterized by intense inflammatory cell infiltration, myocyte necrosis, and scarring. CD68-positive macrophages were the predominant cells present in the lesions. Immunofluorescence staining, following either intravenous injection or tissue section incubation with anti-VAP-1 antibody, revealed moderate VAP-1 positivity at the lesion sites, with occasional VAP-1 staining in the myocardium outside the lesions in immunized rats and in control rats. Immunohistochemical analysis showed a significant presence of αSMA-positive

cells in the myocardial lesions, with only sporadic α-SMA-positive cells in the myocardium outside the lesions in immunized rats or in the myocardium of control rats. CD31 staining indicated the presence of capillary networks within the myocardial lesions, identifying a proportion of CD31-positive endothelial cells (Figure 3). Immunohistochemical staining of the spleen and bone marrow revealed CD68-positive macrophages and VAP-1 positivity in these organs, while staining of the thymus and white adipose tissue showed a high abundance of CD68-positive macrophages.

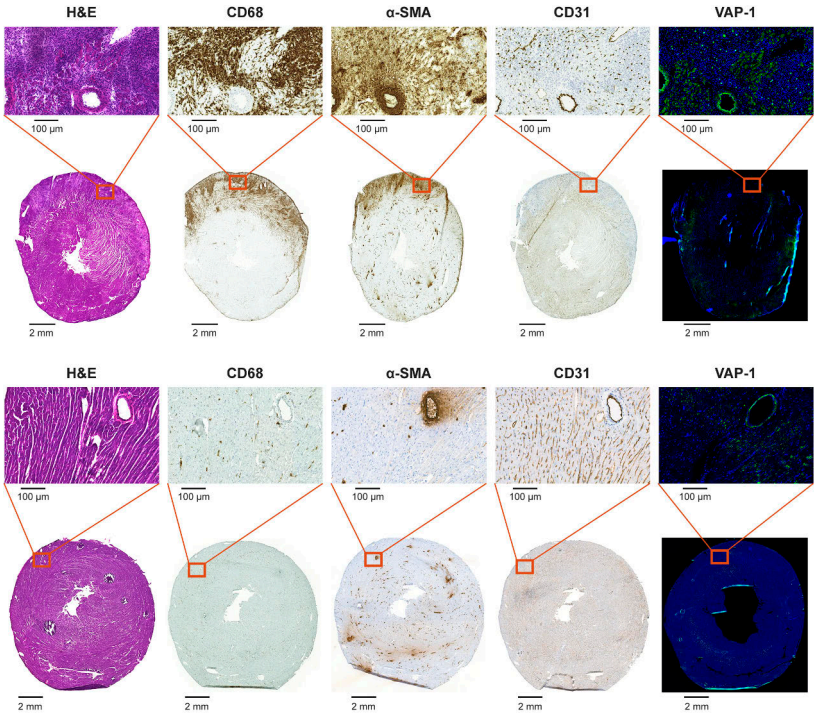

Figure 3. (A) A myocardial lesion from a rat with autoimmune myocarditis identified by hematoxylin and eosin (H&E) staining. A consecutive cryosection stained with immunofluorescence displays intracellular and surface-bound vascular adhesion protein-1 (VAP-1). The rat received an intravenous injection of anti-VAP-1 antibody 10 minutes before sacrifice, and staining was performed using only the secondary antibody. Numerous CD68-positive macrophages and α-smooth muscle actin (α-SMA) on myofibroblasts are present in the inflammatory lesion. Staining with an antibody against CD31 indicates the presence of vascular endothelial cells. (B) Histology and immunohistochemical and immunofluorescence staining of a control rat myocardium. From original publication III.

5.1.2 FR-β and VAP-1 in Human Cardiac Sarcoidosis Samples

To demonstrate the relevance of these factors in human disease, a condition with similar pathological findings was examined.

In SP1, tissue samples of all patients with CS showed FR-β expression in the inflammatory lesions that co-localized with CD68-positive macrophages.

In SP3, all human samples from patients with CS (n = 3) showed VAP-1-positivity in myocardial lesions, which was co-localized with vascular structures. Occasional VAP-1 positivity was also seen in the myocardium outside lesions of patients with CS.

5.2 *In Vivo* PET/CT Imaging Demonstrated Increased Uptake of Novel Tracers in Myocardial Lesions Associated with Autoimmune Myocarditis

Myocardium was clearly visualized by contrast-enhanced CT or a 40 min static [^{18}F]FDG/PET starting at 20 min post-injection.

In SP1, *in vivo* imaging showed distinct focal ^{18}F-FOL uptake in the left ventricular myocardium in all rats with histologically confirmed inflammatory lesions (n = 7), while no myocardial tracer uptake was observed in the immunized rats without histological inflammation (n = 8) or in the control rats (n = 6) at 30–40 minutes post-injection (Figure 4). Histological comparisons indicated that ^{18}F-FOL uptake co-localized with myocardial inflammatory lesions, whereas non-inflamed myocardium exhibited very low radioactivity. Time-activity curves for rats with inflamed lesions showed rapid clearance of ^{18}F-FOL radioactivity from the blood, with consistent uptake in myocardial inflammatory lesions and most other tissues from 20 minutes post-injection. The highest uptake was noted in the kidneys (SUVmean 10.1 ± 4.5), indicating elimination via the urinary system. ^{18}F-FOL uptake in inflammatory lesions was significantly higher than in the non-inflamed myocardium of immunized rats (SUVmean 2.1 ± 1.1 vs. 0.4 ± 0.2; P = 0.004), with a ratio of approximately 5:1 between inflammatory lesions and remote myocardium. Myocardial uptake in non-immunized controls (SUVmean 0.4 ± 0.1) was similar to the uptake in the non-inflamed myocardium of immunized rats (P = 0.4) and significantly lower than in inflammatory lesions (P = 0.003). Tissues adjacent to the heart had lower uptake than inflammatory lesions, with SUVmean values of 0.3 ± 0.1 in LV blood, 0.3 ± 0.1 in lungs, and 1.2 ± 0.4 in liver. Among the kinetic models evaluated, the Logan model provided the best fit to the data (Figure 5A and 5B, Table

5). Logan plots and parametric images of distribution volume (DV) were consistent with ^{18}F-FOL uptake in inflamed myocardium (Figure 5A and 5C). The DV of ^{18}F-FOL was significantly higher in inflamed myocardium compared to non-inflamed myocardium (DV, 4.0 ± 1.7 vs. 0.7 ± 0.2; P = 0.004) or the myocardium of control rats (DV, 0.8 ± 0.2; P = 0.003). SUVmean of ^{18}F-FOL at 30−40 minutes post-injection correlated well with DV.

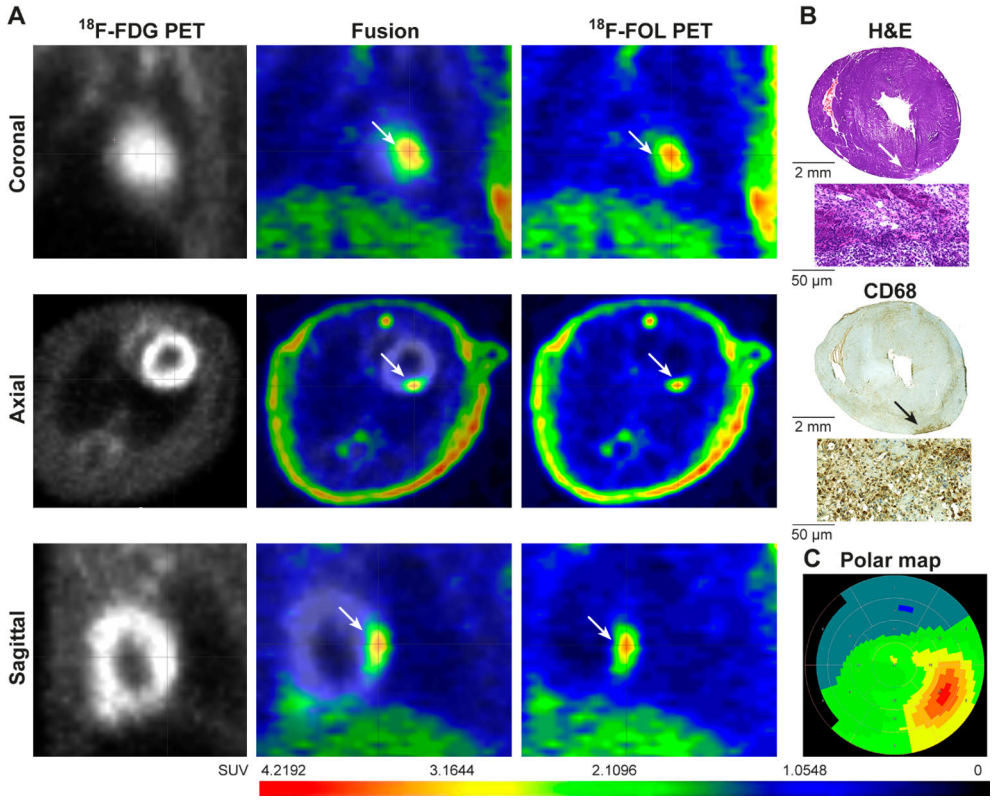

Figure 4. (A) *In vivo* PET images using [^{18}F]FDG and ^{18}F-FOL tracers in a rat with autoimmune myocarditis. The PET images taken 30-40 minutes post-injection show focal ^{18}F-FOL uptake (white arrows) in the posterior wall of the left ventricle (LV). (B) This uptake co-localizes with an inflamed myocardial lesion in the posterior LV wall, as indicated by histological sections stained with hematoxylin and eosin (H&E) and antibodies against CD68 (macrophages). (C) A polar map illustrates ^{18}F-FOL uptake in the posterior wall, with low uptake in other areas of the LV myocardium. From original publication I.

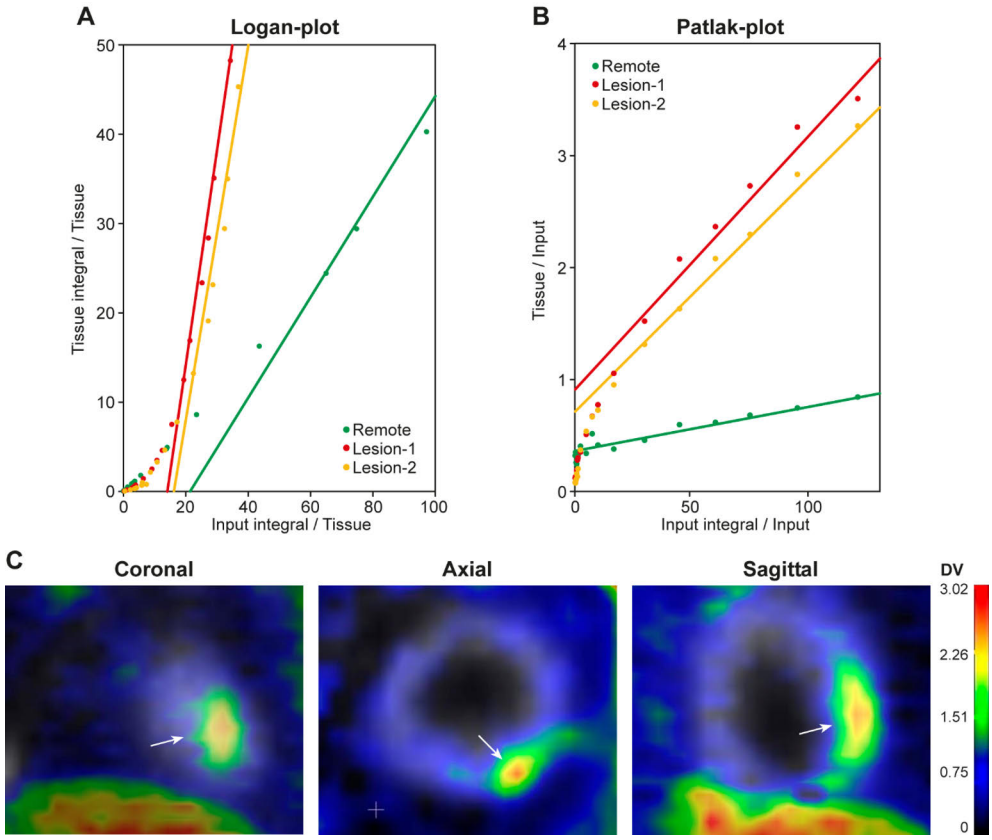

Figure 5. (A) Representative Logan plot of an immunized rat showing two inflammatory lesions in the LV myocardium at 5–60 minutes post-injection, indicating reversible receptor binding of ^{18}F-FOL. (B) Representative Patlak plot of the same immunized rat at 5–60 minutes post-injection, indicating irreversible receptor binding of ^{18}F-FOL due to cell internalization (C) DV generated PET images with ^{18}F-FOL, fused with [^{18}F]FDG PET (grey scale) images, showing distinct and focal ^{18}F-FOL uptake in an inflammatory lesion in the posterior LV wall of a rat with autoimmune myocarditis (white arrows). Metabolite-corrected plasma time-activity curves were used as input functions. Image-derived blood curves measured in the vena cava and LV cavity were converted to metabolite-corrected plasma curves using the group median plasma-to-blood ratio and the percentage of ^{18}F-FOL measured in metabolite analysis. DV and Ki values were calculated from the plot slope 5–60 minutes post-injection. Parametric images of DV were generated using Logan plots and modeling images, and the data were compared with standardized uptake values. From original publication I.

Table 5. Kinetic modeling of ^{18}F-FOL uptake. From original publication I.

Study region	DV	Ki	K1
Inflamed myocardial lesions (n = 8) in four immunized rats	4.0 ± 1.7	0.03 ± 0.02	0.2 ± 0.02
Remote myocardium (n = 4)	0.7 ± 0.2	0.003 ± 0.001	0.04 ± 0.02
Control rats (n = 6)	0.8 ± 0.2	0.004 ± 0.002	0.03 ± 0.01
***P*-values**			
Inflamed myocardium vs. Remote	0.04	0.04	0.000004
Inflamed myocardium vs. Control	0.003	0.003	0.001
Remote vs. Control	0.1	0.4	0.1

Results are expressed as mean ± SD with the probability value (*P*) from a Student's *t*-test. DV = distribution volume (mL/g), Ki = net influx rate (nmol/min/g), K1 = plasma-to-tissue transport rate compartmental model value (mL/min/g).

In SP2, *in vivo* [^{68}Ga]Ga-NODAGA-RGD PET/CT images showed visually increased tracer uptake in the myocardium of all immunized rats with histological inflammation (n = 7), while there was no visible tracer uptake in the myocardium of the immunized rat without inflammation (n = 1) or control rats (n = 8) (Figure 6). Analysis of the kinetics of [^{68}Ga]Ga-NODAGA-RGD uptake based on time activity curves demonstrated that tracer uptake in the inflamed myocardium was most stable after 30 min post-injection. The uptake of the [^{68}Ga]Ga-NODAGA-RGD at 60– 80 min post-injection was significantly higher in the inflamed myocardium compared to the non-inflamed myocardium of control rats (SUVmean, 0.4 ± 0.1 vs. 0.1 ± 0.02; P = 0.00006). The blood SUVmean, was 0.3 ± 0.1 (p = 0.09 vs. inflamed myocardium) and the uptake ratio between inflamed myocardium and blood was 1.4 ± 0.5.

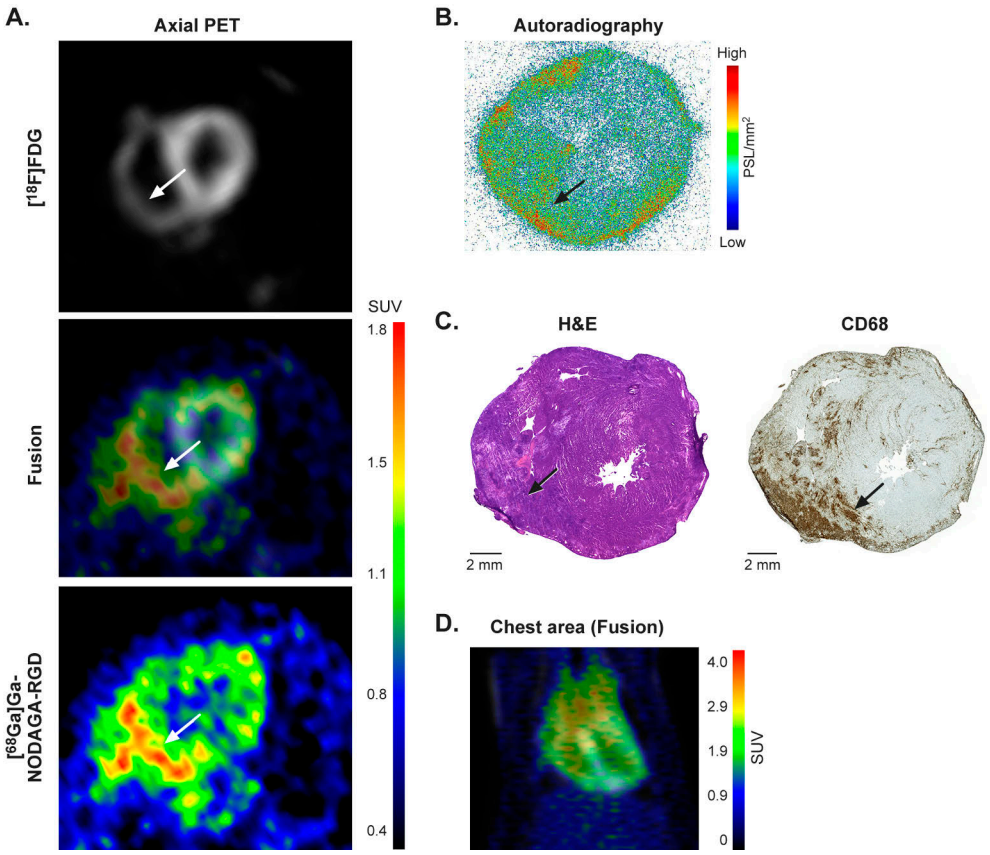

FIGURE 6. (A) *In vivo* PET images using [^{18}F]FDG and [^{68}Ga]Ga-NODAGA-RGD tracers in an immunized rat. PET images taken 60-80 minutes post-injection show [^{68}Ga]Ga-NODAGA-RGD uptake (white arrows) mainly in the inferior wall of the left ventricle, extending to the right ventricular wall. (B) *Ex vivo* autoradiography confirms myocardial [^{68}Ga]Ga-NODAGA-RGD uptake predominantly in the inferior wall of the left ventricle, extending to the right ventricular wall, co-localizing with inflammatory myocardial lesions seen in histological sections stained with hematoxylin and eosin (H&E) and CD68 (macrophages) (C). Note that some tracer uptake and inflammation are also present in the epicardial myocardium near the pericardium. Outside inflammatory lesions, the myocardium exhibits very low uptake. (D) *In vivo* PET image with [^{18}F]FDG (gray) and [^{68}Ga]Ga-NODAGA-RGD (rainbow) tracers showing the chest area in an immunized rat. From original publication II.

In SP3, *in vivo* PET/CT imaging with [^{68}Ga]Ga-DOTA-Siglec-9 enabled the visualization of histologically confirmed myocardial lesions in all eight immunized rats (Figure 7A). No myocardial tracer uptake was observed in the immunized rat without histological lesions or in the control rats (n = 6). Time-activity curves

indicated that [^{68}Ga]Ga-DOTA-Siglec-9 radioactivity was rapidly cleared from the blood, with discernible uptake in myocardial lesions from 30 minutes post-injection. The highest uptake was observed in the kidneys. At 30 to 60 minutes post-injection, [^{68}Ga]Ga-DOTA-Siglec-9 uptake in myocardial lesions was higher than in the myocardium of control rats (SUVmean 0.5 ± 0.1 vs. 0.2 ± 0.03; P = 0.00006). The uptake ratio between myocardial lesions and non-lesioned myocardium was 2.7 ± 0.6, and the lesion-to-blood ratio was 1.4 ± 0.5.

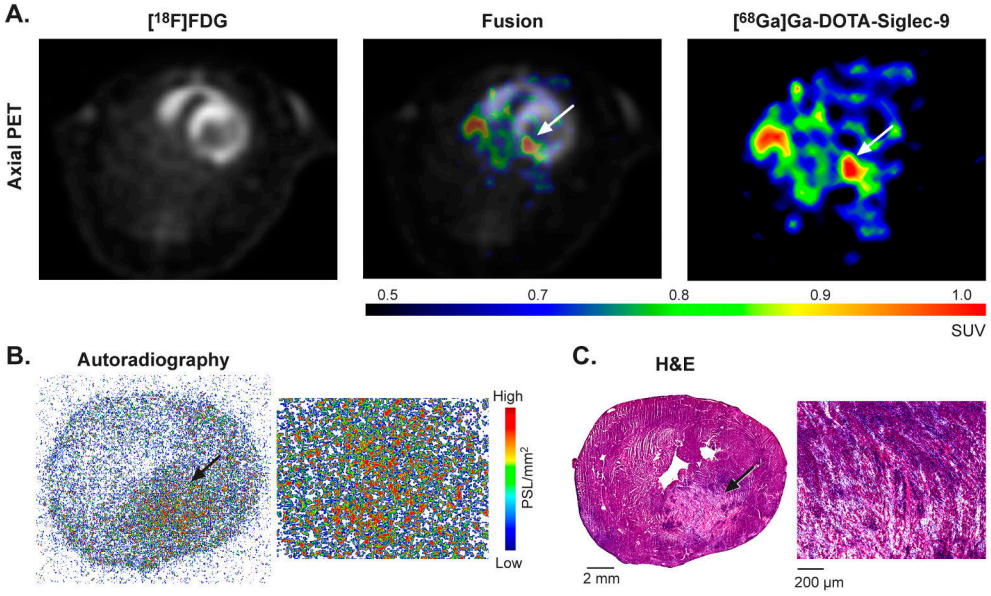

Figure 7. (A) Representative *in vivo* PET images with [^{18}F]-FDG and [^{68}Ga]Ga-DOTA-Siglec-9 tracers in a rat with autoimmune myocarditis. PET images at 30 to 60 minutes post-injection show focal [^{68}Ga]Ga-DOTA-Siglec-9 uptake (white arrows) in the posterior wall of the left ventricle (LV). (B) *Ex vivo* autoradiography of [^{68}Ga]Ga-DOTA-Siglec-9 uptake shows co-localization with edematous and hemorrhagic myocardial lesions in the posterior LV wall, (C) confirmed by consecutive sections stained with hematoxylin and eosin (H&E). From original publication III.

5.3 *Ex Vivo* Autoradiography Revealed co-localization of Novel Tracers and Myocardial Lesions in Autoimmune Myocarditis

To quantify tracer uptake in tissue sections, *ex vivo* autoradiography was performed. In SP1, *ex vivo* autoradiography demonstrated high uptake of ^{18}F-FOL in the inflammatory lesions of immunized rats, contrasting with low uptake in the non-

inflamed myocardium of immunized rats and the myocardium of control rats. The average uptake of ^{18}F-FOL in inflammatory lesions (470 ± 180 PSL/mm2; n = 7) was 7.8 ± 1.4 times higher than in the non-inflamed myocardium of immunized rats (67 ± 43 PSL/mm2; P = 0.0005; n = 7). Control rat myocardium exhibited low activity (39 ± 15 PSL/mm2; P = 0.0002 vs. inflamed lesions; P = 0.19 vs. non-inflamed myocardium of immunized rats; n = 6).

In SP2, *ex vivo* autoradiography revealed focally increased [^{68}Ga]Ga-NODAGA-RGD uptake in the left ventricular (LV) myocardium of immunized rats, co-localizing with histological inflammatory lesions. Tracer uptake was low in the non-inflamed myocardium of immunized rats or the myocardium of controls. Quantitatively, the average [^{68}Ga]Ga-NODAGA-RGD uptake in inflamed areas was 6.7 ± 3.0 times higher than the uptake in non-inflamed areas of immunized rats (19 ± 9.3 vs. 2.9 ± 1.1 PSL/mm2; P = 0.004) and 7.1 ± 3.5 times higher than controls (2.7 ± 0.4 PSL/mm2; n = 8; P = 0.0005).

In SP3, *ex vivo* autoradiography revealed co-localization of [^{68}Ga]Ga-DOTA-Siglec-9 uptake and myocardial lesions. Autoradiography showed a 5.3 ± 1.2 times higher uptake of [^{68}Ga]Ga-DOTA-Siglec-9 in the myocardial lesions of immunized rats (n = 8) than in the myocardium outside lesions (PSL/mm2, 5.3 ± 1.0 vs. 1.1 ± 0.4; P = 0.0002), and 5.5 ± 1.1 times higher uptake than in the myocardium of control rats (PSL/mm2, 1.0 ± 0.1; n = 6; P = 0.00006).

5.4 Specificity of Tracer Binding

In SP1, *in vivo* blocking of ^{18}F-FOL with a 100-fold excess of folate glucosamine in three immunized rats resulted in 77% lower ^{18}F-FOL uptake in inflammatory lesions compared to rats injected with ^{18}F-FOL alone (SUVmean 0.6 ± 0.1 vs. 2.9 ± 0.4; P = 0.02). Folate glucosamine also effectively reduced *in vitro* binding of ^{18}F-FOL in inflamed myocardium in tissue sections (143 ± 27 vs. 2.4 ± 1.5 PSL/mm2; P<0.0001; n = 3).

In SP2, *ex vivo* autoradiography indicated that uptake of non-specific [^{68}Ga]Ga-DOTA-E[c(RGEfK)]2 in histologically confirmed inflammatory lesions of three immunized rats was 76% lower compared to [^{68}Ga]Ga-NODAGA-RGD in inflammatory lesions of seven immunized rats (4.5 ± 0.6 vs. 19 ± 9.3 PSL/mm2; P = 0.04). The average [^{68}Ga]Ga-DOTA-E[c(RGEfK)]2 uptakes in inflamed areas were higher than the uptake in non-inflamed areas of those three immunized rats (4.5 ± 0.6 vs. 0.9 ± 0.3 PSL/mm2; P = 0.004) but lower than the uptake of [^{68}Ga]Ga-NODAGA-RGD in the inflamed areas.

In SP3, *in vivo* studies with [^{68}Ga]Ga-DOTA-control peptide showed a 45% lower uptake ratio (myocardial lesions vs. myocardium outside lesions) than [^{68}Ga]Ga-DOTA-Siglec-9 (1.8 ± 0.5 vs. 1.0 ± 0.05; P = 0.02). According to *ex vivo* autoradiography assessment in immunized rats, [^{68}Ga]Ga-DOTA-control peptide showed a 65% lower uptake ratio (myocardial lesions vs. myocardium outside lesions) than [^{68}Ga]Ga-DOTA-Siglec-9 (1.8 ± 0.2 vs. 5.3 ± 1.2; P = 0.0006). The biodistribution results of [^{68}Ga]Ga-DOTA-control peptide are presented in Table 6. [^{68}Ga]Ga-DOTA-control peptide accumulation was significantly lower in the intestine, kidney, liver, lung, lymph node, and spleen and significantly higher in the plasma of immunized rats compared to the accumulation of [^{68}Ga]Ga-DOTA-Siglec-9. The quantitative *in vitro* autoradiography analysis revealed significantly lower [^{68}Ga]Ga-DOTA-Siglec-9 binding (49% reduction) in sections incubated with a 100-fold molar excess of non-labeled DOTA-Siglec-9 peptide (blocked binding) than with the total [^{68}Ga]Ga-DOTA-Siglec-9 binding (myocardial lesions vs. myocardium outside lesions ratio 1.2 ± 0.1 vs. 2.4 ± 0.2; P = 0.002), indicating specific tracer binding

Table 6. *Ex vivo* biodistribution of [^{68}Ga]Ga-DOTA-Siglec-9 and [^{68}Ga]Ga-DOTA-control peptides in rats at 70 minutes after intravenous injection. From original publication III.

	[^{68}Ga]Ga-DOTA-Siglec-9			[^{68}Ga]Ga-DOTA-control	
	Immunized rats (*n* = 8)	**Control rats** (*n* = 6)	***P*-value**	**Immunized rats** (*n* = 4)	***P*-value**
Blood	0.23 ± 0.08	0.18 ± 0.05	0.21	0.32 ± 0.02	0.06
Heart	0.14 ± 0.04	0.07 ± 0.02	0.007*	0.14 ± 0.03	0.78
Intestine (without content)	0.20 ± 0.06	0.15 ± 0.07	0.24	0.13 ± 0.02	0.04*
Kidney	19.34 ± 9.12	14.37 ± 5.60	0.30	6.69 ± 0.93	0.007*
Liver	1.00 ± 0.62	0.75 ± 0.20	0.40	0.18 ± 0.02	0.004**
Lung	0.45 ± 0.18	0.32 ± 0.15	0.21	0.23 ± 0.01	0.01*
Lymph node	0.23 ± 0.09	0.18 ± 0.06	0.27	0.17 ± 0.01	0.04**
Muscle	0.06 ± 0.01	0.04 ± 0.02	0.13	0.05 ± 0.004	0.46
Plasma	0.44 ± 0.07	0.35 ± 0.12	0.14	0.56 ± 0.05	0.009*
Pancreas	0.11 ± 0.04	0.08 ± 0.02	0.17	0.10 ± 0.02	0.99
Spleen	0.51 ± 0.27	0.41 ± 0.14	0.45	0.21 ± 0.05	0.02*
Thymus	0.15 ± 0.05	0.04 ± 0.01	0.002***	0.08 ± 0.06	0.10
White adipose tissue	0.06 ± 0.02	0.03 ± 0.01	0.05**	0.06 ± 0.01	0.071

The results are expressed as standardized uptake values (SUVs; mean ± SD). *A statistically significant difference based on Student's t,test. **A statistically significant difference based on Mann–Whitney U test. ***A statistically significant difference based on Kolmogorov–Smirnov test.

5.5 *Ex Vivo* Biodistribution revealed Higher Tracer accumulation in the hearts of immunized rats compared with control rats

In SP1, *ex vivo* biodistribution of ^{18}F-FOL at 100 minutes was studied and shown in Table 7. Tracer uptake was higher in the hearts of immunized rats compared with control rats (P = 0.01). Tracer accumulation was significantly higher in the lungs, thymus, and white adipose tissue of the immunized rats compared to control rats.

Table 7. *Ex vivo* biodistribution of ^{18}F-FOL in immunized and control rats at 100 min after intravenous injection. From original publication I.

	Immunized rats (n=7)	**Control rats (n=6)**	***P*-value**
Blood	0.07 ± 0.01	0.08 ± 0.04	0.53
Bone marrow	3.9 ± 1.63	2.92 ± 1.16	0.27
Heart	1.15 ± 0.54	0.39 ± 0.07	0.01*
Intestine without content	1.69 ± 0.37	1.35 ± 0.34	0.14
Kidney	36.56 ± 24.08	26.46 ± 24.86	0.51
Liver	1.48 ± 0.72	0.73 ± 0.31	0.053
Lung	0.73 ± 0.16	0.41 ± 0.15	0.01*
Lymph node	4.65 ± 1.06	3.20 ± 1.58	0.10
Muscle	0.36 ± 0.07	0.29 ± 0.08	0.17
Plasma	0.12 ± 0.02	0.16 ± 0.05	0.86
Pancreas	0.83 ± 0.28	0.57 ± 0.09	0.07
Spleen	4.08 ± 2.80	1.86 ± 0.99	0.12
Thymus	2.45 ± 1.35	0.79 ± 0.21	0.02*
Urine	39.68 ± 27.22	46.37 ± 34.69	0.73
White adipose tissue	0.39 ± 0.13	0.23 ± 0.05	0.02*

The results are expressed as SUVs (mean ± SD).

*A statistically significant difference based on Student's t-test

In SP2, *ex vivo* biodistribution of [^{68}Ga]Ga-NODAGA-RGD at 100 min was studied and shown in Table 8. Tracer uptake was higher in the myocardium than in blood in both immunized and control rats ($P < 0.01$). Compared with control rats, tracer accumulation was higher in the hearts and lymph nodes (mediastinal and axillary) in the immunized rats. Notably, in addition to the heart, inflammation was evident in the lymph nodes of immunized rats by histology.

Table 8. *Ex vivo* biodistribution of [^{68}Ga]Ga-NODAGA-RGD in rats at 100 min after intravenous injection. From original publication II.

	Immunized rats (*n* = 7)	**Control rats** (*n* = 8)	***P*-value**
Blood	0.16 ± 0.10	0.14 ± 0.05	0.80
Heart	0.34 ± 0.10	0.21 ± 0.08	0.029*
Intestine without content	1.44 ± 0.32	2.61 ± 1.37	0.07
Kidney	2.24 ± 0.87	3.19 ± 1.59	0.23
Liver	0.62 ± 0.17	1.12 ± 0.69	0.12
Lung	0.64 ± 0.21	0.89 ± 0.47	0.26
Lymph node	0.72 ± 0.19	0.39 ± 0.72	0.05*
Muscle	0.11 ± 0.03	0.15 ± 0.07	0.29
Plasma	0.32 ± 0.16	0.25 ± 0.10	0.41
Pancreas	0.30 ± 0.08	0.58 ± 0.45	0.18
Spleen	0.8 ± 0.30	1.79 ± 1.42	0.14
Thymus	0.43 ± 0.15	0.40 ± 0.20	0.80
Urine	32.98 ± 6.30	34.42 ± 5.73	0.70
White adipose tissue	0.10 ± 0.03	0.09 ± 0.05	0.84

The results are expressed as SUVs (mean ± SD).

*A statistically significant difference based on Student's t-test

In SP3, *ex vivo* biodistribution of [^{68}Ga]Ga-DOTA-Siglec-9 at 70 min was studied and shown in Table 6. The highest radioactivity concentration in autoradiography was observed in the area where histologically there was edema, hemorrhage, and fibroblasts and scattered inflammatory cells. This area was almost devoid of cardiomyocytes. The number of inflammatory cells appeared to be higher in the surrounding myocardial tissue. In the immunized rats, [^{68}Ga]Ga-DOTA-Siglec-9 accumulation was higher in the heart, thymus, and white adipose tissue than in the control rats. Positivity in autoradiography reflects, at least in part, relatively higher radioactivity in blood/plasma compared to myocardium.

6 Discussion

6.1 Diagnostics of autoimmune Myocarditis

Inflammatory myocarditis is characterized by myocardial infiltration with immune cells and myocyte destruction (Cooper et al.,1997; Lagana et al., 2010), but diagnosing autoimmune myocarditis is challenging, and the gold standard for a definitive diagnosis is histologic confirmation of granulomatous inflammation in EMB from the heart, with exclusion of other causes of granulomatous inflammation. However, EMB is an invasive diagnostic approach which often misses these patchy granulomatous infiltrates, with a sensitivity of only 15-30% in previous studies (Uemura et al., 2005; Ardehali et al., 2005; Patel et al., 2009). This has fueled the development of non-invasive techniques using cardiac imaging such as PET (Schatka & Bengel, 2014), however such imaging techniques have limited specificity. Thus studies have focused on identifying specific PET to detect sites of myocardial inflammation. Useful tracers include [^{18}F]FDG, which is sensitive and has good accuracy for detecting myocardial inflammation (Youssef et al., 2012; Okumura et al., 2004; Mc Ardle et al., 2013). However, [^{18}F]FDG is also taken up by normal myocardium, with undesirable impacts on assessment of abnormal uptake and thus its specificity (Chareonthaitawee et al., 2017). Among the useful targets for tracers are TSPO (Kim et al.,2018), ^{11}C-methionine-PET (Maya et al., 2016), ^{68}Ga-NOTA-MSA (Lee et al.,2017), fluorine-19-based CMR (Van Heeswijk et al., 2013), endothelial cell-surface VAP-1 (Salmi et al., 1992; Elo et al., 2018; Siitonen et al., 2017; Virtanen et al., 2015), and the folate receptor β (FR-β) (Silvola et al., 2018), Several studies on FR-β, which is expressed on activated macrophages during inflammation, have been conducted in rat disease models (Silvola et al., 2018; Elo et al., 2019); and FR-targeted imaging has been investigated in human tumors (Parker et al., 2005; Reddy et al., 2004). VAP-1 is associated with many inflammatory conditions (Merinen et al., 2005; Airas et al., 2006; Salmi et al., 2001), with a role in leukocyte migration during acute and chronic inflammation; it binds Siglec 9 and 10, and [^{68}Ga]Ga-DOTA-Siglec-9 has been studied as a PET tracer for imaging inflammation in both animal-disease models and humans (Ahtinen et al., 2014; Silvola et al., 2016). The potential tracer [^{68}Ga]Ga-NODAGA-RGD binds to

cell-surface αvβ3 integrin receptors that are upregulated during angiogenesis and inflammation in myocarditis.

The three studies (SP1, SP2 and SP3) in this series focused on the evaluation of several targets and tracers for PET/CT scanning, using the well-established EAM rat model. For all rat experiments, we conducted scans and tissue sampling after 21 days, the point of peak inflammation in induced myocarditis, as previously shown histologically and via [^{18}F]FDG PET imaging (Werner et al., 2019). For some investigations we also used cardiac tissue samples obtained at autopsy and from explanted heart from patients with sarcoidosis, whereby FR-β-expressing macrophages are present in CS lesions.

6.2 FR- β as a Target of ^{18}F-FOL PET Tracer (SP1)

We demonstrate that ^{18}F-FOL shows specific uptake in inflamed myocardium in rats with autoimmune myocarditis. Both imaging with ^{18}F-FOL PET and *ex vivo* autoradiography demonstrated high target-to-background ratios for inflamed lesions versus non-inflamed myocardial tissue, indicating favorable kinetics for *in vivo* imaging of inflammation and great potential for imaging myocarditis. Previous studies reported high prevalence of macrophages (both M1- and M2- polarized) and CD3-positive lymphocytes as the usual histological findings in EAM rat model (Kodama et al., 1992; Okura et al., 1997). We expand on previous studies by providing evidence that of the 18 rats, 10 demonstrated focal macrophage-rich inflammatory lesions expressing FR-β, mainly in M1-polarized macrophages, and were co-localized with inflammatory lesions. Our result showed that FR-β-positive macrophages are expressed in inflamed human myocardial tissue samples, indicative of specific uptake of ^{18}F-FOL in FR-β-positive macrophages. Uptake of ^{18}F-FOL in the non-inflamed myocardium of immunized rats and controls was low. *Ex vivo* autoradiography of rat tissue sections confirmed the uptake of ^{18}F-FOL in inflamed myocardium. *In vivo* and *in vitro* blocking studies by a non-labeled FR-β ligand, folate glucosamine, resulted in significant lower ^{18}F-FOL uptake in myocardial inflammatory lesions.

Kinetic modeling through graphical Patlak analysis suggests that ^{18}F-FOL uptake in inflamed myocardium is relatively irreversible, aligning with prior research on folate conjugate internalization into endosomes (Bandara et al., 2014). Nonetheless, the Logan plot provided a superior data fit, implying that some ^{18}F-FOL uptake might be reversible due to partial internalization of ^{18}F-FOL, which aligns with a previous study by (Müller et al. 2006), indicating that 25–35% of FR targeting radiotracers

were internalized into human nasopharyngeal carcinoma cells after 4 hours of incubation at 37°C.

Our findings, consistent with earlier studies (Silvola et al., 2018), indicate that ^{18}F-FOL shows specific uptake in FR-β positive macrophages present in atherosclerotic plaques and possesses favorable kinetics for *in vivo* inflammation imaging. We demonstrated that ^{18}F-FOL PET is a promising method for imaging myocarditis, offering a high target-to-background ratio. Although direct comparisons with other tracers are challenging, ^{18}F-FOL autoradiograms showed a comparable contrast between inflamed and non-inflamed myocardium (7.8 ± 1.4) to that observed with [^{18}F]FDG (3.4 ± 0.7) or ^{11}C-methionine (2.1 ± 0.2) in similar models (Maya et al., 2016). These results are promising, as they demonstrate specific ^{18}F-FOL uptake by macrophages expressing FR-β, which are found in inflammatory lesions in both rats with autoimmune myocarditis and humans with sarcoidosis. This suggests the potential for identifying active myocardial inflammation and assessing myocarditis.

6.3 αvβ3 Integrin Receptors as a Target for [^{68}Ga]Ga-NODAGA-RGD Tracer (SP2)

This tracer has value because it binds to cell-surface αvβ3 integrin receptors, which are expressed by macrophages during angiogenesis and inflammation in inflamed lesions (Brooks et al.,1994; Aguilar-Cazares et al., 2019). There is evidence that αvβ3 is a marker of angiogenesis and is involved in the regulation of macrophage responses during inflammation, therefore uptake of this tracer is associated with angiogenesis in inflammatory lesions, similar to that observed after an ischemic myocardial injury (Grönman et al., 2017).

In rats with autoimmune-induced myocarditis, we observed a significantly higher (although modest) uptake in inflamed myocardium, compared to non-inflamed myocardium in control rats. This relatively high contrast in uptake by inflamed and non-inflamed myocardium (6.7 ± 3.0) was similar (even higher) as with other tracers evaluated in the same rat model, such as [^{18}F]FDG (3.4 ± 0.7), or ^{11}C-methionine (2.1 ± 0.2) (Maya et al., 2016).

Analysis by *ex vivo* autoradiography and histology confirmed that the uptake was co-localized with inflammatory lesions containing αvβ3 integrin-positive capillary-like structures, identified by integrin β3 antibodies, further indicating that [^{68}Ga]Ga-NODAGA-RGD uptake is associated with angiogenesis in inflammation, similar to that observed after ischemic myocardial injury (Grönman et al., 2017).

Inflammatory myocardial lesions were detected histologically in 7 out of the 8 induced-disease rats. These results are further evidence that αvβ3 integrin is expressed in the myocardial tissue at the point of peak inflammation (21 days) in EAM rats.

The specificity of tracer binding in inflamed myocardium was high, as revealed by comparison with non-specific tracer ^{68}Ga-DOTA-E[c(RGEfK)]2 (which demonstrated a 76% lower uptake).

We also found increased accumulation of [^{68}Ga]Ga-NODAGA-RGD in the lymph nodes of the rats with induced myocarditis, which was probably due to inflammation, and is consistent with the common finding of mediastinal lymph-node involvement in inflammatory cardiac disease (Birnie et al., 2017). Not only did we provided evidence that αvβ3 integrin is expressed in the myocardial tissue at peak inflammation (21 days) in EAM rats, but we also added evidence to the potential use of [^{68}Ga]Ga-NODAGA-RGD as a tracer for localizing inflammatory lesions by PET imaging *in vivo*, because of its specific uptake by the target tissues suggesting; it may have a role in the non-invasive assessment of inflammatory activity in human myocarditis.

6.4 VAP-1 as Target for [^{68}Ga]Ga-DOTA-Siglec-9 (SP3)

Several non-invasive molecular-imaging approaches have been studied for the detection of autoimmune myocarditis, including ^{11}C-methionine (Maya et al., 2016), mannosylated human serum albumin ^{68}Ga-NOTA-MSA (Lee et al.,2017), 18-kDa TSPO (Kim et al.,2018), and fluorine-19-based CMR (Van Heeswijk et al., 2013). However, none used VAP-1 targeting PET probe.

We evaluated the potential to target VAP-1. We used [^{68}Ga]Ga-DOTA-Siglec-9 as a tracer with PET/CT imaging on day 21 (as in SP2 and SP3), and found that it was increased in myocardial lesions in rats compared to controls without myocarditis. There was greater uptake in myocardial lesions than in myocardium outside the lesions. Subsequent *ex vivo* autoradiography confirmed localization in the myocardial lesions. Compared with uptake of the tracer shown by *in vivo* PET/CT and *ex vivo* autoradiography assessment, [^{68}Ga]Ga-DOTA-control peptide binding showed a 45% and 65% reduction in the target-to-background ratio, respectively. We used non-labeled DOTA-Siglec-9 peptide in a blocking study, and found a 49% lower target-to-background ratio. The use of a negative control peptide and *in vitro* blocking confirmed the specificity of the [^{68}Ga]Ga-DOTA-Siglec-9 uptake. On *ex vivo* autoradiography, a similar contrast was found for the tracer between myocardial lesions and myocardium outside lesions (5.3 ± 1.2) to that

described for other tracers such as [^{18}F]FDG (3.4 ± 0.7), and ^{11}C-methionine (2.1 ± 0.2) in the same model (Maya et al., 2016).

Histology and immunohistochemistry showed that the myocardial lesions stained positive for VAP-1. Using immunofluorescence staining, we found that VAP-1 is expressed on vascular endothelial cells in myocardial lesions with dense macrophage infiltration; CD31 staining revealed a capillary network in the myocardial lesions. Uptake in the myocardial lesions showed modest lesion-to-background ratios.

Myocardial samples from three patients with CS also showed positive immunohistochemical staining for VAP-1, co-localized with vascular structures.

We also investigated the biodistribution of [^{68}Ga]Ga-DOTA-Siglec-9 in disease-induced rats, and found greater accumulation in the heart, thymus and white adipose tissue than in controls. The high uptake in thymus and white adipose tissue probably relates to the abundance of CD68-positive cells in these organs. CD68-positive cells and VAP-1 expression were also found by immunohistochemical staining of the spleen and bone marrow of the disease-induced rats.

Although the role of VAP-1 in the pathogenesis of myocarditis and sarcoidosis remains unknown, demonstrating the expression of VAP-1 in rats with autoimmune myocarditis and patients with CS suggests a novel potential approach for detecting myocardial inflammation.

6.5 Limitations of The Studies

There were several limitations to these studies. For example, it was not possible to make direct comparison between the uptake of [^{18}F]FDG and ^{18}F-FOL, [^{68}Ga]Ga-NODAGA-RGD or [^{68}Ga]Ga-DOTA-Siglec- 9 in inflamed myocardium. This was because of the need for consistent suppression of physiological [^{18}F]FDG uptake in myocardium. However, it should be noted that other studies in the same rat model found comparable levels of contrast between non-inflamed and inflamed myocardial tissue using [^{18}F]FDG (3.4 ± 0.7) or, ^{11}C-methionine (2.1 ± 0.2) (Maya et al., 2016).

In SP1, assessing ^{18}F-FOL uptake in response to therapy remains to be evaluated in models with a reproducible disease intensity. Notably, FRβ can mediate internalization of folate-linked therapeutic agents into cells (Siegel et al., 2003; Reddy et al., 2004; Turk et al., 2002). A FR-targeted imaging agent has been tested for inflammation imaging in humans (Kraus et al., 2016; Yi, 2016). However, evaluating ^{18}F-FOL uptake in human sarcoid lesions was not feasible due to the absence of a tracer approved for human use. This highlights the need for a study

using a clinically approved tracer to investigate the potential of imaging FR-β in patients with sarcoidosis and myocarditis.

Another limitation in SP1 was that the change in uptake over time was not investigated which could be used in PET guided therapy in inflammatory conditions.

In SP2, there was a relatively weak uptake in inflamed myocardium compared to the adjacent liver in *in vivo* PET using [^{68}Ga]Ga-NODAGA- RGD tracer. Because of the low resolution of PET images and the diffuse inflammatory lesions, we were unable to compare tracer uptake in inflamed and adjacent non-inflamed myocardium of the induced-disease rats in *in vivo* images (although it was revealed by *ex vivo* autoradiography).

In SP3, we found only a modest target-to-background ratio in the *in vivo* PET images. Although we found that VAP-1 is expressed in EAM rat model and human CS, the contribution of VAP-1 in the pathogenesis of CS and GCM remains to be studied.

6.6 Strengths and Future Directions

Consistent with other study findings (Verweij et al., 2020), our results in SP1 indicate the potential of FR-β as a marker of active inflammation in both rats and humans, but further investigation might clarify its role in the pathogenesis of myocarditis. The different results obtained by Patlak and Logan analysis, relating to the reversibility of ^{18}F-FOL uptake and possibly relating to varying degrees of internalization of ^{18}F-FOL, merit further investigation of kinetic modelling. We demonstrated for the first time that macrophages in pathological samples of human cardiac sarcoid lesions express FR-β. Therefore, FR-β could serve as a potential marker of myocardial inflammation in both the EAM rat model and human autoimmune myocarditis. This suggests that anti-folate therapy may reduce inflammation in myocarditis, as seen in other inflammatory conditions (Garcia et al., 2021; Elo et al., 2021). The therapeutic potential of FR-β in myocarditis can be further explored by initiating anti-folate therapy or placebo in EAM rats, where inflammatory lesions have been confirmed by ^{18}F-FOL PET.

The SP2 study was the first to assess the use of [^{68}Ga]Ga-NODAGA-RGD PET imaging for detecting myocardial inflammation in rat models of autoimmune myocarditis. It provided evidence that αvβ3 integrin is expressed at 21 days post-first immunization, which coincides with the peak of acute inflammation in this model.

We demonstrated the expression of VAP-1 in rats with autoimmune myocarditis and in patients with cardiac sarcoidosis for the first time in SP3. The first in-human

study of [^{68}Ga]Ga-DOTA-Siglec-9, used in SP3, has been performed (Viitanen et al., 2021), but there is still room for clinical imaging studies in patients with myocarditis or CS to evaluate the value of this approach. The uptake of VAP-1-targeted [^{68}Ga]Ga-DOTA-Siglec-9 in humans, along with its potential for evaluating responses to therapy, holds promise for future studies. Additionally, investigating CD68-positive cells in non-cardiac tissues, such as the thymus, white adipose tissue, spleen, and bone marrow, also presents significant research potential. Such studies may clarify whether these tissues are indirectly involved in myocarditis.

7 Summary/Conclusions

This study evaluated three PET tracers for the detection of myocardial inflammation.

In SP1, PET imaging with ^{18}F-FOL specifically detected inflamed myocardium containing macrophages expressing FR-β in EAM rat model, which are also present in human cardiac sarcoid lesions.

In SP2, PET imaging with [^{68}Ga]Ga-NODAGA-RGD specifically detected myocardial inflammatory lesions with increased αvβ3 integrin expression in EAM rat model.

In SP3, PET imaging with [^{68}Ga]Ga-DOTA-Siglec-9 showed higher tracer uptake in myocardial lesions with increased VAP-1 expression in EAM rats as compared to control rats. VAP-1 expression was present in human cardiac sarcoid lesions.

The results of these studies provide evidence that targeted PET imaging of FR-β expression, αvβ3 integrin and VAP-1 expression are potential approaches for the detection of active myocardial inflammation.

Acknowledgements

This research was conducted at the Turku PET Centre, within the Institute of Clinical Medicine, Department of Clinical Physiology and Nuclear Medicine, Turku University Hospital, and the University of Turku, between 2018 and 2024. It was supported by the Finnish Centre of Excellence in Cardiovascular and Metabolic Diseases, funded by the Academy of Finland, University of Turku, Turku University Hospital, and Åbo Akademi University.

I would like to extend my deepest gratitude to Professor Juhani Knuuti, Director of the Turku PET Centre, and Professor Jukka Kemppainen, from the Department of Clinical Physiology and Nuclear Medicine, for providing excellent research facilities. The financial support from the Clinical Research Doctoral Programme, University of Turku Graduate School, and the Finnish Foundation for Cardiovascular Research was invaluable, for which I am profoundly grateful.

I am especially indebted to my supervisors, Professor Antti Saraste and Professor Anne Roivainen. Antti, no words can fully capture my deep appreciation for your guidance, enthusiasm, knowledge, and ambition throughout this journey. Your unwavering support and the freedom you granted me in my research helped me grow as an independent researcher. Anne, your patience, determination, and positive outlook have been a constant source of inspiration. Your expertise in preclinical imaging was a cornerstone of my work, and your creative mindset was an invaluable asset.

I am sincerely grateful to Docent Johanna Magga and Docent Kalle Sipilä for their thorough review of my thesis. Your expert feedback significantly enhanced the quality of my work and broadened my understanding of the field. I also wish to thank Professor Kirsi Timonen for kindly accepting the role of my opponent.

I would also like to thank my Follow-Up Committee members, Professor Juhani Knuuti and Docent Tytti Vuorinen, for their insightful comments and guidance throughout this process. I am thankful for the Directors of the Clinical Research Doctoral Programme, Professor Antti Saraste, the past and present coordinators of the programme, Kristiina Nuutila, Tiia Forsström, and Mikko Tähtö-Pakkanen, and the Chief Academic Officer, Outi Irjala, for their support during my doctoral studies.

This thesis would not have been possible without the collaborative efforts of many esteemed colleagues. I warmly thank Professor Sirpa Jalkanen, Professor Pekka Taimen, Professor Tiina Salminen, Professor Jukka Lehtonen, Docent Mikko Mäyränpää, and Professor Philip Low for their productive collaborations. My heartfelt thanks go to Docent Ville Kytö, Päivi Marjamäki, Noora Rajala, Alix Marion, and Qingshou Chen for their contributions to the success of these projects.

I am also grateful to Mia Ståhle for your expertise in preclinical PET studies and for your friendship during the most challenging moments. A special thank you to my dear friend Jenni Virta—your unwavering support, both in the lab and outside of it, made this journey far more enjoyable. Sauli Uotila is warmly thanked for giving me an introduction to myocarditis studies. The animal studies would not have been possible without the help of Heidi Liljenbäck, and Aake Honkaniemi, whose flexibility and expertise I deeply appreciate. My sincere thanks go to Assistant Professor Xiang-Guo Li, Olli Moisio, Maxwell Miner, and Jesse Ponkamo for their dedication to producing the tracers. Vesa Oikonen's assistance in kinetic modeling was also invaluable, and I wish to thank him for his input.

I also extend my thanks to Erica Nyman, Marja-Riitta Kajaala, and Sari Mäki for their tremendous efforts in histotechnology, as well as to Markus Peurla for his help with microscopy. The support from Emrah Yatkin and the staff at the Central Animal Laboratory, particularly Nina Kulmala and Aila Saari, was essential, and I thank them for their care of the study subjects. Additionally, I am grateful to Timo Kattelus for his skill in formatting the figures in the manuscript. I wish to thank the expert personnel at Turku PET Centre, including the radiochemists, physicists, physicians, radiographers, laboratory technicians, study nurses, IT experts, secretaries, and all other staff members.

To my present and former colleagues in the Roivainen-Saraste group—Helena, Max, Mia, Riikka, Petri, Heidi, Jenni, Olli, Maxwell, Senthil, Andriana, Imran, Erika, Päivi, Prince, Ella, Arman, Achol, Shiva, Mitra, and Erki—I am incredibly grateful for your support. You made the intense days brighter and kept the spirit high. A special thanks to Maria Grönman for being a wonderful coworker and neighbor. Your friendship and determination have been invaluable, and I am so lucky to have you as a lifelong friend.

I am blessed to have had so many incredible friends who helped me balance life and research. To my amazing friends, Dr. Simin Jamaly and Dr. Mehrdad Rakaee, thank you for broadening my perspective, inspiring me, and motivating me to reach my goals. Your influence has profoundly shaped both my academic journey and personal growth. A heartfelt thank you to my dearest friend Atefeh for always being there for me. Your unwavering friendship, constant presence, and willingness to listen and support me have made everything so much easier. I would also like to express my deepest gratitude to Robin, Zamaneh, Vahid, and all the other friends

who have become like family to me over these years. Your steadfast support has been invaluable, turning a new country into a true home.

Lastly, my deepest thanks go to my family. To my parents, Jila and Ali (who, sadly, is no longer with us), your constant support has meant the world to me. To Elena, my sweet daughter, thank you for making me a mommy and filling my days with love, laughter, and wonder. You are my sunshine, and I love you more than words can say. And to Milad, the love of my life—thank you for your unwavering love, support, and encouragement. You are my everything, and I eagerly await our next adventures together.

Turku, November 2024

Arghavan Jahandideh

References

Aalto, K., Autio, A., Kiss, E.A., Elima, K., Nymalm, Y., Veres, T. Z., Marttila-Ichihara, F., Elovaara, H., Saanijoki, T., Crocker, P. R., Maksimow, M., Bligt, E., Salminen, T. A., Salmi, M., Roivainen, A. & Jalkanen, S., 2011. Siglec-9 is a novel leukocyte ligand for vascular adhesion protein-1 and can be used in PET imaging of inflammation and cancer. *Blood*, 118(13), p. 3725-33.

Abeler, V., 1979. Sarcoidosis of the cardiac conducting system. *American Heart Journal*, 97(6), p. 701-7.

Aguilar-Cazares, D., Chavez-Dominguez, R., Carlos-Reyes, A., Lopez-Camarillo, C., Hernadez de la Cruz, O. N. & Lopez-Gonzalez, J. S., 2019. Contribution of Angiogenesis to Inflammation and Cancer. *Frontiers in Oncology*, 9, p. 1399.

Ahtinen, H., Kulkova, J., Lindholm, L., Eerola, E., Hakanen, A. J, Moritz, N., Söderström, M., Saanijoki, T., Jalkanen, S., Roivainen, A. & Aro H. T., 2014. (68)Ga-DOTA-Siglec-9 PET/CT imaging of peri-implant tissue responses and staphylococcal infections. *EJNMMI Research*, 4:45.

Airas, L., Mikkola, J., Vainio, J. M., Elovaara, I. & Smith, D. J., 2006. Elevated serum soluble vascular adhesion protein-1 (VAP-1) in patients with active relapsing remitting multiple sclerosis. *Journal of Neuroimmunology*, 177(1-2), p. 132-5.

Aitken, M., Chan, M. V, Urzua Fresno, C., Farrell, A., Islam, N., McInnes, M. D. F., Iwanochko, M., Balter, M., Moayedi, Y., Thavendiranathan, P., Metser, U., Veit-Haibach, P. & Hanneman, K., 2022. Diagnostic Accuracy of Cardiac MRI versus FDG PET for Cardiac Sarcoidosis: A Systematic Review and Meta-Analysis. *Radiology*, 304(3), p. 566-579.

Aitken, M., Davidson, M., Chan, M. V., Urzua Fresno, C., Vasquez, L. I., Huo, Y. R., McAllister, B. J., Broncano, J., Thavendiranathan, P., McInnes, M. D. F., Iwanochko, M. R., Balter, M., Moayedi, Y., Farrell, A. & Hanneman, K., 2023. Prognostic Value of Cardiac MRI and FDG PET in Cardiac Sarcoidosis: A Systematic Review and Meta-Analysis. *Radiology*, 307(2), p. e222483.

Akashi, H., Kato, T.S., Takayama, H., Naka, Y., Farr, M., Mancini, D. & Schulze, P. C., 2012. Outcome of patients with cardiac sarcoidosis undergoing cardiac transplantation--single-center retrospective analysis. *Journal of Cardiology*, 60(5), p. 407-10.

Allison, A. C. & Eugui, E. M., 2000. Mycophenolate mofetil and its mechanisms of action. *Immunopharmacology*, 47(2-3), p. 85-118.

Allison, A. C., 2005. Mechanisms of action of mycophenolate mofetil. *Lupus*, 14 Suppl 1, p. s2-8.

Ammirati, E., Oliva, F., Belli, O., Bonacina, E., Pedrotti, P., Turazza, F.M., Roghi, A., Paino, R., Martinelli, L. & Frigerio, M., 2016. Giant cell myocarditis successfully treated with antithymocyte globuline and extracorporeal membrane oxygenation for 21 days. *Journal of Cardiovascular Medicine*, 17 Suppl 2, p. e151-e153.

Antoniou, K. M, Tzouvelekis, A., Alexandrakis, M. G., Sfiridaki, K., Tsiligianni, I., Rachiotis, G., Tzanakis, N., Bouros, D., Milic-Emili, J. & Siafakas, N. M., 2006. Different angiogenic activity in pulmonary sarcoidosis and idiopathic pulmonary fibrosis. *Chest*, 130(4), p. 982-8.

Antonov, A. S., Antonova, G. N., Munn, D. H., Mivechi, N., Lucas, R., Catravas, J. D. & Verin, A. D., 2011. αVβ3 integrin regulates macrophage inflammatory responses via PI3 kinase/Akt-dependent NF-κB activation. J*ournal of Cell Physiology*, 226(2), p. 469-76.

Antonov, A. S., Kolodgie, F. D., Munn, D. H. & Gerrity, R. G., 2004. Regulation of macrophage foam cell formation by alphaVbeta3 integrin: potential role in human atherosclerosis. *American Journal of Pathology*, 165, p. 247–58.

Arango Duque, G. & Descoteaux, A., 2014. Macrophage cytokines: involvement in immunity and infectious diseases. *Frontiers in Immunology*, 5, p. 491.

Ardehali, H., Howard, D. L., Hariri, A., Qasim, A., Hare, J. M., Baughman, K. L. & Kasper, E. K., 2005. A positive endomyocardial biopsy result for sarcoid is associated with poor prognosis in patients with initially unexplained cardiomyopathy. *American Heart Journal*, 150(3), p. 459-63.

Ayoub, C., Pena, E., Ohira, H., Dick, A., Leung, E., Nery, P. B., Birnie, D. & Beanlands, R. S., 2015. Advanced imaging of cardiac sarcoidosis. *Current Cardiology Reports*, 17(4), p. 17.

Bandara, N. A., Hansen, M. J. & Low, P. S., 2014. Effect of receptor occupancy on folate receptor internalization. *Molecular Pharmaceutics*, 11, p. 1007-1013.

Barbarinia, G. & Barbaro, G., 2003. Incidence of the involvement of the cardiovascular system in HIV infection. *AIDS*, 1, p. S46-50.

Barton, J. C., & Edwards, C. Q., 2018. Hemochromatosis: Genetics, pathophysiology, diagnosis and treatment. *The Journal of the American Medical Association*. 284(12), p. 1581.

Baughman, R.P. & Lower, E. E., 2004. Leflunomide for chronic sarcoidosis. *Sarcoidosis, Vasculitis and Diffuse Lung Diseases*, 21(1), p. 43-8.

Baughman, R. P., Valeyre, D., Korsten, P., Mathioudakis, A. G., Wuyts, W. A., Wells, A., Rottoli, P., Nunes, H., Lower, E. E., Judson, M. A., Israel-Biet, D., Grutters, J. C., Drent, M., Culver, D. A., Bonella, F., Antoniou, K., Martone, F., Quadder, B., Spitzer, G., Nagavci, B., Tonia, T., Rigau, D. & Ouellette, D.R., 2021. ERS clinical practice guidelines on treatment of sarcoidosis. *European Respiratory Journal*, 58(6), p. 2004079.

Baughman, R. P., Winget, D. B. & Lower, E.E., 2000. Methotrexate is steroid sparing in acute sarcoidosis: results of a double blind, randomized trial. *Sarcoidosis*, *Vasculitis and Diffuse Lung Diseases*, 17(1), p. 60-6.

Belperio, J.A., Keane, M.P., Lynch, J.P., Fishbein, M.C., & Strieter, R.M., 2001. The Role of Interleukin-6 in Pulmonary Fibrosis. *Chest*, 120(1), p. 249-254.

Bengel, F. M., Higuchi, T., Javadi, M. S. & Lautamaki, R., 2009. Cardiac positron emission tomography. *Journal of American College of Cardiology*, 54, p. 1–15.

Benotti, J. R., Grossman, W. & Cohn, P. F., 1980. Clinical profile of restrictive cardiomyopathy. *Circulation*, 61(6), p. 1206-12.

Betensky, B. P., Tschabrunn, C. M., Zado, E. S., Goldberg, L. R., Marchlinski, F. E., Garcia, F. C. & Cooper, J. M., 2012. Long-term follow-up of patients with cardiac sarcoidosis and implantable cardioverter-defibrillators. *Heart Rhythm*, 9(6), p. 884-91.

Birnie, D. H., Kandolin, R., Nery, P.B. & Kupari, M., 2017. Cardiac manifestations of sarcoidosis: diagnosis and management. *European Heart Journal*, 38, p. 2663–2670.

Birnie, D. H., Nery, P. B., Ha, A. C. & Beanlands, R. S., 2016. Cardiac Sarcoidosis. *Journal of the American College of Cardiology*, 68(4), p. 411-21.

Birnie, D. H., Sauer, W. H., Bogun, F., Cooper, J. M., Culver, D. A., Duvernoy, C. S., Judson, M. A., Kron, J., Mehta, D., Cosedis Nielsen, J., Patel, A. R., Ohe, T., Raatikainen, P. & Soejima, K., 2014. HRS expert consensus statement on the diagnosis and management of arrhythmias associated with cardiac sarcoidosis. *Heart Rhythm*, 11(7), p. 1305-23.

Blankstein, R., Osborne, M., Naya, M., Waller, A., Kim, C. K., Murthy, V. L., Kazemian, P., Kwong R. Y., Tokuda, M., Skali, H., Padera, R., Hainer, J., Stevenson, W. G., Dorbala, S., Di Carli, M.F., 2014. Cardiac positron emission tomography enhances prognostic assessments of patients with suspected cardiac sarcoidosis. *Journal of American College of Cardiology*, 63(4),p. 329-36.

Bligt-Linden, E., Pihlavisto, M., Szatmari, I., Otwinowski, Z., Smith, D. J., Lazar, L., Fulop, F. & Salminen, T. A., 2013. Novel Pyridazinone Inhibitors for Vascular Adhesion Protein-1 (VAP-1): Old target – New Inhibition Mode. *Journal of Medical Chemistry*, 56(24), p. 9837-9848.

Błyszczuk, P., 2019. Myocarditis in Humans and in Experimental Animal Models. *Frontiers in Cardiovascular Medicine*, 16(6), p. 64.

Boesen, K., Hansen, B. F., 1981. A case of giant cell myocarditis. *Acta Medica Scandinavica*, 210, p. 521-522.

Bogabathina, H., Olson, P., Rathi, V. K. & Biederman, R. W. W., 2012. Cardiac Sarcoidosis or Giant Cell Myocarditis? On Treatment Improvement of Fulminant Myocarditis as Demonstrated by Cardiovascular Magnetic Resonance Imaging. *Case Reports in Cardiology*, 647041.

Bono P, Salmi M, Smith DJ, Jalkanen S, 1998. Cloning and characterization of mouse vascular adhesion protein-1 reveals a novel molecule with enzymatic activity. *Journal of Immunology*, 160(11), p. 5563-71.

Boughdad, S., Latifyan, S., Fenwick, C., Bouchaab, H., Suffiotti, M., Moslehi, J.J., Salem, J. E., Schaefer, N., Nicod-Lalonde, M., Costes, J., Perreau, M., Michielin, O., Peters, S., Prior, J. O. & Obeid, M., 2021. ^{68}Ga-DOTATOC PET/CT to detect immune checkpoint inhibitor-related myocarditis. *Journal for ImmunoTherapy of Cancer*, 9(10), p. e003594.

Brociek, E., Tymińska, A., Giordani, A. S., Caforio, A. L. P., Wojnicz, R., Grabowski, M. & Ozierański, K., 2023. Myocarditis: Etiology, Pathogenesis, and Their Implications in Clinical Practice. *Biology*, 12(6), p. 874.

Brodbeck, W. G. & Anderson, J. M., 2009. Giant cell formation and function. *Current Opinion in Hematology*, 16(1), p. 53-57.

Brooks, P. C., Montgomery, A. M., Rosenfeld, M., Reisfeld, R. A., Hu, T., Klier, G. & Cheresh, D. A., 1994. Integrin alpha v beta 3 antagonists promote tumor regression by inducing apoptosis of angiogenic blood vessels . *Cell*, 79(7), p. 1157-64.

Buist, M. R., Molthoff, C., Kenemans, P. & Meijer, C. J., 1995. Distribution of OV-TL 3 and MOv18 in normal and malignant ovarian tissue. *Journal of Clinical Pathology*, 48(7), p. 631-6.

Burstow, D.J. , Tajik, A. J., Bailey, K. R., DeRemee, R. A. & Taliercio, C. P., 1989. Two-dimensional echocardiographic findings in systemic sarcoidosis. *American Journal of Cardiology*, 63, p. 478–82.

Cacoub, P., Chapelon-Abric, C., Resche-Rigon, M., Saadoun, D., Desbois, A.C. & Biard, L., 2020. Cardiac sarcoidosis: A long term follow up study. *PLoS One*, 15(9), p. e0238391.

Cai, M., Ren, L., Yin, X., Guo, Z., Li, Y., He, T., Tang, Y., Long, T., Liu, Y., Liu, G., Zhang, X., & Hu, S., 2016. PET monitoring angiogenesis of infarcted myocardium after treatment with vascular endothelial growth factor and bone marrow mesenchymal stem cells. *Amino Acids*, 48(3), p. 811–820.

Camaré, C., Pucelle, M., Nègre-Salvayre, A. & Salvayre, R., 2017. Angiogenesis in the atherosclerotic plaque. *Redox Biology*, 12, p. 18–34.

Campbell, I. G., Jones, T. A., Foulkes, W. D., Trowsdale, J., 1991. Folate-binding protein is a marker for ovarian cancer. *Cancer Research*, 51(19), p. 5329-38.

Cao, Z., Jia, Y., & Zhu, B., 2019. BNP and NT-proBNP as Diagnostic Biomarkers for Cardiac Dysfunction in Both Clinical and Forensic Medicine. *International Journal of Molecular Sciences*, 20(8), p. 1820.

Chapelon-Abric, C., Sene, D., Saadoun, D., Cluzel, P., Vignaux, O., Costedoat-Chalumeau, N., Piette, J. C., Cacoub, P., 2017. Cardiac sarcoidosis: Diagnosis, therapeutic management and prognostic factors. Archives of Cardiovascular Diseases, 110(8-9), p. 456-465.

Chareonthaitawee, P., Beanlands, R. S., Chen, W., Dorbala, S., Miller, E. J., Murthy, V. L., Birnie, D. H., Chen, E. S., Cooper, L. T., Tung, R. H. & White, E. S., 2017. Joint SNMMI-ASNC expert consensus document on the role of ^{18}F-FDG PET/CT in cardiac sarcoid detection and therapy monitoring. *Journal of Nuclear Medicine*, 58, p. 1341–53.

Chen, H., Niu, G., Wu, H. & Chen, X., 2016. Clinical Application of Radiolabeled RGD Peptides for PET Imaging of Integrin αvβ3. *Theranostics*, 6, p. 78–92.

Chung, E. S., Packer, M., Lo, K. H., Fasanmade, A. A, Willerson, J. T., 2003. Anti-TNF Therapy Against Congestive Heart Failure Investigators. Randomized, double-blind, placebo-controlled,

pilot trial of infliximab, a chimeric monoclonal antibody to tumor necrosis factor-alpha, in patients with moderate-to-severe heart failure: results of the anti-TNF Therapy Against Congestive Heart Failure (ATTACH) trial. *Circulation*, 107(25), p. 3133-40.

Cihakova, D. & Rose, N. R., 2008. Pathogenesis of myocarditis and dilated cardiomyopathy. *Advanced Immunology*, 99, p. 95-114.

Cochain, C. & Zernecke, A., 2015. Macrophages and immune cells in atherosclerosis: recent advances and novel concepts. *Basic Research in Cardiology*, 110, p. 34.

Colin, S., Chinetti-Gbaguidi, G. & Staels, B., 2014. Macrophage phenotypes in atherosclerosis. *Immunological Reviews*, 262, p. 153–166.

Collyns, J. A. H., 1959. Isolated granulomatous myocarditis. *American Heart Journal*, 58, p. 630-636.

Cooper, L. T., Berry, G. J & Shabetai, R., 1997. Idiopathic giant-cell myocarditis--natural history and treatment. Multicenter Giant Cell Myocarditis Study Group Investigators. *New England Journal of Medicine*, 336(26),p. 1860-6.

Cooper, L. T., Hare, J. M, Tazelaar, H. D., Edwards, W. D., Starling, R. C., Deng, M. C., Menon, S., Mullen, G. M., Jaski, B., Bailey, K. R., Cunningham, M. W. & Dec, G. W., 2008. Giant Cell Myocarditis Treatment Trial Investigators. Usefulness of immunosuppression for giant cell myocarditis. *American Journal of Cardiology*, 102(11), p. 1535-9.

Cooper, L. T., 2007. Giant Cell Myocarditis in Children. *Progress in Pediatric Cardiology*, 24, p. 47–9.

Crown Human Genome Center, Department of Molecular Genetics, and The Weizmann Institute of Science., 2013. FOLR4 expression in normal human tissues (normalized intensities). *Genecard.com. Genecard.org*.

Crown Human Genome Center, Department of Molecular Genetics, and The Weizmann Institute of Science., 2012. RTBDN expression in normal human tissues. *Genecard.com. Genecard.org*.

Crum-Cianflone, N. F., 2008. Bacterial, fungal, parasitic, and viral myositis. *Clinical Microbiology Reviews*, 21(3), p. 473-94.

Darlington, P., Gabrielsen, A., Sörensson, P., Cederlund, K., Eklund, A. & Grunewald, J., 2014. Cardiac involvement in Caucasian patients with pulmonary sarcoidosis. *Respiratory Research*, 15(1), p. 15.

Davies, M. J., Pomerance, A. & Teare, R. D., 1975. Idiopathic giant cell myocarditis: A distinctive clinico-pathological entity. *British Heart Journal*, 37, p. 192-195.

DeFilippis, E. M, Narain, S., Sobol, I., Narula, N., Bass, A. & Erkan, D., 2015. Rapidly Progressive Cardiac Failure Due to Giant Cell Myocarditis. *Musculoskeletal Journal of Hospital for Special Surgery*, 11(2), p. 182–186.

Demeter, S. L., 1988. Myocardial sarcoidosis unresponsive to steroids. Treatment with cyclophosphamide. *Chest,* 94(1), p. 202-3.

Dhôte, R., Vignaux, O., Blanche, P., Duboc, D., Dusser, D., Brezin, A., Devaux, J. Y., Christoforov, B. & Legmann, P., 2003. Apport de l'IRM dans l'exploration de l'atteinte cardiaque au cours de la sarcoïdose [Value of MRI for the diagnosis of cardiac involvement in sarcoidosis]. *Revue de Médecine Interne*, 24(3), p. 151-7.

Dieplinger, B., & Januzzi, J.L., 2015. Soluble ST2 as a Biomarker for Heart Failure and Other Cardiovascular Diseases: The Evolving State of the Art. *Clinica Chimica Acta*, 443, p. 48-56.

Doughan, A. R. & Williams, B. R., 2006. Cardiac sarcoidosis. *Heart*, 92, p. 282–8.

Ekstrom, K., Lehtonen, J., Kandolin, R., Raisanen-Sokolowski, A., Salmenkivi, K. & Kupari, M., 2016. Incidence, risk factors, and outcome of life-threatening ventricular arrhythmias in giant cell myocarditis. *Circulation: Arrhythmia and Electrophysiology*, 9, e004559.

Ekström, K., Lehtonen, J., Kandolin, R., Räisänen-Sokolowski, A., Salmenkivi, K. & Kupari, M., 2016. Long-term outcome and its predictors in giant cell myocarditis. *European Journal of Heart Failure*, 18(12), p. 1452-1458.

Ekström, K., Lehtonen, J., Nordenswan, H. K., Mäyränpää, M. I., Räisänen-Sokolowski, A., Kandolin, R., Simonen, P., Pietilä-Effati, P., Alatalo, A., Utriainen, S., Rissanen, T. T, Haataja, P., Kokkonen,

J., Vihinen, T., Miettinen, H., Kaikkonen, K., Kerola, T. & Kupari, M., 2019. Sudden death in cardiac sarcoidosis: an analysis of nationwide clinical and cause-of-death registries. *European Heart Journal*, 40, p. 3121–8.

Ekström, K., Räisänen-Sokolowski, A., Lehtonen, J., Nordenswan, H. K., Mäyränpää, M. I. & Kupari, M., 2020. Idiopathic giant cell myocarditis or cardiac sarcoidosis? A retrospective audit of a nationwide case series. *ESC Heart* Failure, 7(3), p. 1362-1370.

Elezkurtaj, S., Lassner, D., Schultheiss, H. P. & Escher, F., 2013. Vascular involvement in cardiac giant cell myocarditis: a new pathophysiological aspect. *Clinical Research of Cardiology*, 103, p. 161–3.

Elo, P., Li, X. G., Liljenbäck, H., Gardberg, M., Moisio, O., Miner, M., Virta, J., Saraste, A., Srinivasarao, M., Pugh, M., Low, P. S., Knuuti, J., Jalkanen, S., Airas, L., Lu, Y. J. & Roivainen, A., 2021. Efficacy and tolerability of folate-aminopterin therapy in a rat focal model of multiple sclerosis. *Journal of Neuroinflammation*, 18(1), p. 30.

Elo, P., Li, X. G., Liljenbäck, H., Helin, S., Teuho, J., Koskensalo, K., Saunavaara, V., Marjamäki, P., Oikonen, V., Virta, J., Chen, Q., Low, P. S., Knuuti, J., Jalkanen, S., Airas, L. & Roivainen, A., 2019. Folate receptor-targeted positron emission tomography of experimental autoimmune encephalomyelitis in rats. *Journal of Neuroinflammation*, 16, p. 252.

Elo, P., Tadayon, S., Liljenbäck, H., Teuho, J., Käkelä, M., Koskensalo, K., Saunavaara, V., Virta, J., Veres, T. Z., Kiviniemi, A., Saraste, A., Marjamäki, P., Airas, L., Jalkanen, S. & Roivainen, A., 2018. Vascular adhesion protein-1 is actively involved in the development of inflammatory lesions in rat models of multiple sclerosis. *Journal of Neuroinflammation*, 15(1), p. 128.

Elshabrawy, H. A., Chen, Z., Volin, M. V., Ravella, S., Virupannavar, S. & Shahrara, S., 2015. The pathogenic role of angiogenesis in rheumatoid arthritis. *Angiogenesis*, 18, p. 433–48.

Eo, J. S. & Jeong, J. M., 2016. Angiogenesis Imaging Using (68)Ga-RGD PET/CT: Therapeutic Implications. *Seminars in Nuclear Medicine*. 46(5), p. 419-27.

DeFilippis, E. M., Narain, S., Sobol, I., Narula, N., Bass, A. & Erkan, D., 2015. Rapidly Progressive Cardiac Failure Due to Giant Cell Myocarditis: A Clinical Pathology Conference Held by the Division of Rheumatology at Hospital for Special Surgery. *HSS Journal*, 11(2), p. 182-6.

Fairweather, D., Coronado, M. J., Garton, A. E., Dziedzic, J. L., Bucek, A., Cooper, L. T, Brandt, J. E., Alikhan, F. S., Wang, H., Endres, C. J., Choi, J., Pomper, M. G. & Guilarte, T. R. , 2014. Sex differences in translocator protein 18 kDa (TSPO) in the heart: implications for imaging myocardial inflammation. *Journal of Cardiovascular Translational Research*, 7(2), p. 192-202.

Fairweather, D., & Rose, N. R., 2007. Coxsackievirus-induced myocarditis in mice: A model of autoimmune disease for studying immunotoxicity. *Methods*, 41(1), p. 118-122.

Fazelpour, S., Sadek, M. M., Nery, P. B., Beanlands, R. S., Tzemos, N., Toma, M. & Birnie, D. H., 2021. Corticosteroid and Immunosuppressant Therapy for Cardiac Sarcoidosis: A Systematic Review. *Journal of the American Heart Association*, 10(17), e021183.

Fernández. M., Javaid, F. & Chudasama, V., 2017. Advances in targeting the folate receptor in the treatment/imaging of cancers. *Chemical Science*, 9(4), p. 790-810.

Finke, D., Heckmann, M. B., Herpel, E., Katus, H. A., Haberkorn, U., Leuschner, F. & Lehmann, L. H., 2021. Early Detection of Checkpoint Inhibitor-Associated Myocarditis Using ^{68}Ga-FAPI PET/CT. *Frontiers of Cardiovascular Medicine*, 8, 614997.

Fleming, H. A. & Bailey, S. M., 1986. The prognosis of sarcoid heart disease in the United Kingdom. *Annals of the New York Academy of Sciences,* 465,p. 543–50.

Fox, R. I., Herrmann, M. L., Frangou, C. G., Wahl, G. M., Morris, R. E., Strand, V. & Kirschbaum, B. J., 1999. Mechanism of action for leflunomide in rheumatoid arthritis. *Clinical Immunology*, 93(3), p. 198-208.

Friedrich, M. G, Sechtem, U., Schulz-Menger. J., Holmvang, G., Alakija, P., Cooper, L. T., White, J. A., Abdel-Aty, H., Gutberlet, M., Prasad, S., Aletras, A., Laissy, J. P., Paterson, I., Filipchuk, N. G., Kumar, A., Pauschinger, M. & Liu, P., 2009. International Consensus Group on Cardiovascular

Magnetic Resonance in Myocarditis. Cardiovascular magnetic resonance in myocarditis: A JACC White Paper. *Journal of American College of Cardiology*, 53(17), p. 1475-87.

Furusho, Y., Miyata, M., Matsuyama, T., Nagai, T., Li, H., Akasaki, Y., Hamada, N., Miyauchi, T., Ikeda, Y., Shirasawa, T., Ide, K. & Tei, C., 2012. Novel therapy for atherosclerosis using recombinant immunotoxin against folate receptor betaexpressing macrophages. *Journal of American Heart Association,* 1, e003079.

Fuse, K., Kodama, M., Ito, M., Okura, Y., Kato, K., Hanawa, H., Aoki, S. & Aizawa, Y., 2003. Polarity of helper T cell subsets represents disease nature and clinical course of experimental autoimmune myocarditis in rats. *Clinical and Experimental Immunology*, 134(3), p. 403-8.

Gadela, N. V., Krishnan, A. M., Mukarram, O. & Sthalekar, N., 2021. Giant cell myocarditis. *Proceedings (Baylor University Medical Center)*, 34(3), p. 401-402.

Gao, H., Lang, L., Guo, N., Cao, F., Quan, Q., Hu, S., Kiesewetter, D. O., Niu, G., & Chen, X., 2012. PET imaging of angiogenesis after myocardial infarction/reperfusion using a one-step labeled integrin-targeted tracer ^{18}F-AlF-NOTA-PRGD2. *European Journal of Nuclear Medicine and Molecular Imaging*, 39(4), p. 683–692.

Garcia, G. E., Lu, Y. J., Truong, L. D., Roncal-Jiménez, C. A., Miyazaki, M., Miyazaki-Anzai S, Cara-Fuente,s G., Andres-Hernando, A., Lanaspa, M., Johnson, R. J., Leamon, C. P., 2021. A Novel Treatment for Glomerular Disease: Targeting the Activated Macrophage Folate Receptor with a Trojan Horse Therapy in Rats. *Cells*, 10(8), 2113.

Garin-Chesa, P., Campbell, I., Saigo, P. E., Lewis, J. L, Old, L. J. & Rettig, W. J., 1993. Trophoblast and ovarian cancer antigen LK26. Sensitivity and specificity in immunopathology and molecular identification as a folate-binding protein. *American Journal of Pathology*, 142(2), p. 557-67.

Gerke, A. K., 2020. Treatment of Sarcoidosis: A Multidisciplinary Approach. *Frontiers in Immunology*, 11, 545413.

Ginhoux, F. & Jung, S., 2014. Monocytes and macrophages: developmental pathways and tissue homeostasis. *Nature Reviews Immunology*, 14, p. 392–404.

Griffin, J. M., Chasler, J., Wand, A. L., Okada, D. R., Smith, J. N., Saad, E., Tandri, H., Chrispin, J., Sharp, M., Kasper, E. K., Chen, E. S. & Gilotra, N. A., 2021. Management of Cardiac Sarcoidosis Using Mycophenolate Mofetil as a Steroid-Sparing Agent. *Journal of Cardiac Failure*, 27(12), p. 1348-1358.

Grönman, M., Tarkia, M., Kiviniemi, T., Halonen, P., Kuivanen, A., Savunen, T., Tolvanen, T., Teuho, J., Käkelä, M., Metsälä, O., Pietilä, M., Saukko, P., Ylä-Herttuala, S., Knuuti, J., Roivainen, A. & Saraste, A., 2017. Imaging of αvβ3 integrin expression in experimental myocardial ischemia with [^{68}Ga]NODAGA-RGD positron emission tomography. *Journal of Translational Medicine*, 15(1), 144.

Guérard, S. & Pouliot, R., 2012. The role of angiogenesis in the pathogenesis of psoriasis: mechanisms and clinical implications. *Journal of Clinical Experimental Dermatology Research*, S2, 007.

Gutierrez, F. R., Sesti-Costa, R., Silva, G. K., Trujillo, M. L., Guedes, P. M., Silva, J. S., 2014. Regulation of the immune response during infectious myocarditis. *Expert Review of Cardiovascular Therapy,* 12(2), p. 187-200.

Hales, S.A., Theaker, J. M. & Gatter, K. C., 1987. Giant cell myocarditis associated with lymphoma: An immunocytochemical study (1987). *Journal of Clinical Pathology*, 40, p. 1310-1313.

Hanawa, H., Kodama, M., Inomata, T., Izumi, T., Shibata, A., Tuchida, M., Matsumoto, Y. & Abo, T., 1994. Anti-alpha beta T cell receptor antibody prevents the progression of experimental autoimmune myocarditis. *Clinical and Experimental Immunology*, 96(3), p. 470-5.

Harper, L.J., McCarthy, M., Ribeiro Neto, M. L., Hachamovitch, R., Pearson, K., Bonanno, B., Shaia, J., Brunken, R., Joyce, E. & Culver, D. A., 2019. Infliximab for Refractory Cardiac Sarcoidosis. *American Journal of Cardiology*,124(10), p. 1630-1635.

Havakuk, O., Rezkalla, S. H. & Kloner, R. A., 2017. The Cardiovascular Effects of Cocaine. Journal of the American College of Cardiology, 70(1), p. 101-113.

Herrmann, M.L., Schleyerbach, R. & Kirschbaum, B.J., 2000. Leflunomide: an immunomodulatory drug for the treatment of rheumatoid arthritis and other autoimmune diseases (2000). *Immunopharmacology*, 47(2-3), p. 273-89.

Higuchi, T., Bengel, F. M., Seidl, S., Watzlowik, P., Kessler, H., Hegenloh, R., Reder, S., Nekolla, S.G., Wester, H. J., & Schwaiger, M., 2008. Assessment of alphavbeta3 integrin expression after myocardial infarction by positron emission tomography. *Cardiovascular Research*, 78(2), p. 395–403.

Hiraga, H., Yuwai, K., Hiroe, M., 1993. Guideline for Diagnosis of Cardiac Sarcoidosis: Study Report on Diffuse Pulmonary Diseases From the Japanese Ministry of Health and Welfare. *Tokyo: Japanese Ministry of Health and Welfare*, p. 23–24.

Hoffbrand, A. V. & Weir, D. G., 2001. The history of folic acid. *British Journal of Haematology*, 113(3), p. 579-89.

Hu, Y., Wang, B., Shen, J., Low, S. A., Putt, K. S., Niessen, H. W. M., Matteson, E. L., Murphy, L., Ruppert, C., Jansen, G., Oliver, S. J., Feng, Y., Dimitrov, D. S., Nickerson-Nutter, C. & Low, P. S., 2019. Depletion of activated macrophages with a folate receptor-beta-specific antibody improves symptoms in mouse models of rheumatoid arthritis. *Arthritis Research and Therapy*, 21(1), p. 143.

Hunninghake, G. W. & Crystal, R. G., 1981. Pulmonary sarcoidosis: a disorder mediated by excess helper T-lymphocyte activity at sites of disease activity. *New England Journal of Medicine*, 305(8), p. 429-34.

Iannuzzi, M. C., Rybicki, B. A. & Teirstein, A. S. , 2007. Sarcoidosis. *New England Journal of Medicine*, 357, p. 2153–65.

Italiani, P. & Boraschi, D., 2015. New Insights Into Tissue Macrophages: From their origin to the development of memory. *Immune Network*, 15, p. 167-176.

Iwai, K., Sekiguti, M., Hosoda, Y., DeRemee, R. A., Tazelaar, H., D., Sharma, O. P., Maheshwari, A. & Noguchi, T. I., 1994. Racial difference in cardiac sarcoidosis incidence observed at autopsy. *Sarcoidosis*, 11(1), p. 26-31.

Jaakkola, K., Nikula, T., Holopainen, R., Vähäsilta, T., Matikainen, M. T., Laukkanen, M. L., Huupponen, R., Halkola, L., Nieminen, L., Hiltunen, J., Parviainen, S., Clark, M. R., Knuuti, J., Savunen, T., Kääpä, P., Voipio-Pulkki, L. M. & Jalkanen, S., 2000. In vivo detection of vascular adhesion protein-1 in experimental inflammation. *American Journal of Pathology*, 157, p. 463–71.

Jamar, F., Buscombe, J., Chiti, A., Christian, P.E., Delbeke, D., Donohoe, K. J., Israel, O., Martin-Comin, J. & Signore, A., 2013. EANM/SNMMI guideline for ^{18}F-FDG use in inflammation and infection. *Journal of Nuclear Medicine*. 54(4), p. 647-58.

Jefic, D., Joel, B., Good, E., Morady, F., Rosman, H., Knight, B. & Bogun, F., 2009. Role of radiofrequency catheter ablation of ventricular tachycardia in cardiac sarcoidosis: report from a multicenter registry. *Heart Rhythm*, 6(2),p. 189-95.

Jeserich, M., Konstantinides, S., Pavlik, G., Bode, C. & Geibel, A., 2009. Non-invasive imaging in the diagnosis of acute viral myocarditis. *Clinical Research of Cardiology*, 98(12), p. 753-63.

Kadkhodayan, A., Chareonthaitawee, P., Raman, S. V., Cooper, L. T., 2016. Imaging of inflammation in unexplained cardiomyopathy. *Journal of the American College of Cardiology Cardiovasc Imaging*, 9, p. 603-617.

Kamen, B. A., Wang, M. T., Streckfuss, A. J., Peryea, X., Anderson, R. G., 1988. Delivery of folates to the cytoplasm of MA104 cells is mediated by a surface membrane receptor that recycles. *Journal of Biological Chemistry,* 263(27), 13602-9.

Kandolin, R., Lehtonen, J., Airaksinen, J., Vihinen, T., Miettinen, H., Ylitalo, K., Kaikkonen, K., Tuohinen, S., Haataja, P., Kerola, T., Kokkonen, J., Pelkonen, M., Pietilä-Effati, P., Utrianen, S., Kupari, M., 2015. Cardiac sarcoidosis: epidemiology, characteristics, and outcome over 25 years in a nationwide study. *Circulation*, 131, p. 624-32.

Kandolin, R., Lehtonen, J., Salmenkivi, K., Räisänen-Sokolowski, A., Lommi , J. & Kupari, M., 2013. Diagnosis, treatment, and outcome of giant-cell myocarditis in the era of combined immunosuppression. *Circulation: Heart Failure*, 6(1), p. 15–22.

Kaplan, M. H., 1958. Immunologic studies of heart tissue. I. Production in rabbits of antibodies reactive with an autologous myocardial antigen following immunization with heterologous heart tissue. *Journal of Immunology*, 80, p. 254-67.

Kapp, T. G., Rechenmacher, F., Neubauer, S., Maltsev, O. V., Cavalcanti-Adam, E. A., Zarka, R., Reuning, U., Notni, J., Wester, H. J., Mas-Moruno, C., Spatz, J., Geiger, B., & Kessler, H., 2017. A comprehensive evaluation of the activity and selectivity profile of ligands for RGD-binding integrins. *Scientific Reports*, 7, p. 1–13.

Karjalainen, J. & Heikkilä, J., 1999. Incidence of three presentations of acute myocarditis in young men in military service. A 20-year experience. *European Heart Journal*, 20(15), p. 1120-5.

Keramari, S., Poutoglidis, A., Chatzis, S., Keramaris, M., Savopoulos, C., Kaiafa, G., 2022. Parvovirus B19-Associated Myocarditis: A Literature Review of Pediatric Cases. *Cureus*, 14(1), e21726.

Kilgallen, C. M., Jackson, E., Bankoff, M., Salomon, R. N. & Surks, H. K., 1998. A case of giant cell myocarditis and malignant thymoma: a postmortem diagnosis by needle biopsy. *Clinical Cardiology*, 21(1), p. 48-51.

Kim, G.R., Paeng, J. C., Jung, J. H., Moon, B. S., Lopalco, A., Denora, N., Lee, B. C., Kim, S. E., 2018. Assessment of TSPO in a Rat Experimental Autoimmune Myocarditis Model: A Comparison Study between [^{18}F]Fluoromethyl-PBR28 and [^{18}F]CB251. I*nternational Journal of Molecular Sciences*, 19(1), p. 276.

Kim, J. S., Judson, M. A., Donnino, R., Gold, M., Cooper, L. T., Prystowsky, E. N. & Prystowsky, S,.2009. Cardiac sarcoidosis. *American Heart Journal*, 157(1), p. 9-21.

Kim SJ, Pak K, Kim K, 2020. Diagnostic performance of F-18 FDG PET for detection of cardiac sarcoidosis; A systematic review and meta-analysis. Journal of Nuclear Cardiology. 27(6), p. 2103-2115.

Kircher, M. & Lapa, C., 2020. Infection and Inflammation Imaging: Beyond FDG. *PET Clinics*,15(2), p. 215-229.

Kishimoto, C., & Sasayama, S., 2003. The T cell receptor transgenic mouse model of myocarditis. *Trends in Cardiovascular Medicine*, 13(1), p. 19-24.

Kittleson, M. M., Minhas, K. M., Irizarry, R. A., Ye, S. Q., Edness, G., Breton, E., Conte, J. V., Tomaselli, G., Garcia, J. G. & Hare, J. M., 2005. Gene expression in giant cell myocarditis: Altered expression of immune response genes. *International Journal of Cardiology*, 102(2), p. 333-40.

Kiugel, M., Dijkgraaf, I., Kytö, V., Helin, S., Liljenbäck, H., Saanijoki, T., Yim, C. B., Oikonen, V., Saukko, P., Knuuti, J., Roivainen, A. & Saraste, A., 2014. Dimeric [(^{68})Ga]DOTA-RGD peptide targeting αvβ 3 integrin reveals extracellular matrix alterations after myocardial infarction. *Molecular Imaging and Biology*, 16(6), p. 793-801.

Kivi, E., Elima, K., Aalto, K., Nymalm, Y., Auvinen, K., Koivunen, E., Otto, D. M., Crocker, P. R., Salminen, T. A., Salmi, M. & Jalkanen, S., 2009. Human Siglec-10 can bind to vascular adhesion protein-1 and serves as its substrate. *Blood*, 114(26), p. 5385-92.

Klein, I., & Danzi, S., 2007. Thyroid disease and the heart. *Circulation*, 116(15), p. 1725-1735.

Kodama, M., Matsumo, Y., Fujiwara, M., Masani, F., Izumi, T. & Shibata, A., 1990. A novel experimental model of giant cell myocarditis induced in rats by immunization with cardiac myosin fraction. *Clinical Immunology and Immunopathology*, 57(2), p. 250–262.

Kodama, M., Matsumoto, Y., Fujiwara, M., Zhang, S. S., Hanawa, H., Itoh, E., Tsuda, T., Izumi, T. & Shibata, A., 1991. Characteristics of giant cells and factors related to the formation of giant cells in myocarditis. *Circulation Research*, 69(4), p. 1042-50.

Kodama, M., Zhang, S., Hanawa, H. & Shibata, A., 1992. Immunohistochemical characterization of infiltrating mononuclear cells in the rat heart with experimental autoimmune giant cell myocarditis. Clinical and Experimental Immunology, 90, p. 330-335.

Koplan, B. A., Soejima, K., Baughman, K., Epstein, L. M. & Stevenson, W. G., 2006. Refractory ventricular tachycardia secondary to cardiac sarcoid: electrophysiologic characteristics, mapping, and ablation. *Heart Rhythm*, 3(8), p. 924-9.

Kotanidis, C. P., Bazmpani, M. A., Haidich, A. B., Karvounis, C., Antoniades, C. & Karamitsos, T. D., 2018. Diagnostic accuracy of cardiovascular magnetic resonance in acute myocarditis: a systematic review and meta-analysis. *Journal of American College of Cardiology Imging*, 11, p. 1583–90.

Kotyla, P. J., 2018. Bimodal Function of Anti-TNF Treatment: Shall We Be Concerned about Anti-TNF Treatment in Patients with Rheumatoid Arthritis and Heart Failure?. *International Journal of Molecular Sciences*, 19(6), p. 1739.

Kraus, V. B., McDaniel, G., Huebner, J. L., Stabler, T. V., Pieper, C. F., Shipes, S. W., Petry, N. A., Low, P. S., Shen, J., McNearney, T. A. & Mitchell, P., 2016. Direct in vivo evidence of activated macrophages in human osteoarthritis. *Osteoarthritis Cartilage*, 24, p. 1613-1621.

Kron, J., Sauer, W., Schuller, J., Bogun, F., Crawford, T., Sarsam, S., Rosenfeld, L., Mitiku, T. Y., Cooper, J. M., Mehta, D., Greenspon, A. J., Ortman, M., Delurgio, D. B., Valadri, R., Narasimhan, C., Swapna, N., Singh, J. P., Danik, S., Markowitz, S. M., Almquist, A. K., Krahn, A. D., Wolfe, L. G., Feinstein, S. & Ellenbogen, K. A., 2013. Efficacy and safety of implantable cardiac defibrillators for treatment of ventricular arrhythmias in patients with cardiac sarcoidosis. *Europace*, 15(3), p. 347-54.

Kurkijärvi, R., Adams, D. H., Leino, R., Möttönen, T., Jalkanen, S. & Salmi, M., 1998. Circulating form of human vascular adhesion protein-1 (VAP-1): increased serum levels in inflammatory liver diseases. *Journal of Immunology*, 161(3), p. 1549-57.

Kurkijärvi, R., Yegutkin, G.G., Gunson, B. K., Jalkanen, S., Salmi, M. & Adams, D. H., 2000. Circulating soluble vascular adhesion protein 1 accounts for the increased serum monoamine oxidase activity in chronic liver disease. *Gastroenterology*, 119(4), p. 1096-103.

Kytö, V., Saukko, P., Lignitz, E., Schwesinger, G., Henn, V., Saraste, A. & Voipio-Pulkki, L. M., 2005. Diagnosis and presentation of fatal myocarditis. *Human Pathology*, 36(9), 1003-7.

Lagan, J., Schmitt, M. & Miller, C. A., 2018. Clinical applications of multi-parametric CMR in myocarditis and systemic inflammatory diseases. *International Journsl of Cardiovascular Imaging*, 34, p. 35–54.

Lagana, S. M., Parwani, A. V. & Nichols, L. C., 2010. Cardiac sarcoidosis: a pathology-focused review. *Archives of Pathology and Laboratory Medicine*, 134(7), p. 1039-46.

Laitinen, I., Notni, J., Pohle, K., Rudelius, M., Farrell, E., Nekolla, S. G., Henriksen, G., Neubauer, S., Kessler, H., Wester, H.-J., & Schwaiger, M. Comparison of cyclic RGD peptides for αvβ3 integrin detection in a rat model of myocardial infarction (2013). *EJNMMI Research*, 3(1), p. 38.

Lamacie MM, Almufleh A, Nair V, Stadnick E, Birnie D, Beanlands RSB, Chih S, 2020. Serial ^{18}F-Fluorodeoxyglucose Positron Emission Tomography Imaging in a Patient With Giant Cell Myocarditis. *Circulation: Cardiovascular Imaging*. 13(2), p. e009940.

Lay, G., Poquet, Y., Salek-Peyron, P., Puissegur, M. P., Botanch, C., Bon, H., Levillain, F., Duteyrat, J. L., Emile, J. F. & Altare, F., 2007. Langhans giant cells from M tuberculosisinduced human granulomas cannot mediate mycobacterial uptake. *Journal of Pathology*, 211, p. 76–85.

Lee, S. P., Im, H. J., Kang, S., Chung, S. J., Cho, Y. S., Kang, H., Park, H. S., Hwang, D. W., Park, J. B., Paeng, J. C., Cheon, G. J., Lee, Y. S., Jeong, J. M. & Kim, Y. J., 2017. Noninvasive Imaging of Myocardial Inflammation in Myocarditis using ^{68}Ga-tagged Mannosylated Human Serum Albumin Positron Emission Tomography. *Theranostics*, 7(2), p. 413-424.

Leong, T., Wong, J., Rice, A., Zidan, M., Hamilton, A., Ariff, B., Chester, R., Rahman Haley, S. L., Kelion, A., Burke, M. M., Mitchell, A. G., Banner, N. & Mittal, T. K., 2012. Giant cell myocarditis in the CMR era. *Journal of Cardiovascular Magnetic Resonans*, 14(Suppl 1), M2.

Litovsky, S. H., Burke, A. P. & Virmani, R., 1996. Giant cell myocarditis: an entity distinct from sarcoidosis characterized by multiphasic myocyte destruction by cytotoxic T cells and histiocytic giant cells. *Modern Pathology*, 9, p. 1126–34.

Lok, S.I., Van der Meer, P., de la Porte, P.W.B.A., Lipsic, E., Van Wijngaarden, J., Hillege, H.L., Van Veldhuisen, D.J., & Voors, A.A., 2013. Prognostic value of galectin-3, a novel marker of fibrosis, in patients with chronic heart failure: data from the DEAL-HF study. *Clinical Research in Cardiology*, 102, p. 323-331.

Lonsdale, D., 2006. A review of the biochemistry, metabolism and clinical benefits of thiamin(e) and its derivatives. *Evidence-Based Complementary and Alternative Medicine*, 3(1), p. 49-59.

Lopes de Carvalho, L., Elovaara, H., de Ruyck, J., Vergoten, G., Jalkanen, S., Guedez, G. & Salminen, T. A., 2018. Mapping the interaction site and effect of the Siglec-9 inflammatory biomarker on human primary amine oxidase. *Scientific Reports*, 8, 2086.

Lower, E. E. & Baughman, R. P., 1990. The use of low dose methotrexate in refractory sarcoidosis. *American Journal of the Medical Sciences*, 299(3), p. 153-7.

Lu, Y. J., Wheeler, L. W., Chu, H., Kleindl, P. J., Pugh, M., You, F., Rao, S., Garcia, G., Wu, H. Y., da Cunha, A. P., Johnson, R., Westrick, E., Cross, V., Lloyd, A., Dircksen, C., Klein, P. J., Vlahov, I. R., Low, P. S. & Leamon, C. P., 2021. Targeting folate receptor beta on monocytes/macrophages renders rapid inflammation resolution independent of root causes. *Cell Reports Medicine*, 2(10), p. 100422.

Magnani, J. W. & Dec, G. W., 2006. Myocarditis: current trends in diagnosis and treatment. Circulation, 113(6), p. 876-90.

Mahrholdt, H., Wagner, A., Deluigi, C. C., Kispert, E., Hager, S., Meinhardt, G., Vogelsberg, H., Fritz, P., Dippon, J., Bock, C. T., Klingel, K., Kandolf, R. & Sechtem, U., 2006. Presentation, patterns of myocardial damage, and clinical course of viral myocarditis. *Circulation*, 114(15), p. 1581-90.

Maisch, B., 2019. Cardio-Immunology of Myocarditis: Focus on Immune Mechanisms and Treatment Options. *Frontiers in Cardiovascular Medicine*, 6, p. 48.

Maleszewski, J. J., Orellana, V. M., Hodge, D. O., Kuhl, U., Schultheiss, H. P., Cooper, L. T., 2015. Long-term risk of recurrence, morbidity and mortality in giant cell myocarditis. *American Journal of Cardiology,* 115(12), p. 1733–1738.

Mann, D. L., McMurray, J. J., Packer, M., Swedberg, K., Borer, J. S., Colucci, W. S., Djian, J., Drexler, H., Feldman, A., Kober, L., Krum, H., Liu, P., Nieminen, M., Tavazzi, L., van Veldhuisen, D. J., Waldenstrom, A., Warren, M., Westheim, A., Zannad, F. & Fleming, T., 2004. Targeted anticytokine therapy in patients with chronic heart failure: results of the Randomized Etanercept Worldwide Evaluation (RENEWAL). *Circulation,* 109(13), p. 1594-602.

Marrelli, A., Cipriani, P., Liakouli, V., Carubbi, F., Perricone, C., Perricone, R. & Giacomelli, R., 2011. Angiogenesis in rheumatoid arthritis: a disease specific process or a common response to chronic inflammation?. *Autoimmune Revision*. 10(10), p. 595-8.

Mathias, C. J., Lewis, M. R., Reichert, D. E., Laforest, R., Sharp, T. L., Lewis, J. S., Yang, Z. F., Waters, D. J., Snyder, P. W., Low, P. S., Welch, M. J. & Green, M. A., 2003. Preparation of ^{66}Ga- and ^{68}Ga-labeled Ga(III)-deferoxamine-folate as potential folate-receptor-targeted PET radiopharmaceuticals. *Nuclear Medicine and Biology*, 30, p. 725-731.

Matoh, F., Satoh, H., Shiraki, K., Odagiri, K., Saitoh, T., Urushida, T., Katoh, H., Takehara, Y., Sakahara, H. & Hayashi, H., 2008. The usefulness of delayed enhancement magnetic resonance imaging for diagnosis and evaluation of cardiac function in patients with cardiac sarcoidosis. *Journal of Cardiology*, 51(3), p. 179-88.

Matsui, Y., Iwai, K., Tachibana, T., Fruie, T., Shigematsu, N., Izumi, T., Homma, A. H., Mikami, R., Hongo, O., Hiraga, Y. & Yamamoto, M., 1976. Clinicopathological study of fatal myocardial sarcoidosis. *Annals of the New York Academy of Sciences* , 278, p. 455-69.

Maya, Y., Werner, R. A., Schütz, C., Wakabayashi, H., Samnick, S., Lapa, C., Zechmeister, C., Jahns, R., Jahns, V., Higuchi, T., 2016. ^{11}C-Methionine PET of Myocardial Inflammation in a Rat Model of Experimental Autoimmune Myocarditis. *Journal of Nuclear Medicine*, 57, p. 1985–1990.

Mc Ardle, B. A., Leung, E., Ohira, H., Cocker, M. S., deKemp, R. A., DaSilva, J., Birnie, D., Beanlands, R. S., Nery, P. B., 2013. The role of F(18)-fluorodeoxyglucose positron emission tomography in

guiding diagnosis and management in patients with known or suspected cardiac sarcoidosis. *Journal of Nuclear Cardiology*, 20(2), p. 297-306.

Mehta, D., Lubitz, S. A., Frankel, Z., Wisnivesky, J. P., Einstein, A. J., Goldman, M., Machac, J. & Teirstein, A., 2008. Cardiac involvement in patients with sarcoidosis: diagnostic and prognostic value of outpatient testing. *Chest*, 133(6), p. 1426-1435.

Menichetti, L., Kusmic, C., Panetta, D., Arosio, D., Petroni, D., Matteucci, M., Salvadori, P. A., Casagrande, C., L'Abbate, A., & Manzoni, L., 2013. MicroPET/CT imaging of $\alpha v\beta_3$ integrin via a novel ^{68}Ga-NOTA-RGD peptidomimetic conjugate in rat myocardial infarction. *European Journal of Nuclear Medicine and Molecular Imaging*, 40(8), p. 1265–1274.

Merinen, M., Irjala, H., Salmi, M., Jaakkola, I., Hänninen, A. & Jalkanen, S., 2005. Vascular adhesion protein-1 is involved in both acute and chronic inflammation in the mouse. *American Journal of Pathology*, 166(3), p. 793-800.

Mezu-Ndubuisi, O. J. & Maheshwari, A., 2021. The role of integrins in inflammation and angiogenesis. Pediatric Research, 89(7), p. 1619-1626.

Miron, R. J. & Bosshardt, D. D., 2018. Multinucleated Giant Cells: Good Guys or Bad Guys?. *Tissue Engineering Part B Revision*, 24(1), p. 53-65.

Miron, R. J. & Bosshardt, D. D., 2016. OsteoMacs: Key players around bone biomaterials. *Biomaterials*, 82, p. 1-19.

Mosser, D. M. & Edwards, J. P., 2008. Exploring the full spectrum of macrophage activation. *Nature Reviews Immunology*, 8, p. 958–969.

Mou, T., Zhang, X., Yi, T., Tian, J. & Li, X., 2022. PET/CT Myocardial Inflammation Imaging in Myocarditis Rats by Using a Translocator Protein Tracer ^{18}F-FDPA. *Journal of Nuclear Medicine*, 63 (supplement 2) 3331.

Nagai, S., Yokomatsu, T., Tanizawa, K., Ikezoe, K., Handa, T., Ito, Y., Ogino, S. & Izumi, T., 2014. Treatment with methotrexate and low-dose corticosteroids in sarcoidosis patients with cardiac lesions. *Internal Medicine*, 53(23), p. 2761.

Nagai, T., Kohsaka, S., Okuda, S., Anzai, T., Asano, K. & Fukuda, K., 2014. Incidence and prognostic significance of myocardial late gadolinium enhancement in patients with sarcoidosis without cardiac manifestation. *Chest*, 146(4), p. 1064-1072.

Nagai, T., Nagano, N., Sugano, Y., Asaumi, Y., Aiba, T., Kanzaki, H., Kusano, K., Noguchi, T., Yasuda, S., Ogawa, H. & Anzai, T., 2015. Effect of Corticosteroid Therapy on Long-Term Clinical Outcome and Left Ventricular Function in Patients With Cardiac Sarcoidosis. *Circulation*, 79(7), p. 1593-600.

Nensa, F., Kloth, J., Tezgah, E., Poeppel, T. D., Heusch, P., Goebel, J., Nassenstein, K. & Schlosser, T., 2018. Feasibility of FDG-PET in myocarditis: Comparison to CMR using integrated PET/MRI. *Journal of Nuclear Cardiology*, 25(3), p. 785-794.

Ni, N. C., Jin, C. S., Cui, L., Shao, Z., Wu, J,. Li, S. H., Weisel, R. D., Zheng, G., Li, R. K., 2016. Non-invasive Macrophage Tracking Using Novel Porphysome Nanoparticles in the Post-myocardial Infarction Murine Heart. *Molecular Imaging and Biology*, 18(4), p. 557-68.

Nindl, V., Maier, R., Ratering, D., De Giuli, R., Züst, R., Thiel, V., Scandella, E., Di Padova, F., Kopf, M., Rudin, M., Rülicke, T., Ludewig, B., 2012. Cooperation of Th1 and Th17 cells determines transition from autoimmune myocarditis to dilated cardiomyopathy. *European Journal of Immunology*, 42(9), p. 2311-21.

Nordenswan, H. K., Lehtonen, J., Ekström, K., Räisänen-Sokolowski, A., Mäyränpää, M. I,. Vihinen, T., Miettinen, H., Kaikkonen, K., Haataja, P., Kerola, T., Rissanen, T. T., Kokkonen, J., Alatalo, A., Pietilä-Effati, P., Utriainen, S. & Kupari, M. , 2021. Manifestations and Outcome of Cardiac Sarcoidosis and Idiopathic Giant Cell Myocarditis by 25-Year Nationwide Cohorts. *Journal of American Heart Association*,10(6), e019415.

Jager, N. A., Teteloshvili, N., Zeebregts, C. J., Westra, J. & Bijl, M., 2012. Macrophage folate receptor-β (FR-β) expression in auto-immune inflammatory rheumatic diseases: A forthcoming marker for cardiovascular risk?. *Autoimmunity Reviews*, 11(9), p. 621-6.

Obi, O. N., Lower, E. E. & Baughman, R. P., 2022. Controversies in the Treatment of Cardiac Sarcoidosis. *Sarcoidosis Vasculitis and Diffuse Lung Diseases*, 39(2), e2022015.

Ogino, M. H. & Tadi, P., 2022. Cyclophosphamide. *StatPearls. Treasure Island (FL)*.

Ohira H, Tsujino I, Ishimaru S, Oyama N, Takei T, Tsukamoto E, Miura M, Sakaue S, Tamaki N, Nishimura M, 2008. Myocardial imaging with ^{18}F-fluoro-2-deoxyglucose positron emission tomography and magnetic resonance imaging in sarcoidosis. *European Journal of Nuclear Medicine and Molecular Imaging*. 35(5), p. 933-41.

Okada, R. & Wakafuji, S., 1985. Myocarditis in autopsy. *Heart and Vessels Supplement*, 1, p. 23 – 9.

Okuda, K., Fu, H. Y., Matsuzaki, T., Araki, R., Tsuchida, S., Thanikachalam, P. V., Fukuta, T., Asai, T., Yamato, M., Sanada, S., Asanuma, H., Asano, Y., Asakura, M., Hanawa, H., Hao, H., Oku, N., Takashima, S., Kitakaze, M., Sakata, Y. & Minamino, T., 2016. Targeted Therapy for Acute Autoimmune Myocarditis with Nano-Sized Liposomal FK506 in Rats. *PLoS One*, 11(8), e0160944.

Okumura, W., Iwasaki, T., Toyama, T., Iso, T., Arai, M., Oriuchi, N., Endo, K., Yokoyama, T., Suzuki, T. & Kurabayashi, M., 2004. Usefulness of fasting ^{18}F-FDG PET in identification of cardiac sarcoidosis. *Journal of Nuclear Medicine*, 45(12), p. 1989-98.

Okura, Y., Dec, G. W., Hare, J. M., Kodama, M., Berry, G. J., Tazelaar, H. D., Bailey, K. R., Cooper, L. T., 2003. A clinical and histopathologic comparison of cardiac sarcoidosis and idiopathic giant cell myocarditis. *Journal of the American College of Cardiology*, 41(2), p. 322-9.

Okura, Y., Yamamoto, T., Goto, S., Inomata, T., Hirono, S., Hanawa, H., Feng, L., Wilson, C. B., Kihara, I., Izumi, T., Shibata, A., Aizawa, Y., Seki, S. & Abo, T., 1997. Characterization of cytokine and iNOS mRNA expression in situ during the course of experimental autoimmune myocarditis in rats. *Journal of Molecular and Cellular Cardiology*. 29, p. 491-502.

Olsen, E.G.J., 1985. What is myocarditis?. *Heart Vessels*, 1, 1–3.

Pang, X., He, X., Qiu, Z., Zhang, H., Xie, R., Liu, Z., Gu, Y., Zhao, N., Xiang, Q., Cui, Y., 2003. Targeting integrin pathways: mechanisms and advances in therapy. *Signal Transduction and Targeted Therapy*, 8(1), 1.

Parker, N., Turk, M. J., Westrick, E., Lewis, J. D., Low, P. S. & Leamon, C. P., 2005. Folate receptor expression in carcinomas and normal tissues determined by a quantitative radioligand binding assay. *Analytical Biochemistry*, 338(2), p. 284-93.

Parrish, J.A., 1956. Fiedler's myocarditis. *British Heart Journal*, 27, p. 458-461.

Patel, A. R., Klein, M. R., Chandra, S., Spencer, K. T., Decara, J. M., Lang, R. M., Burke, M. C., Garrity, E. R., Hogarth, D. K., Archer, S. L., Sweiss, N. J. & Beshai, J. F., 2011. Myocardial damage in patients with sarcoidosis and preserved left ventricular systolic function: an observational study. *European Journal of Heart Failur*e, 13(11), p. 1231-7.

Patel, M. R., Cawley, P. J., Heitner, J. F., Klem, I., Parker, M. A., Jaroudi, W. A., Meine, T. J., White, J. B., Elliott, M. D., Kim, H. W., Judd, R. M. & Kim, R. J., 2009. Detection of myocardial damage in patients with sarcoidosis. *Circulation*, 120(20) , p. 1969-77.

Paulos, C. M., Turk, M. J., Breur, G. J. & Low, P. S., 2004. Folate receptor-mediated targeting of therapeutic and imaging agents to activated macrophages in rheumatoid arthritis. *Advanced Drug Delivery Reviews*, 56, p. 1205–1217.

Paulos, C. M., Varghese, B., Widmer, W. R., Breur, G. J., Vlashi, E. & Low, P. S., 2006. Folate-targeted immunotherapy effectively treats established adjuvant and collagen-induced arthritis. *Arthritis Research*, 8, R77.

Perkel, D., Czer, L. S., Morrissey, R.P., Ruzza, A., Rafiei, M., Awad, M., Patel, J. & Kobashigawa, J.A., 2013. Heart transplantation for end-stage heart failure due to cardiac sarcoidosis. *Transplantation Proceedings*, 45(6), p. 2384-6.

Prejbisz, A., Lenders, J. W., Eisenhofer, G., & Januszewicz, A., 2011. Cardiovascular manifestations of phaeochromocytoma. *Journal of Hypertension*, 29(11), p. 2049-2060.

Puig-Kröger, A., Sierra-Filardi, E., Domínguez-Soto, A., Samaniego, R., Corcuera, M. T., Gómez-Aguado, F., Ratnam, M., Sánchez-Mateos, P. & Corbí, A.L., 2009. Folate receptor beta is

expressed by tumor-associated macrophages and constitutes a marker for M2 anti-inflammatory/regulatory macrophages. *Cancer Research*, 69(24), p. 9395-403.

Pyun, K. S., Kim, Y. H., Katzenstein, R. E., Kikkawa, Y., 1970. Giant cell myocarditis. *Archives of Pathology*, 90, p. 181-188.

Rahaghi, F.F., Baughman, R.P., Saketkoo, L.A., Sweiss, N.J., Barney, J.B., Birring, S.S., Costabel, U., Crouser, E.D., Drent, M., Gerke, A.K., Grutters, J. C., Hamzeh, N. Y., Huizar, I., Ennis James, W., Kalra, S., Kullberg, S., Li, H., Lower, E. E., Maier, L. A., Mirsaeidi, M., Müller-Quernheim, J., Carmona Porquera, E. M., Samavati, L., Valeyre, D. & Scholand, M. B., 2020. Delphi consensus recommendations for a treatment algorithm in pulmonary sarcoidosis. *European Respiratory Review*, 29(155), p. 190146.

Reddy, J. A., Haneline, L. S., Srour, E. F., Antony, A.C., Clapp, D. W. & Low, P.S., 1999. Expression and functional characterization of the beta-isoform of the folate receptor on CD34(+) cells. *Blood*, 93(11), p. 3940-8.

Reddy, J. A., L. C. Xu, N. Parker, M. Vetzel, & C. P. Leamon., 2004. Preclinical evaluation of (99m)Tc-EC20 for imaging folate receptor-positive tumors. *Journal of Nuclear Medicin*e, 45, p. 857-866.

Rezzola, S., Loda, A., Corsini, M., Semeraro, F., Annese, T., Presta, M. & Ribatti, D., 2020. Angiogenesis-Inflammation Cross Talk in Diabetic Retinopathy: Novel Insights From the Chick Embryo Chorioallantoic Membrane/Human Vitreous Platform. *Frontiers in Immunology*, 11, 581288.

Roberts, W. C., McAllister, H. A. & Ferrans, V. J., 1977. Sarcoidosis of the heart. A clinicopathologic study of 35 necropsy patients (group 1) and review of 78 previously described necropsy patients (group 11). *American Journal of Medicine*, 63(1), p. 86-108.

Roberts, W. C., Roberts, C. C., Ko, J. M., Filardo, G., Capehart, J. E. & Hall, S. A., 2014. Morphologic features of the recipient heart in patients having cardiac transplantation and analysis of the congruence or incongruence between the clinical and morphologic diagnoses. *Medicine (Baltimore)*, 93(5), p. 211-235.

Rosen, Y., 2022. Pathology of Granulomatous Pulmonary Diseases. *Archives of Pathology & Laboratory Medicine*, 146 (2), p. 233–251.

Ross, J. F., Chaudhuri, P. K. & Ratnam, M., 1994. Differential regulation of folate receptor isoforms in normal and malignant tissues in vivo and in established cell lines. *Physiologic and clinical implications. Cancer*, 73(9), p. 2432-43.

Rossides, M., Kullberg, S., Di Giuseppe, D., Eklund, A., Grunewald, J., Askling, J. & Arkema, E. V., 2021. Infection risk in sarcoidosis patients treated with methotrexate compared to azathioprine: A retrospective 'target trial' emulated with Swedish real-world data. *Respirology*, 26(5), p. 452-460.

Rothberg, K. G., Ying, Y. S., Kolhouse, J. F., Kamen, B. A. & Anderson, R. G., 1990. The glycophospholipid-linked folate receptor internalizes folate without entering the clathrin-coated pit endocytic pathway. J*ournal of Cell Biology*, 110(3), p. 637-49.

Rybicki, B. A., Iannuzzi, M. C., Frederick, M.M., Thompson, B. W., Rossman, M. D., Bresnitz, E. A., Terrin, M. L., Moller, D. R., Barnard, J., Baughman, R. P., DePalo, L., Hunninghake, G., Johns, C., Judson, M. A., Knatterud, G. L., McLennan, G., Newman, L. S., Rabin, D. L., Rose, C., Teirstein, A. S., Weinberger, S. E., Yeager, H. & Cherniack, R., 2001. Familial aggregation of sarcoidosis. A case-control etiologic study of sarcoidosis (ACCESS). *American Journal of Respiratory and Critical Care Medicin*e, 164(11), p. 2085-91.

Sahoo, D.H., Bandyopadhyay, D., Xu, M., Pearson, K., Parambil, J. G., Lazar, C. A., Chapman, J. T. & Culver, D. A., 2011. Effectiveness and safety of leflunomide for pulmonary and extrapulmonary sarcoidosis. European Respiratory Journal, 38(5), p. 1145-50.

Saidha, S., Sotirchos, E. S. & Eckstein, C., 2012. Etiology of sarcoidosis: does infection play a role?. *Yale Journal of Biology and Medicine*, 85(1), p. 133-41.

Salazar, M. D. & Ratnam, M., 2007. The folate receptor: What does it promise in tissue targeted therapeutics?. *Cancer Metastasis Reviews*. 26(1), p. 141–152.

Salmi, M. & Jalkanen, S., 2001. VAP-1: an adhesin and an enzyme (2001). Trends in Immunology, 22, 211–6.

Salmi, M. & Jalkanen, S., 1992. A 90-kilodalton endothelial cell molecule mediating lymphocyte binding in humans. *Science*, 257, p. 1407–1409.

Saltykow, S., 1905. Uber Diffuse Myokarditis. *Virchows Archiv. A pathol Anat*, 182, p. 1–39.

Sarrazy, V., Koehler, A., Chow, M. L., Zimina, E., Li, C. X., Kato, H., Caldarone, C. A. & Hinz, B., 2014. Integrins αvβ5 and αvβ3 promote latent TGF-β1 activation by human cardiac fibroblast contraction. *Cardiovascular Research*. 102, p. 407–417.

Sato, H., Woodhead, F. A., Ahmad, T., Grutters, J. C., Spagnolo, P., van den Bosch, J. M., Maier, L. A., Newman, L. S., Nagai, S., Izumi, T., Wells, A. U., du Bois, R. M. & Welsh, K. I., 2010. Sarcoidosis HLA class II genotyping distinguishes differences of clinical phenotype across ethnic groups. *Human Molecular Genetics*. 19(20), p. 4100-11.

Schatka, I. & Bengel, F. M., 2014. Advanced imaging of cardiac sarcoidosis. *Journal of Nuclear Medicine*, 55, p. 99–106.

Schniering, J., Benešová, M., Brunner, M., Haller, S., Cohrs, S., Frauenfelder, T., Vrugt, B., Feghali-Bostwick, C., Schibli, R., Distler, O., Müller, C. & Maurer, B., 2019. ^{18}F-AzaFol for Detection of Folate Receptor-β Positive Macrophages in Experimental Interstitial Lung Disease—A Proof-of-Concept Study. *Frontiers of Immunology*, 10, p. 2724.

Schuller, J. L., Lowery, C. M., Zipse, M., Aleong, R. G., Varosy, P. D., Weinberger, H. D. & Sauer, W. H., 2011. Diagnostic utility of signal-averaged electrocardiography for detection of cardiac sarcoidosis. *Annals of Noninvasive Electrocardiology*, 16(1), p .70-6.

Schuller, J. L., Olson, M. D., Zipse, M. M., Schneider, P. M., Aleong, R. G., Wienberger, H. D., Varosy, P. D., Sauer, W. H., 2011. Electrocardiographic characteristics in patients with pulmonary sarcoidosis indicating cardiac involvement. *Journal of Cardiovascular Electrophysiology*, 22(11), p. 1243-8.

Schultz, J. C., Hilliard, A. A., Cooper, L. T. & Rihal, C. S., 2009. Diagnosis and treatment of viral myocarditis. *Mayo Clinic Proceedings*, 84(11), p. 1001-9.

Sekhri, V., Sanal, S., Delorenzo, L. J., Aronow, W. S. & Maguire, G. P., 2011. Cardiac sarcoidosis: a comprehensive review. *Archives of Medical Science*, 7(4), p. 546-54.

Shah, C. P. & Moreb, J. S., 2019. Cardiotoxicity due to targeted anticancer agents: a growing challenge. *Therapeutic advances in cardiovascular disease*, 13, 1753944719843435.

Sharma, O. P., 2008. Sarcoidosis around the world. *Clinical Chest Medicine*, 29(3), p. 357-63.

Shen, F., Ross, J. F., Wang, X. & Ratnam, M., 1994. Identification of a novel folate receptor, a truncated receptor, and receptor type beta in hematopoietic cells: cDNA cloning, expression, immunoreactivity, and tissue specificity. *Biochemistry*, 33, p. 1209–1215.

Shen, F., Wu, M., Ross, J. F., Miller, D., Ratnam, M., 1995. Folate receptor type gamma is primarily a secretory protein due to lack of an efficient signal for glycosylphosphatidylinositol modification: protein characterization and cell type specificity. *Biochemistry*, 34, p. 5660–5665.

Shen, J., Hilgenbrink, A. R., Xia, W., Feng, Y., Dimitrov, D. S., Lockwood, M. B., Amato, R. J. & Low, P. S., 2014. Folate receptor-β constitutes a marker for human proinflammatory monocytes. Journal of Leukocyte Biology, 96(4), p. 563-70.

Shen, J., Putt, K. S., Visscher, D. W., Murphy, L., Cohen, C., Singhal, S., Sandusky, G., Feng, Y., Dimitrov, D. & Low, P. S., 2015. Assessment of folate receptor β expression in human neoplastic tissues. Oncotarget, 6(16), p. 14700-14709.

Shen, J., Chelvam, V., Cresswell, G. & Low, P. S., 2013. Use of folate-conjugated imaging agents to target alternatively activated macrophages in a murine model of asthma. *Molecular Pharmacology*, 10, p. 1918-1927.

Sherif, H. M., Saraste, A., Nekolla, S. G., Weidl, E., Reder, S., Tapfer, A., Rudelius M, Higuchi T, Botnar, R. M., Wester, H. J. & Schwaiger, M., 2012. Molecular imaging of early αvβ3 integrin expression predicts long-term left-ventricle remodeling after myocardial infarction in rats. *Journal of Nuclear Medicine*, 53, p. 318– 23.

Shields, R. C., Tazelaar, H. D., Berry, G. J. & Cooper, L. T., 2002. The role of right ventricular endomyocardial biopsy for idiopathic giant cell myocarditis. *Journal of Cardiac Failure*. 8(2), p. 74-8.

Siegel, B. A., F. Dehdashti, D. G. Mutch, D. A. Podoloff, R. Wendt, G. P. Sutton, R. W. Burt, P. R. Ellis, C. J. Mathias, C. J., Green, M. A. & Gershenson, D. M., 2003. Evaluation of 111InDTPA-folate as a receptor-targeted diagnostic agent for ovarian cancer: initial clinical results. *Journal of Nuclear Medicine*, 44, p. 700-707.

Siitonen, R., Pietikäinen, A., Liljenbäck, H., Käkelä, M., Söderström, M., Jalkanen, S., Hytönen, J. & Roivainen, A., 2017. Targeting of vascular adhesion protein-1 by positron emission tomography visualizes sites of inflammation in Borrelia burgdorferi-infected mice. *Arthritis Research and Therapy*, 19, p. 254.

Silvola, J. M., Virtanen, H., Siitonen, R., Hellberg, S., Liljenbäck, H., Metsälä, O., Ståhle, M., Saanijoki, T., Käkelä, M., Hakovirta, H., Ylä-Herttuala, S., Saukko, P., Jauhiainen, M., Veres, T. Z., Jalkanen, S., Knuuti, J., Saraste, A. & Roivainen, A., 2016. Leukocyte trafficking-associated vascular adhesion protein 1 is expressed and functionally active in atherosclerotic plaques. *Scientific Reports*, 6, p. 35089.

Silvola, J. M., Li, X. G., Virta, J., Marjamäki, P., Liljenbäck, H., Hytönen, J. P., Tarkia, M., Saunavaara, V., Hurme, S., Palani, S., Hakovirta, H., Ylä-Herttuala, S., Saukko, P., Chen, Q., Low, P. S., Knuuti, J., Saraste, A. & Roivainen, A., 2018. Aluminum fluoride-18 labeled folate enables in vivo detection of atherosclerotic plaque inflammation by positron emission tomography. *Scientific Reports*, 8(1), p. 9720.

Smedema, J. P., Snoep, G., van Kroonenburgh, M. P., van Geuns, R. J., Dassen, W. R., Gorgels, A. P. & Crijns, H. J., 2005. Cardiac involvement in patients with pulmonary sarcoidosis assessed at two university medical centers in the Netherlands. *Chest*, 128(1), p. 30-5.

Sobernheim, J. F., 1837. Praktische Diagnostik der inneren Krankheiten mit vorzueglicher Ruecksicht auf pathologische Anatomie. *Hirschwald, Berlin*, p 117.

Sozzi, F. B., Gherbesi, E., Faggiano, A., Gnan, E., Maruccio, A., Schiavone, M., Iacuzio, L., Carugo, S., 2022. Viral Myocarditis: Classification, Diagnosis, and Clinical Implications. *Frontiers in Cardiovascular Medicine*, 9, 908663.

Spiegelstein, O., Eudy, J. D. & Finnell, R. H., 2000. Identification of two putative novel folate receptor genes in humans and mouse. Gene, 258(1-2), p. 117-25.

Ståhle, M., Kytö, V., Kiugel, M., Liljenbäck, H., Metsälä, O., Käkelä, M., Li, X. G., Oikonen, V., Saukko, P., Saukko, P., Nuutila, P.,Knuuti, J., Roivainen, A. & Saraste, A., 2020. Glucagon-like peptide-1 receptor expression after myocardial infarction: Imaging study using ^{68}Ga-NODAGA-exendin-4 positron emission tomography. J*ournal of Nuclear Cardiology*, 27(6), p. 2386-2397.

Statement on sarcoidosis., 1999. Joint Statement of the American Thoracic Society (ATS), the European Respiratory Society (ERS) and the World Association of Sarcoidosis and Other Granulomatous Disorders (WASOG) adopted by the ATS Board of Directors and by the ERS Executive Committee. *American Journal of Respiratory and Critical Care Medicin*e, 160, p. 736–55.

Stievenart, J., Le Guenno, G., Ruivard, M., Rieu, V., André, M. & Grobost, V., 2022. Cardiac sarcoidosis: systematic review of the literature on corticosteroid and immunosuppressive therapies. *European Respiratory Journal*, 59(5), 2100449.

Sverrild, A., Backer, V., Kyvik, K. O., Kaprio, J., Milman, N., Svendsen, C. B. & Thomsen, S. F. , 2008. Heredity in sarcoidosis: a registry-based twin study. *Thorax*, 63(10), p. 894-6.

Tam, P. E., 2006. Coxsackievirus myocarditis: interplay between virus and host in the pathogenesis of heart disease. *Viral Immunology*, 19(2), p. 133-46.

Tavora, F., Cresswell, N., Li, L., Ripple, M., Solomon, C. & Burke, A., 2009. Comparison of necropsy findings in patients with sarcoidosis dying suddenly from cardiac sarcoidosis versus dying suddenly from other causes. *American Journal of Cardiology*, 104(4), p. 571-7.

Terasaki, F., Azuma, A., Anzai, T., Ishizaka, N., Ishida, Y., Isobe, M., Inomata, T., Ishibashi-Ueda, H., Eishi, Y., Kitakaze, M., Kusano, K., Sakata, Y., Shijubo, N., Tsuchida, A., Tsutsui, H., Nakajima, T., Nakatani, S., Horii, T., Yazaki, Y., Yamaguchi, E., Yamaguchi, T., Ide, T., Okamura, H., Kato, Y., Goya, M., Sakakibara, M., Soejima, K., Nagai, T., Nakamura, H., Noda, T., Hasegawa, T., Morita, H., Ohe, T., Kihara, Y., Saito, Y., Sugiyama, Y., Morimoto, S. I. & Yamashina, A., 2019. Japanese Circulation Society Joint Working Group. JCS 2016 Guideline on Diagnosis and Treatment of Cardiac Sarcoidosis - Digest Version. *Circulation Journal*, 83(11), p. 2329-2388.

Tesluk, H., 1956. Giant cell versus granulomatous myocarditis. *American Journal of Clinical Pathology*, 26, p. 1326-1333.

Tezuka D, Terashima M, Kato Y, Toriihara A, Hirasawa K, Sasaoka T, Yoshikawa S, Maejima Y, Ashikaga T, Suzuki J, Hirao K, Isobe M, 2015. Clinical characteristics of definite or suspected isolated cardiac sarcoidosis: application of cardiac magnetic resonance imaging and ^{18}F-Fluoro-2-deoxyglucose positron-emission tomography/computerized tomography. *Journal of Cardiac Failure*. 21(4), p. 313-22.

Theaker, J. M., Gatter, K. C., Evans, D. J. & McGee, J. O., 1985. Giant cell myocarditis: Evidence for the macrophage origin of the giant cells. *Journal of Clinical Pathology*, 38, p. 160-164.

Toffoli, G., Cernigoi, C., Russo, A., Gallo Bagnoli, M. & Boiocchi, M., 1997. Overexpression of folate binding protein in ovarian cancers. *International Journal of Cancer*, 74(2), 193-8.

Tsuneyoshi, Y., Tanaka, M., Nagai, T., Sunahara, N., Matsuda, T., Sonoda, T., Ijiri, K., Komiya, S. & Matsuyama, T., 2012. Functional folate receptor beta-expressing macrophages in osteoarthritis synovium and their M1/M2 expression profiles. *Scandinavian Journal of Rheumatology*, 41(2), p. 132-40.

Tubbs, R. R., Sheibani, K. & Hawk, W. A., 1980. Giant cell myocarditis. Archives of Pathology & Laboratory Medicine, 104, 245-246.

Turk, M. J., Breur, G. J., Widmer, W. R., Paulos, C. M., Xu, L. C., Grote, L. A. & Low, P. S., 2002. Folate-targeted imaging of activated macrophages in rats with adjuvant-induced arthritis. *Arthritis & Rheumatology*, 46, p. 1947-1955.

Turkington, T.G., 2001. Introduction to PET Instrumentation. *Journal of Nuclear Medicine Technology*, 29, p. 1–8.

Uemura, A., Morimoto, S., Kato, Y., Hiramitsu, S., Ohtsuki, M., Kato, S., Sugiura, A., Miyagishima, K., Iwase, M. & Hishida, H., 2005. Relationship between basal thinning of the interventricular septum and atrioventricular block in patients with cardiac sarcoidosis. *Sarcoidosis, Vasculitis and Diffuse Lung Diseases*, 22(1), p. 63-5.

Upadhrasta, S., Elias, H., Patel, K. & Zheng, L., 2019. Managing cardiotoxicity associated with immune checkpoint inhibitors. *Chronic Diseases and Translational Medicine*. 5(1), p. 6-14.

Van den Borne, S. W., Isobe, S., Verjans, J. W., Petrov, A., Lovhaug, D., Li, P., Zandbergen, H. R., Ni, Y., Frederik, P., Zhou, J., Arbo, B., Rogstad, A., Cuthbertson, A., Chettibi, S., Reutelingsperger, C., Blankesteijn, W. M., Smits, J. F., Daemen, M. J., Zannad, F., Vannan, M. A., Narula, N., Pitt, B., Hofstra, L. & Narula, J., 2008. Molecular imaging of interstitial alterations in remodeling myocardium after myocardial infarction. *Journal of American College of Cardiology*, 52(24), p. 2017-28.

Van Der Gucht, A., Pomoni, A., Jreige, M., Allemann, P., & Prior, J. O., 2016. ^{68}Ga-NODAGARGDyK PET/CT Imaging in Esophageal Cancer. *Clinical Nuclear Medicine*, 00(00), p. 1.

Van Heeswijk, R. B., De Blois, J., Kania G, Gonzales, C., Blyszczuk, P., Stuber, M., Eriksson, U. & Schwitter, J., 2013. Selective in vivo visualization of immune-cell infiltration in a mouse model of autoimmune myocarditis by fluorine-19 cardiac magnetic resonance. *Circulation: Cardiovascular Imaging* . 6, p. 277-284.

Van Maarsseveen, T. C., Vos, W., & Van Diest, P. J., 2009. Giant cell formation in sarcoidosis: cell fusion or proliferation with non-division?. Clinical and Experimental Immunology, 155(3), p. 476–486.

Varghese, B., Haase, N. & Low, P. S., 2007. Depletion of folate-receptor-positive macrophages leads to alleviation of symptoms and prolonged survival in two murine models of systemic lupus erythematosus. *Molecular Pharmacology*, 4(5), p. 679-85.

Verweij, N. J. F., Yaqub, M., Bruijnen, S. T. G., Pieplenbosch, S., Ter Wee, M. M., Jansen, G., Chen, Q., Low, P. S., Windhorst, A. D., Lammertsma, A. A., Hoekstra, O. S., Voskuyl, A. E. & van der Laken, C. J., 2020. First in man study of [^{18}F]fluoro-PEG-folate PET: a novel macrophage imaging technique to visualize rheumatoid arthritis. *Scientific Reports*, 10(1), p. 1047.

Vignaux, O., Dhote, R., Duboc, D., Blanche, P., Devaux, J. Y., Weber, S. & Legmann, P., 2002. Detection of myocardial involvement in patients with sarcoidosis applying T2-weighted, contrast-enhanced, and cine magnetic resonance imaging: initial results of a prospective study. *Journal of Computer Assisted Tomography*, 26(5), p. 762-7.

Viitanen, R., Moisio, O., Lankinen, P., Li, X. G., Koivumäki, M., Suilamo, S., Tolvanen, T., Taimen, K., Mali, M., Kohonen, I., Koskivirta, I., Oikonen, V., Virtanen, H., Santalahti, K., Autio, A., Saraste, A., Pirilä, L., Nuutila, P., Knuuti, J., Jalkanen, S. & Roivainen, A., 2021. First-in-Humans Study of ^{68}Ga-DOTA-Siglec-9, a PET Ligand Targeting Vascular Adhesion Protein 1. *Journal of Nuclear Medicine*, 62(4), p. 577-583.

Virtanen, H., Autio, A., Siitonen, R., Liljenbäck, H., Saanijoki, T., Lankinen, P., Mäkilä, J., Käkelä, M., Teuho, J., Savisto, N., Jaakkola, K., Jalkanen, S. & Roivainen, A., 2015. ^{68}Ga-DOTA-Siglec-9--a new imaging tool to detect synovitis. *Arthritis Research and Therapy*, 17, p. 308.

Vorselaars, A. D. M., Wuyts, W. A., Vorselaars, V. M. M., Zanen, P., Deneer, V. H. M., Veltkamp, M., Thomeer, M., van Moorsel, C. H. M. & Grutters, J. C., 2013. Methotrexate vs azathioprine in second-line therapy of sarcoidosis. *Chest*, 144(3), p. 805-812.

Wada, A. M., Kudo, Y., & Tanaka, S., 2001. T-cell transfer model of autoimmune myocarditis. *Nature Immunology*, 2(1), p. 44-50.

Wang, A., Singh, K., Ibrahim, W., King, B. & Damsky, W., 2020. The Promise of JAK Inhibitors for Treatment of Sarcoidosis and Other Inflammatory Disorders with Macrophage Activation: A Review of the Literature. *Yale Journal of Biology and Medicine*, 93(1),p. 187-195.

Watanabe, M., Panetta, G. L., Piccirillo, F., Spoto, S., Myers, J., Serino, F. M., Costantino, S. & Di Sciascio, G., 2019. Acute Epstein-Barr related myocarditis: An unusual but life-threatening disease in an immunocompetent patient. *Journal of Cardiology Cases*, 21(4), p. 137-140.

Weitman, S. D., Weinberg, A. G., Coney, L. R., Zurawski, V. R., Jennings, D. S., Kamen, B. A., 1992. Cellular localization of the folate receptor: potential role in drug toxicity and folate homeostasis. *Cancer Research*, 52(23), p. 6708-11.

Werner, R. A., Wakabayashi, H., Bauer, J., Schütz, C., Zechmeister, C., Hayakawa, N., Javadi, M. S., Lapa, C., Jahns, R., Ergün, S., Jahns, V. & Higuchi, T., 2019. Longitudinal ^{18}F-FDG PET imaging in a rat model of autoimmune myocarditis. *European Heart Journal of Cardiovascular Imaging*, 20, p. 467-474.

Whitehead, R., 1965. Isolated myocarditis. *British Heart Journal*, 27, p. 220 – 30.

Wibowo, A. S., Singh, M., Reeder, K. M., Carter, J. J., Kovach, A. R., Meng, W., Ratnam, M., Zhang, F. & Dann, C. A., 2013. Structures of human folate receptors reveal biological trafficking states and diversity in folate and antifolate recognition. *Proceedings of the National Academy of Sciences of the United States of America*, 110(38), p. 15180–15188.

Wu, M., Gunning, W. & Ratnam, M., 1999. Expression of folate receptor type alpha in relation to cell type, malignancy, and differentiation in ovary, uterus, and cervix. *Cancer Epidemiology, Biomarkers & Prevention*, 8(9), p. 775-82.

Wu, W., Li, X., Zuo, G., Pu, J., Wu, X. & Chen, S., 2018. The role of angiogenesis in coronary artery disease: a double-edged sword: intraplaque angiogenesis in physiopathology and therapeutic angiogenesis for treatment. *Current Pharmaceutical Design*, 24, p. 451–64.

Wu, Y., Li, P., Zhang, H., Shi, Y., Wu, H., Zhang, J., Qian, Y., Li, C. & Yang, J., 2013. Diagnostic value of fluorine 18 fluorodeoxyglucose positron emission tomography/computed tomography for

the detection of metastases in non-small-cell lung cancer patients. *International Journal of Cancer*, 132(2), p. E37-47.

Xia, W., Hilgenbrink, A. R., Matteson, E. L., Lockwood, M. B., Cheng, J. X. & Low, P. S., 2009. A functional folate receptor is induced during macrophage activation and can be used to target drugs to activated macrophages. *Blood*, 113(2), p. 438-46.

Xu, J. & Brooks, E. G., 2016. Giant Cell Myocarditis: A Brief Review. *Archives of Pathology & Laboratory Medicine,* 140(12), p. 1429-1434.

Yala-Lopez, W., Xia, W., Varghese, B. & Low, P. S., 2010. Imaging of atherosclerosis in apoliprotein e knockout mice: targeting of a folate-conjugated radiopharmaceutical to activated macrophages. *Journal of Nuclear Medicine*, 51, p. 768-774.

Yang, J., Chen, H., Vlahov, I. R., Cheng, J. X. & Low, P. S., 2007. Characterization of the pH of folate receptor-containing endosomes and the rate of hydrolysis of internalized acid-labile folate-drug conjugates. *Journal of Pharmacology and Experimental Therapeutics*, 321(2), p. 462-8.

Yashima, Y. & Ohgane, T., 2001. [Pharmacological profiles of mycophenolate mofetil (CellCept), a new immunosuppressive agent]. *Nihon Yakurigaku Zasshi*, 117(2), p. 131-7.

Yasutake, H., Seino, Y., Kashiwagi, M., Honma, H., Matsuzaki, T., Takano, T., 2005. Detection of cardiac sarcoidosis using cardiac markers and myocardial integrated backscatter. *International Journal of Cardiology*, 102, p. 259–68.

Yazaki, Y., Isobe, M., Hiramitsu, S., Morimoto, S., Hiroe, M., Omichi, C., Nakano, T., Saeki, M., Izumi, T. & Sekiguchi, M., 1998. Comparison of clinical features and prognosis of cardiac sarcoidosis and idiopathic dilated cardiomyopathy. *American Journal of Cardiology*, 82(4), p. 537-40.

Yazaki, Y., Isobe, M., Hiroe, M., Morimoto, S., Hiramitsu, S., Nakano, T., Izumi, T. & Sekiguchi, M., 2001. Central Japan Heart Study Group. Prognostic determinants of long-term survival in Japanese patients with cardiac sarcoidosis treated with prednisone. *American Journal of Cardiology*, 88(9), p. 1006-10.

Yi, Y. S., Yala-Lopez, W., Kularatne, S. A. & Low, P. S., 2009. Folate-targeted hapten immunotherapy of adjuvant-induced arthritis: comparison of hapten potencies. *Molecular Pharmacology*, 6, p. 1228-1236.

Yi, Y. S., 2016. Folate Receptor-Targeted Diagnostics and Therapeutics for Inflammatory Diseases. *Immune Network*, 16(6), p. 337–343.

Yilmaz, A., Kindermann, I., Kindermann, M., Mahfoud, F., Ukena, C., Athanasiadis, A., Hill, S., Mahrholdt, H., Voehringer, M., Schieber, M., Klingel, K., Kandolf, R., Böhm, M. & Sechtem, U., 2010. Comparative evaluation of left and right ventricular endomyocardial biopsy: differences in complication rate and diagnostic performance. *Circulation*, 122(9), p. 900-9.

Yoshida, T., Maekawa, N., Wada, Y., Suzuki, M., Kobayashi, M., & Shirai, T., 1999. Autoimmune myocarditis in MRL-lpr/lpr mice: Presence of myocarditis-related autoantigens in subcellular fractions of heart muscle. *Journal of Autoimmunity*, 13(2), p. 169-176 .

Yoshida A, Ishibashi-Ueda H, Yamada N, Kanzaki H, Hasegawa T, Takahama H, Amaki M, Asakura M, Kitakaze M, 2013. Direct comparison of the diagnostic capability of cardiac magnetic resonance and endomyocardial biopsy in patients with heart failure. *European Journal of Heart Failure*. 15(2), p. 166-75.

Youssef, G., Leung, E., Mylonas, I., Nery, P., Williams, K., Wisenberg, G., Gulenchyn, K. Y., Dekemp, R. A., Dasilva, J., Birnie, D., Wells, G. A. & Beanlands, R. S., 2012. The use of ^{18}F-FDG PET in the diagnosis of cardiac sarcoidosis: a systematic review and metaanalysis including the Ontario experience. *Journal of Nuclear Medicine*, 53(2), p. 241-8.

Zhang, M., Tavora, F., Huebner, T., Heath, J. & Burke, A., 2012. Allograft pathology in patients transplanted for idiopathic dilated cardiomyopathy. *American Journal of Surgical Pathology*, 36(3), p. 389-95.

Zhang, S., Kodama, M., Hanawa, H., Izumi, T., Shibata, A. & Masani, F., 1993. Effects of cyclosporine, prednisolone, and aspirin on rat autoimmune giant cell myocarditis. *Journal of the American College of Cardiology*, 21(5), p. 254–260.

Ziora, D., Jastrzębski, D., Adamek, M., Czuba, Z., Kozielski, J. J., Grzanka, A. & Kasperska-Zajac, A., 2015. Circulating concentration of markers of angiogenic activity in patients with sarcoidosis and idiopathic pulmonary fibrosis. *BMC Pulmunary Medicine*, 15, p. 113.

Zipse, M. M. & Sauer, W. H., 2014. Cardiac sarcoidosis. *Current Cardiology Reports*, 16, p. 514–10.

Zipse, M. M, & Sauer, W. H., 2013. Electrophysiologic manifestations of cardiac sarcoidosis. *Current Opinion in Pulmonary Medicine*, 19, p. 485–92.

TURUN
YLIOPISTO
UNIVERSITY
OF TURKU

Painosalama, Turku, Finland 2024

ISBN 978-951-29-9994-1 (PRINT)
ISBN 978-951-29-9995-8 (PDF)
ISSN 0355-9483 (Print)
ISSN 2343-3213 (Online)